European Journal of Pharmaceutical Sciences 104 (2017) 114–123

Contents lists available at ScienceDirect

European Journal of Pharmaceutical Sciences

journal homepage: www.elsevier.com/locate/ejps

Statistically optimized fast dissolving microneedle transdermal patch of meloxicam: A patient friendly approach to manage arthritis

Sejal Amodwala, Praveen Kumar, Hetal P. Thakkar*

Shri G. H. Patel Pharmacy Building, Faculty of Pharmacy, The Maharaja Sayajirao University of Baroda, Fatehgunj, Vadodara 390 002, Gujarat, INDIA.

ARTICLE INFO

Keywords:
Meloxicam
Fast-dissolving microneedle
Micromolding technique
Transdermal patch
Permeation enhancement

ABSTRACT

Introduction: The long term administration of Meloxicam for the management of arthritis, a chronic disorder, results in gastrointestinal disturbances leading to poor patient compliance. Considering the favorable molecular weight, therapeutic dose, biological half-life and log P value of meloxicam for transdermal delivery, its fast dissolving microneedle patch, with an ability to breach the *stratum corneum* and efficiently deliver the cargo to deeper skin layers, were developed.

Methods: Microneedle patch of low molecular weight polyvinyl alcohol and polyvinylpyrrolidone was prepared using Polydimethylsiloxane micromolds. The ratio of polyvinyl alcohol to polyvinyl pyrrolidone and solid content of matrix solution was optimized to achieve maximum needle strength. The optimized batch was extensively evaluated for *in vitro* dissolution, drug release, stability, *ex vivo* skin permeation/deposition, histopathology and *in vivo* pharmacodynamic study.

Results: The patch containing 9:1 polyvinyl alcohol to polyvinylpyrrolidone ratio with 50% solid content had shown maximum axial needle fracture force (0.9 N) suitable for penetrating the skin. The optimized batch was found to be fast dissolving and released almost 100% drug in 60 min following dissolution controlled kinetics. The formulation showed a significant drug deposition within skin (63.37%) and an improved transdermal flux (1.60 μg/cm^2/h) with a 2.58 fold enhancement in permeation as compared to plain drug solution. The formulation showed a comparable anti-inflammatory activity in rats when compared to its existing approved marketed oral tablet. Histopathology and stability evaluations demonstrated acceptable safety and shelf-life of the developed formulation.

Conclusion: The successful verification of safety, efficacy and stability of microneedle patch advocated the suitability of the formulation for transdermal use.

1. Introduction

Arthritis, an acute or chronic inflammation of a joint is often characterized by pain and structural changes and is associated with diverse causes such as inflammation, crystal deposition, injury, abnormal metabolism, infections and immune system dysfunction. Based on National Health Interview Survey (NHIS) data of 2010–2012, an estimated 22.7% of adults had self-reported doctor-diagnosed arthritis while 9.8% of those with arthritis have arthritis-attributable activity limitation (Prevention, 2013). Out of different forms of arthritis, the most common types are osteoarthritis and rheumatoid arthritis. Osteoarthritis is the most frequent and symptomatic health problem for middle aged and elderly people (Buckwalter and Martin, 2006) which is characterized by cartilage degenerative changes and bone proliferation while Rheumatoid arthritis is an autoimmune disease which causes chronic inflammation of the joints and most often starts at the age of 45–55 years (Saad et al., 2016). Nonsteroidal anti-inflammatory drugs such as diclofenac, aceclofenac, piroxicam, meloxicam, celecoxib, rofecoxib, mefenamic acid *etc*. are widely used for the management of osteoarthritis and rheumatoid arthritis. However, orally administered non-steroidal anti-inflammatory drugs cause various side effects like nausea, vomiting, abdominal pain, heartburn, dizziness and headache (USFDA, 2007).

Meloxicam is an oxicam derivative having a molecular weight of 351.401 g/mol, LogP of 3.43 and half-life of 15 to 20 h (Dowd et al., 2016). Commercially, it is available as oral suspension, tablet and capsule dosage forms at two different strengths of 7.5 mg and 15 mg (Wishart et al., 2005). Orally administered meloxicam causes the common side effects as associated with other non-steroidal anti-inflammatory drugs. The drugs used in the management of arthritis are usually required to be taken for very long periods as it is a chronic disorder. The occurrence of gastrointestinal side effects leads to poor

* Corresponding author at: Pharmacy Department, Faculty of Pharmacy, The Maharaja Sayajirao University of Baroda, PO Box No. 51, Kalabhavan, Vadodara 390 001, Gujarat, INDIA.
E-mail address: hetal.thakkar-pharmacy@msubaroda.ac.in (H.P. Thakkar).

http://dx.doi.org/10.1016/j.ejps.2017.04.001
Received 21 February 2017; Received in revised form 30 March 2017; Accepted 1 April 2017
Available online 03 April 2017
0928-0987/

patient compliance. As described above, meloxicam possess favorable characteristics for transdermal route. Transdermal delivery offers several potential advantages, including avoidance of hepatic first pass metabolism, reduction of the severe adverse effects on the gastrointestinal tract associated with oral drug administration, provides sustained drug release for a prolonged period of time and ease of drug delivery termination in case of the occurrence of toxicity. However, transdermal delivery of drugs is limited due to highly efficient protective barrier *i.e. stratum* corneum (SC) and usually various physical, chemical or formulation based penetration enhancement approaches have been employed to modulate the barrier function of the skin (Bharkatiya and Nema, 2009). Use of chemicals as penetration enhancers often leads to skin irritation while stability and scale up problems are associated with formulation approach. Physical approaches like iontophoresis, sonophoresis, electroporation (Ranade and Cannon, 2011) *etc.* are needed to achieve the desired plasma concentration. However, these techniques have inherent limitations such as requirement of application of electric current or sound energy, usually self- treatment is not feasible and also it may cause pain to the patient (Prausnitz, 1996). Design of a formulation which could potentiate the skin permeability and avoid the side effects of currently available oral marketed formulations would lead to an increased patient compliance due to avoidance of gastrointestinal side effects. One of the interesting physical penetration enhancement technique is the use of microneedles array, which is composed of small micron-sized needles which, when applied on the skin, disrupt the SC barrier by creating large aqueous microchannels that allow for the passage of molecules through the skin without damaging it (Singh and Yadav, 2016). They do not touch the nerve endings and thus are devoid of pain. Microneedles are made up of different types of materials such as silicon, rubber, titanium, glass, stainless steel and various polymers (Hong et al., 2013; Pamornpathomkul et al., 2015). Based on these materials, microneedles can be classified into two categories: (i) Non-biodegradable microneedles which can be fabricated using different metals or nondegradable polymers such as polycarbonate, polymethylmethacrylate and photolithographic epoxy. Non-biodegradable microneedles may break and leave residue in the skin causing toxicity and discomfort to the patient (Brady and Donnelly, 2016). On the other hand, (ii) Biodegradable microneedles that encapsulate drugs and fully or partially dissolve in the skin can be fabricated using different biodegradable polymers such as polylactides, polyglycolides, poly (lactide-co-glycolides), maltose, amylopectin *etc.* (Hong et al., 2013). They can be used for controlled or rapid release of active pharmaceutical ingredients by choosing the proper polymers. Hydrophilic polymers such as polyvinyl alcohol, polyvinylpyrrolidone and sugars have been used to produce fast dissolving microneedle array (Lee et al., 2015). Meloxicam is a poorly water soluble drug and in microneedles, it needs to be in solubilized state. Thus, polyvinyl alcohol was selected as a polymer to prepare a microneedle as it also acts as a solubilizer (Brough et al., 2016).

Thus, the aim of the present investigation was to prepare fast dissolving microneedle patches containing meloxicam in order to potentiate the skin permeability and to avoid the side effects of currently available oral marketed formulations.

2. Materials and methods

2.1. Materials

Meloxicam was kindly gifted by Bharat Parenterals Ltd., India. Derma Stamp (L4001, 1.5 mm needle length) was purchased from Guangzhou Junguan Beauty Co. Ltd., China. Sylgard® 184 (polydimethylsiloxane) was purchased from Dow Corning, USA. Polyvinyl alcohol (molecular weight, 6000 Da) and polyvinylpyrrolidone (molecular weight, 3500 Da) were purchased from Acros Organics, India. High adhesion double coated medical tape (1567) was obtained as a gift sample from 3M, USA. All the other materials and solvents used were of analytical reagent grade.

2.2. Methods

2.2.1. Fabrication of meloxicam loaded microneedle patch

Meloxicam loaded microneedle patches were prepared using micromolding technique (Bediz et al., 2014) with slight modifications described underneath.

2.2.1.1. Preparation of polydimethylsiloxane micromold. Derma Stamp containing 35 conical (circular cross section) microneedles of 1.5 mm length was used as master structure and polydimethylsiloxane micromolds as inverse replicas of this master structure were prepared. Briefly, one portion of curing agent was uniformly mixed with 10 portions of silicone base and the resulting solution was transferred into a suitable molding container. The molding container was kept in a vacuum desiccator to remove air bubbles. After removing air bubbles, the Derma Stamp was vertically inserted in to the solution and kept in place for 24 h for curing. Later, the Derma Stamp as well as the micromold was retrieved from molding container. Various dimensions of resulting micromolds were measured using optical microscopy.

2.2.1.2. Fabrication of microneedle patch. Aqueous blend containing polyvinyl alcohol, polyvinylpyrrolidone and meloxicam were used to fabricate fast dissolving microneedle patches. As specified in Table 1, 1 mg of meloxicam and varying amounts of polyvinyl alcohol and polyvinylpyrrolidone were dissolved in different volumes of phosphate buffer (pH 7.4) and applying gentle heat using waterbath. Phosphate buffer (pH 7.4) was selected as solvent owing to better solubility of drug in it as compared to distilled water. These polymer matrix solutions were transferred into polydimethylsiloxane micromolds, centrifuged for 10 min at 3000 rpm and allowed to dry in vacuum desiccator for 24 h. After 24 h, microneedle patches were retrieved from micromolds using high adhesion double coated medical tape and preserved in a moisture resistant container along with silica

Table 1
Randomized combined d-optimal mixture design matrix with experimentally determined values of axial needle fracture force as response variable.

Run order	Formulation code	Factors			ANFF (N)
		A[#]	B[#]	C[#]	
7	MNP_1	80 (0)	20 (0)	0.23 (0)	0.38
3	MNP_2	90 (1)	10 (−1)	0.23 (0)	0.10
1	MNP_3	80 (0)	20 (0)	0.20 (−1)	0.42
4	MNP_4	80 (0)	20 (0)	0.25 (1)	0.12
9	MNP_5	70 (−1)	30 (1)	0.20 (−1)	0.19
17	MNP_6	70 (−1)	30 (1)	0.25 (1)	0.06
18	MNP_7	70 (−1)	30 (1)	0.23 (0)	0.11
15	MNP_8	90 (1)	10 (−1)	0.20 (−1)	0.90
16	MNP_9	90 (1)	10 (−1)	0.25 (1)	0.37
19	MNP_{10}	75 (−0.5)	25 (0.5)	0.21 (−0.5)	0.17
12	MNP_{11}	75 (−0.5)	25 (0.5)	0.24 (0.5)	0.09
6	MNP_{12}	85 (0.5)	15 (−0.5)	0.21 (−0.5)	0.08
14	MNP_{13}	85 (0.5)	15 (−0.5)	0.24 (0.5)	0.09
2	MNP_{14}	70 (−1)	30 (1)	0.21 (−0.5)	0.10
13	MNP_{15}	90 (1)	10 (−1)	0.25 (1)	0.37
5	MNP_{16}	90 (1)	10 (−1)	0.20 (−1)	0.90
10	MNP_{17}	70 (−1)	30 (1)	0.25 (1)	0.06
11	MNP_{18}	70 (−1)	30 (1)	0.20 (−1)	0.19
8	MNP_{19}	80 (0)	20 (0)	0.25 (1)	0.50

[#] Actual values (coded values). A, amount of polyvinyl alcohol (mg); B, amount of polyvinylpyrrolidone (in mg); C, volume of phosphate buffer, pH 7.4 (in ml); ANFF, axial needle fracture force; MNP, microneedle patch.

gel as a desiccant.

Similarly, placebo microneedle patch and plain patch without microneedles were also prepared for comparison purpose during *ex vivo* and/or *in vivo* studies. The same method was used while omitting the drug addition or centrifugation step, respectively.

2.2.2. Formulation optimization using combined d-optimal mixture design

Among several formulation characteristics, microneedle strength was recognized as critical which is mainly responsible for creating microchannels in skin. Hence, axial needle fracture force, an indicative of microneedle strength, was selected as response variable. Preliminary trials were performed to study the effect of formulation as well as process variables on microneedle strength and to identify the key factors among them. The ratio of polyvinyl alcohol to polyvinylpyrrolidone in polymer matrix solution and percent solid content of these solutions were found to have significant influence on microneedle strength. Combined d-optimal mixture design, capable of analyzing a mixture component together with other numerical factors, was utilized to statistically optimize the formulation composition. The amount of polyvinyl alcohol was varied from 70 mg (−1 level) to 90 mg (+1 level) and the amount of polyvinylpyrrolidone was varied from 10 mg (−1 level) to 30 mg (+1 level) while keeping the total weight of polymer mixture as 100 mg. The volume of phosphate buffer (pH 7.4) was altered from 0.20 ml (−1 level) to 0.25 ml (−1 level) to result polymer matrix solution of percent solid content ranging from 50 to 40% w/v, respectively. Design Expert v7.0 software (Stat-Ease Inc., Minneapolis) was used to apply the design, statistically analyze the factor-response relationship and provide optimization solution with maximum desirability. The design was validated using check point analysis.

2.2.2.1. Measurement of axial needle fracture force. Axial needle fracture force is defined as minimum force, applied parallel to the microneedle axis, required to deform or break the microneedle (needle failure). Axial needle fracture force was measured using a CT3 Texture Analyzer (Brookfield, USA). The microneedle patch was stuck on a fixed cylindrical platform using two-sided adhesive tape. The instrument was programmed to axially compress the single microneedle on each occasion by a cylindrical probe (TA-39; diameter: 2 mm) travelling at a speed of 0.1 mm/s and to a distance of 2 mm. A graph showing force (in newton) applied by moving probe while compressing the microneedle to preprogrammed distance was generated by TexturePro CT software. A sudden drop in force was considered as needle failure and maximum force applied immediately before this deflection was reported as axial needle fracture force (Demir et al., 2013).

2.2.3. In vitro evaluation of optimized meloxicam loaded microneedle patch

2.2.3.1. Optical microscopy. The morphology of optimized microneedle patch was minutely observed under Eclipse inverted microscope (Nikon, Japan) and the images were captured using Nikon Imaging Integrated Software, Version 4.00.

2.2.3.2. Scanning electron microscopy. For a better understanding of surface morphology and microneedle dimensions, scanning electron microscopy was performed. The optimized patch was attached to sample stub using two side adhesive tape and viewed in JSM-5610LV, (JEOL, Japan) at various magnifications using an accelerating voltage of 20 kV.

2.2.3.3. Microneedle dissolution study. The gelatin block mimicking the hydration level of stratum corneum (Silva et al., 2007) was prepared and used to demonstrate the fast-dissolving behavior of optimized microneedle patch. Briefly, 6.5 g gelatin was added to 10 ml water and allowed to hydrate for about 30 min. The mixture was heated at 60 °C in a water bath and gently stirred till complete dissolution of gelatin. This solution was poured into a glass petridish and water was allowed to evaporate to achieve the final weight of 10 g. The obtained gelatin block with 35% w/w water was cut into small Square shaped pieces. Optimized microneedle patches were inserted into the gelatin block for 30 and 60 s, removed and observed under Eclipse H600L inverted microscope (Nikon, Japan) for morphological changes. The experiment was performed in triplicate.

2.2.3.4. Drug content. The optimized microneedle patch was added to a beaker containing 20 ml of phosphate buffer saline (pH 7.4) and the content was kept for 1 h under mild stirring to ensure complete dissolution of the microneedle patch. 1 ml of the resulting solution was withdrawn and diluted up to 5 ml with phosphate buffer saline (pH 7.4). The drug present in this dilute solution was analyzed using UV-Spectrophotometer at 363 nm λ_{max} (Jain and Pathak, 2010) against phosphate buffer saline (pH 7.4) as a blank. Percent drug content was calculated using formula (1).

$$\text{Percent drug content} = \left(\frac{\text{Amount of drug estimated}}{\text{Amount of drug added}}\right) \times 100 \quad (1)$$

2.2.3.5. Drug release. The *in vitro* drug release study was carried out using custom made diffusion cell with 7 ml of receptor chamber volume. Microneedle patch was inserted in Parafilm M® and mounted between donor and receptor chamber keeping the base towards donor side and microneedle tip towards receptor side. The receptor chamber was filled with phosphate buffer saline (pH 7.4) as release media. The assembly was placed on a magnetic stirrer and gently stirred throughout the study. At 0, 1, 2, 5, 10, 20, 30, 45 and 60 min, 1 ml sample was withdrawn from receptor chamber and the volume was immediately replenished with fresh phosphate buffer saline (pH 7.4). The concentration of drug in withdrawn samples was determined by using UV-spectrophotometer at a λ_{max} of 363 nm. The kinetics of drug release was studied by applying various mathematical release models and comparing the resulting regression coefficient (R^2) values (Quinn et al., 2015).

2.2.4. Ex vivo evaluation of optimized meloxicam loaded microneedle patch

2.2.4.1. Drug permeation and deposition study. Freshly excised rat abdominal skin was used for the study. The experimental protocol (protocol no. MSU/IAEC/2016–17/1624) was approved by institutional animal ethics committee of Faculty of Pharmacy, The Maharaja Sayajirao University of Baroda, India. Abdominal skin of euthanized male Wistar rats was shaved using electrical clipper, washed with phosphate buffer saline (pH 7.4) and excised. The subcutaneous fat was removed by scalpel and the skin was placed on a stack of filter papers previously moistened with phosphate buffer saline (pH 7.4) to provide mechanical support. Plain as well as microneedle patches containing 1 mg of drug were applied over stratum corneum side of skin using a gentle pressure of thumb. The skin were immediately mounted between donor and receptor chambers of diffusion cells with the patch facing towards donor side. The receptor chamber was filled with 7 ml phosphate buffer saline (pH 7.4) as diffusion medium and the content of diffusion media was subjected to gentle stirring using magnetic stirrer. At 0, 0.25, 0.50, 1, 2, 3, 4, 6, 8, 20 and 24 h, 1 ml of sample was withdrawn from the receptor chamber and the equal volume was replenished each time with fresh diffusion medium. Quantitative estimation of drug in withdrawn samples was done and percent drug permeated across skin was calculated. A graph of cumulative amount permeated as a function of time was generated and the steady-state flux (Jss, μg/cm^2/h) was calculated from the slope of the linear portion of this graph. Permeation enhancement ratio (PER) as compared to plain drug solution (control) in phosphate buffer (pH 7.4) was calculated from steady-state flux using formula (2).

$$PER = \frac{J_{SS}^{test}}{J_{SS}^{control}} \quad (2)$$

Where,

J_{SS}^{test} = steady − state flux obtained *via* optimized patches;

$J_{SS}^{control}$ = steady − state flux obtained *via* plain drug solution.

On completion of 24 h, the skin was removed and drug present on skin surface was washed three times with 5 ml of fresh phosphate buffer saline (pH 7.4). These washings were combined and the drug present in it was quantified to calculate percent drug retained on skin surface. Subsequently, the washed skin was minced with a chopper, collected in 10 ml of phosphate buffer saline (pH 7.4) and subjected to homogenization for 5 min under cold conditions followed by bath sonication for 15 min. The tissue debris were made to settle by centrifugation at 5000 rpm for 10 min and the supernatant containing extracted drug was collected. The drug content of supernatant was quantified to calculate percent drug deposited within the skin. UV spectrophotometric method (Khan et al., 2012) at 363 nm λ_{max} was used for drug quantification in all *ex vivo* samples.

2.2.4.2. Histopathology study. The safety aspect of breaching stratum corneum with microneedles was studied on freshly excised pig ear skin. Briefly, application of optimized microneedle patch on the skin and set up of diffusion cell was done in a similar manner as described in previous section. After 6 hours, the skin was retrieved and immediately preserved in 10% formalin solution as fixative. The skin sectioning and HE staining was done using the method described earlier (Thakkar et al., 2016). The prepared slides were observed under inverted microscope at 10 × magnification and the skin layers were minutely examined for any pathological changes as a measure of safety. Sections of skin treated with phosphate buffer saline (pH 7.4) and isopropyl alcohol were also obtained in similar manner to serve as negative and positive control, respectively.

2.2.5. In vivo pharmacodynamic study

The experimental protocol was approved by institutional animal ethics committee (protocol no. MSU/IAEC/2016–17/1624) and the experiments were conducted in accordance with the guidelines of 'committee for the purpose of control and supervision of experiments on animals'. Thirty female Sprague Dawley rats of (240–250 g) were procured and housed for five days for acclimatization in suitable cages. All animals had free access to potable water and standard animal diet. The environmental conditions viz., 22 ± 3 °C room temperature, 55 ± 5% relative humidity and 12 h light/dark cycle, were maintained. After acclimatization, Animals were randomly allocated to five groups of six animals each to administer different formulations as per the schedule given in Table 2. Animals of group II to IV were shaved on neck region using electric clipper for application of transdermal formulations. The animal dose of meloxicam was calculated as per United States Food and Drug Administration guidelines (USFDA, 2005) using formula (3) and similar dose (0.77 mg/kg) was loaded in formulations given to the animals of group III to V.

$$AED = \frac{HED \times HK_M}{AK_M} \quad (3)$$

Where,
AED = animal equivalent dose (mg/kg),
HED = Human equivalent dose (0.125 mg/kg),
HK_M = Human constant (37),
AK_M = Animal constant (6).

After half an hour of formulation treatment, animals of all the five groups were administered with 0.1% w/v carrageenan suspension in normal saline by sub-planter injection into right hind paw to induce inflammation. The paw thickness (in mm) of all the animals was measured using vernier caliper at 0.5, 1, 2, 3, 4, 6, 8 and 24 h. The percent inhibition of inflammation was then calculated using the following formula (4) (Singh et al., 2010).

$$\%Inhibition = \frac{T_0 - T_t}{T_0} \times 100 \quad (4)$$

Where,
T_t = Paw thickness of vehicle or test group at time t.
T_0 = Paw thickness of model control group at time t.

2.2.6. Stability study

The stability of optimized formulation at 30 ± 2 °C / 65 ± 5% RH was assessed for three months. The optimized microneedle patches were placed in three different airtight containers (three patches per container) together with silica gel bags as desiccant. The containers were further wrapped within Parafilm M® followed by aluminum foil to prevent moisture gain and stored under specified environmental condition in a stability chamber. After each month, one container was withdrawn and the patches were characterized for axial needle fracture force and percent drug content as stability indicating parameters.

Table 2
Treatment plan for pharmacodynamic study in different animal groups.

Group	Treatment
I: Model control	0.1%, w/v carrageenan suspension (0.1 ml) in normal saline[#] (A)
II: Vehicle control	Placebo microneedle patch transdermally followed by A
III: Test group-I	Plain patch of Meloxicam transdermally followed by A
IV: Test group-II	Microneedle patch of Meloxicam transdermally followed by A
V: Standard control	Suspension of marketed Meloxicam tablet orally followed by A

[#] by sub-planter injection in to right hind paw.

3. Results and discussion

Fast dissolving microneedles hold great promise over metal or other non-biocompatible microneedles by eliminating the risk of cross contamination or accidental breakage, promoting self-application *via* patient friendly design and providing rapid release of cargo to enhance their uptake by skin. Micromolding technology simplified the fabrication of these microneedles to a great extent by markedly reducing the production time as well as the production cost and boosting their large scale production with a variety of materials (Kolli, 2015). Further, reports on sterile manufacture of polymeric microneedle suggested the possibility of aseptic processing of pre-sterilized micromolds as well as active ingredient or terminal sterilization of developed patches to keep the bioburden within acceptable limits (McCrudden et al., 2015).

The image of prepared polydimethylsiloxane micromold is shown in Fig. 1. The geometry of microneedles in master structure and needle cavities in polydimethylsiloxane micromold were found to be almost identical in their microscopic images (Fig. 2) confirming that the developed polydimethylsiloxane micromolds were inverse replicas of microneedle master. These micromolds were further utilized to fabricate meloxicam loaded microneedle patches.

3.1. Formulation and optimization of microneedle patch

Based on literatures (Donnelly et al., 2014) and preliminary trials, the optimum level of various process variables like centrifugation speed, centrifugation time and drying time were decided which are mentioned in Methods section. However, the combined d-optimal mixture design was used to analyze the effect of key formulation variables on axial needle fracture force and also to obtain their optimum levels. A total 19 batches were prepared based on the randomized design matrix generated by the software. The axial needle

Fig. 1. Image of polydimethylsiloxane micromolds. Microneedle cavities are indicated by arrows.

fracture force of these 19 batches were determined and the values were entered in software for statistical analysis. The software suggested linear model for mix order with P-value of 0.0005 while quadratic model for process order with P-value of 0.0017. Software based analysis of variance for combined linear and quadratic model revealed the significance of suggested model [P-value; 0.0002] with an insignificant lack of fit [P-value; 0.4149] which was desired. The adjusted and predicted R^2 values were found to be 0.7519 and 0.7192, respectively which were in good agreement indicating the suitability of the suggested model. The adequate precision, a measure of signal to noise ratio, was found to be 10.425 which indicated adequate signal. The mathematical Eq. (5) consisting of various linear as well as quadratic model terms along with their coefficients was generated by the software in terms of coded factors. The positive or negative signs before coefficients of different model terms indicate a direct or inverse relation, respectively between model terms and response variable.

Table 3
Regression coefficients and their P-values for axial needle fracture force.

Source*	Axial needle fracture force	
	Coefficients	P-value
Model	–	*0.0002*
A	*0.092*	*0.0003*
B	*0.14*	(linear mixture)
AC	*− 0.22*	*0.0022*
BC	− 0.028	0.6290
AC^2	*0.54*	*0.0005*
BC^2	− 0.015	0.8978
Residual: lack of fit	–	0.4149

A, amount of polyvinyl alcohol (mg); B, amount of polyvinylpyrrolidone (mg); C, volume of phosphate buffer (pH 7.4).

* Significant terms having P-value < 0.05 were represented in italics.

$$ANFF=0.092A + 0.14B - 0.22\,AC - 0.028\,BC + 0.54\,AC^2 - 0.015BC^2 \quad (5)$$

As shown in Table 3, the linear mixture of A and B, interactive term AC and quadratic term AC^2 were found to affect the axial needle fracture force substantially considering P-value < 0.05 as significant. Two dimensional contour plot as well as three dimensional response surface plot (Fig. 3) were further utilized to reveal the influence of polymer ratio and their total quantity in microneedle matrix solution on microneedle strength. It can be seen in Fig. 3 that as the amount of polyvinyl alcohol was increased, the axial needle fracture force was found to increase. The result indicated the significant influence of

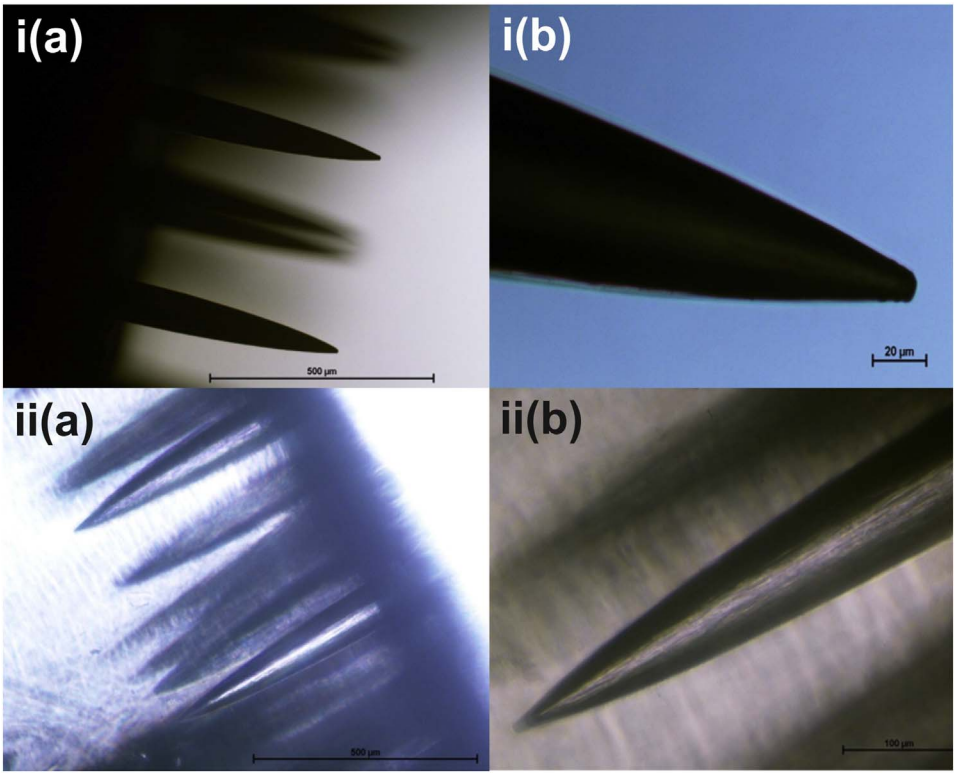

Fig. 2. Microscopic image of (i) microneedles in master structure at (a) 4 × as well as (b) 20 × magnification; and (ii) microneedle cavity in polydimethylsiloxane micromold at (a) 4 × as well as 10 × magnification.

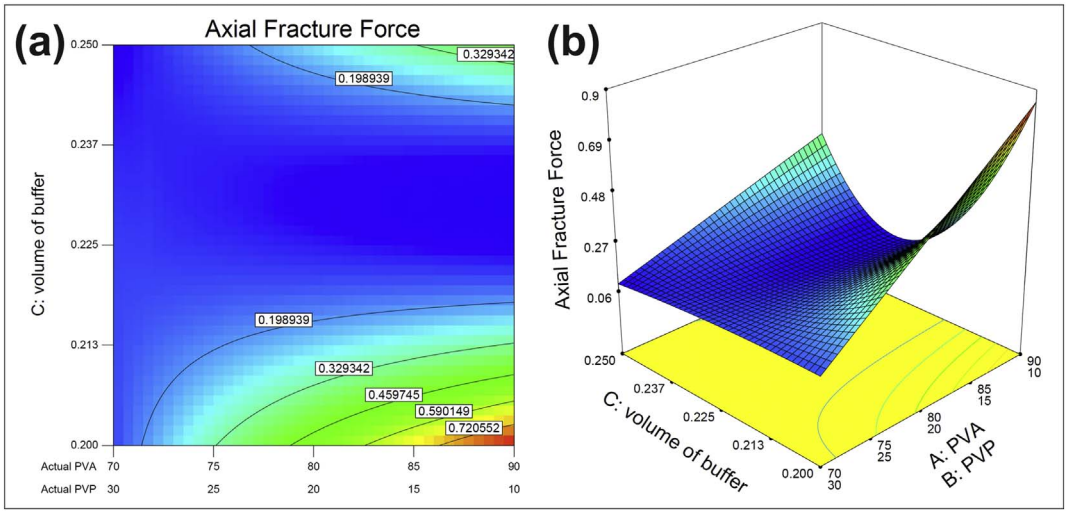

Fig. 3. (a) 2-D contour and (b) 3-D response surface mix-process plot generated by Design Expert® software for d-optimal mixture design.

Table 4
Optimized batch composition provided by Design-Expert® software based on preselected desirability criteria.

Variables	Goal	Solutions	Desirability
polyvinyl alcohol	in range	90 mg	0.942
polyvinylpyrrolidone	in range	10 mg	
Phosphate buffer (pH 7.4)	in range	0.20 ml	
Axial needle fracture force	maximize	0.850955 N	

polyvinyl alcohol for providing strength to microneedles as compared to polyvinylpyrrolidone. This supports the earlier findings where polyvinyl alcohol has been reported to offer strength to the microneedles while polyvinylpyrrolidone played a role of filler during microneedle fabrication (Chu et al., 2010). Similarly, the axial needle fracture force was also found to increase on increasing the total solid content of polymers in matrix solution. Here, the high solid content with less solvent for evaporation could have led to a faster drying with negligible shrinkage resulting in a compact microneedles with maximum strength. Table 4 summarizes the optimization solution provided by the software with a desirability of 0.942 for prefixed criteria of keeping all the factors in range and maximizing the axial needle fracture force. The images of optimized microneedle patch prepared using 90 mg polyvinyl alcohol and 10 mg polyvinylpyrrolidone in 0.2 ml phosphate buffer (pH 7.4) has been shown in Fig. 4(i). For validation of the selected model, the statistical comparision of axial needle fracture force observed for check point batches and the axial needle fracture force predicted by selected model for these batches was performed using student's *t*-test. A lower $T_{calculated}$ than $T_{tabulated}$ indicated insignificant difference (P-value < 0.05) between the mean of experimentally obtained values and predicted values (Table 5) advocating the validity of the selected model.

3.2. In vitro evaluation of optimized meloxicam loaded microneedle patch

3.2.1. Microscopic evaluations

The meloxicam loaded microneedle patch was found to possess smooth surface and similar geometry to that of microneedle master when observed under Nikon microscope [Fig. 4(ii)]. For accurate measurements of microneedle dimensions and a better morphological evaluation of microneedle surface, scanning electron microscopic images under magnification of 50 and 270 × were taken [Fig. 4(iii)]. The images showed a smooth microneedle surface with 10 µm tip and 250 µm base diameter. The length of single microneedle was found to be 1.5 mm and the distance between two needles were 500 µm. The geometry of microneedle array was found to be within acceptable range that have been reported in literatures and suggested to be essential to pierce the skin with minimal damage (Akhtar, 2014).

3.2.2. Percent drug content

The mean percent drug content of optimized microneedle patch was found to be 98.17% with only 0.5% standard deviation. The results demonstrated the suitability of the formulation as well as the method of its preparation posing insignificant effect over drug's stability and providing a better content uniformity.

3.2.3. Microneedle dissolution study

The insertion of an optimized microneedle patch in gelatin blocks with similar hydration level to that of stratum corneum resulted in rapid dissolution of Microneedles. It can be seen in Fig. 5 that the needle length was significantly reduced in the first 30 s and almost shrank to base in the next 30 s owing to its dissolution. The results could be attributed to the use of polyvinylpyrrolidone as a filler that not only aid polyvinyl alcohol in providing strength to the microneedles but also, being highly hydrophilic, dissolves rapidly to create aqueous channels for faster dissolution of polyvinyl alcohol.

3.2.4. Drug release

The *in vitro* cumulative percent drug release at different sampling times has been shown in Fig. 6. Almost 100% of drug was released in 60 min indicating the fast dissolving behavior of polymer matrix. These release data were fitted in various mathematical models viz., Zero order, First order, Higuchi and Hixson-Crowell models to determine the kinetics of drug release and the correlation coefficient (R^2) values obtained were 0.931, 0.733, 0.959 and 0.992, respectively. The best linear correlation between drug release and time was obtained with Hixson Crowell cube root model suggesting that the drug release was governed by dissolution. The release exponent value of Korsmeyer Peppas model was also found to be 1.01 signifying that the drug release followed case II transport (Patel et al., 2015). The case II transport corresponds to time independent zero order release which is reported to be associated with relaxation process of the polymer occurring upon water imbibition into the system as the rate-controlling step (Siepmann and Peppas, 2001). Case II transport in our case might be observed owing to the faster dissolution of polyvinylpyrrolidone creating aqueous channel for water imbibition which ultimately leads to quick dissolution of polyvinyl alcohol.

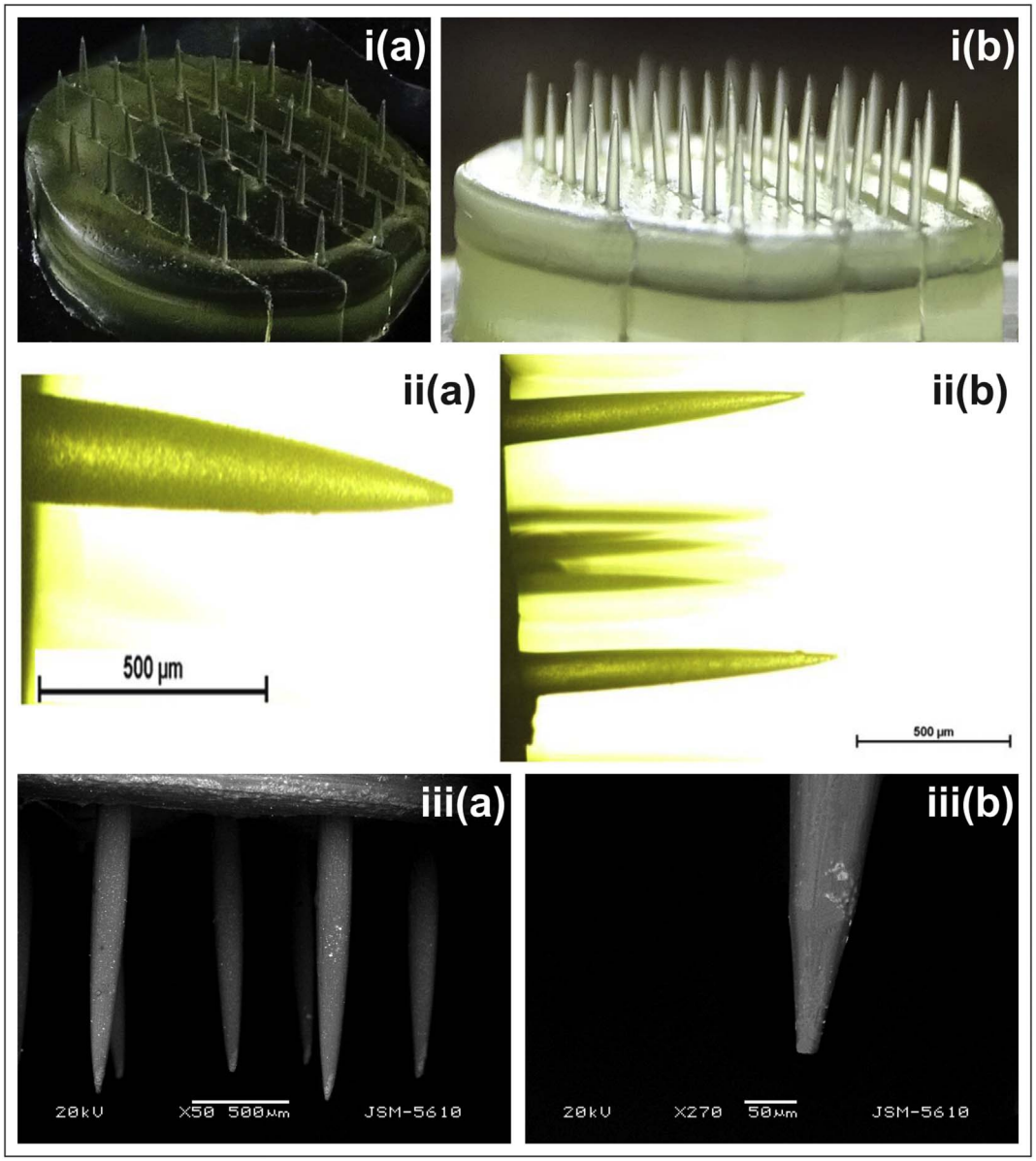

Fig. 4. (i) Normal, (ii) optical microscopic and (iii) scanning electron microscopic images of meloxicam loaded optimized microneedle patch at ii (a) 10 ×, ii(b) 4 ×, iii(a) 50 × and iii(b) 270 × magnifications.

Table 5
Composition of checkpoint batches and their evaluation.

Batch	Independent variables			Response variable	
	Mixture		Numeric	Axial needle fracture force	
	A[#]	B[#]	C[#]	Predicted	Observed
CP_1	90 (1)	10 (0)	0.20 (− 1)	0.85	0.90
CP_2	90 (1)	10 (0)	0.25 (1)	0.40	0.37
CP_3	70 (0)	30 (1)	0.20 (− 1)	0.15	0.19
t-test	$T_{calculated}$			0.51	
	$T_{tabulated}$			4.30	

A, amount of polyvinyl alcohol (mg); B, amount of polyvinyl pyrrolidone (mg); C, volume of phosphate buffer (pH 7.4); CP, check point.
[#] Actual values (coded values).

3.3. Ex vivo drug permeation and deposition study

The *ex vivo* meloxicam permeation and deposition *via* microneedle patch across rat skin was studied and compared with that of drug solution and plain patch (Fig. 7, Table 6). The drug permeation from its plain solution was found to be 13.34% at a steady state flux of 0.623 µg/cm^2/h. The drug permeation *via* plain patch was initially slow but the overall permeation (15.07%) was found to be slightly more as compared to plain drug solution (PER, 1.42). The initial lag might be attributed to the time required for dissolution of polymer matrix which is essential to solubilize the drug before its transportation. On the contrary, the surfactant nature of polyvinyl alcohol could have contributed to certain extent in higher drug transport (Jss, 0.885 µg/cm^2/h) across intact rat skin. A higher deposition of drug within skin after 24 h *via* plain drug solution (21.67%) as compared to plain patch (18.48%) indicated drugs inherent nature to create depot in more lipophilic epidermis region owing to its moderately high log P-value (3.43) and thus less partitioning in to more hydrophilic dermal layer. This result also reflected the role of polyvinyl alcohol in improving the

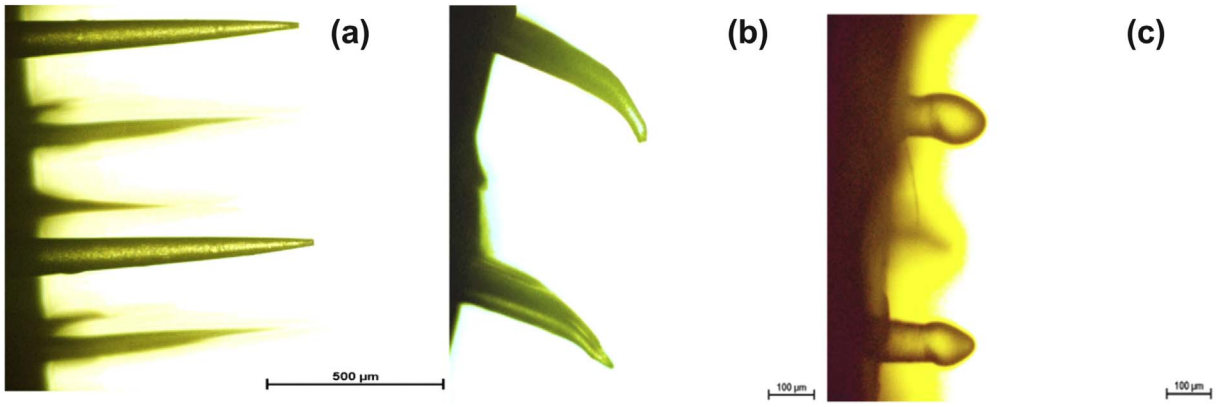

Fig. 5. Microscopic images showing microneedle dissolution in gelatin block (a) before insertion, (b) after 30 s and (c) after 60 s at 4 × magnification.

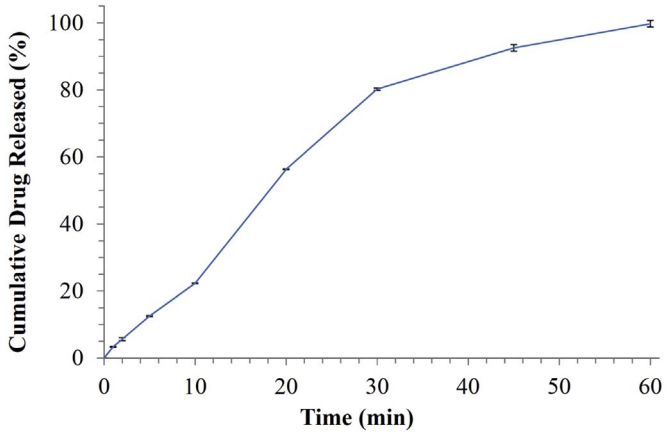

Fig. 6. Cumulative percent drug released from optimized microneedle patch *in vitro* (n = 3).

partitioning of drug in dermal layer and thus facilitating its permeation *via* plain patch. On application of microneedle patch, the drug deposition and permeation both were significantly increased (63.37 and 26.30%, respectively). A 2.58 fold rise in permeation was observed with a flux of 1.608 µg/cm^2/h as compared to plain drug solution. It could be attributed to the successful breaching of stratum corneum by developed microneedle patches forming microchannels to ease the drug transport to deeper skin layers. In addition, the occlusive condition might further have contributed to the high skin transportation of drug *via* prolonged opening of these microchannels (Akhtar, 2014). The significantly high skin deposition seen with microneedle patch might be helpful in improving the effectiveness of the formulations on local application to desired site.

Table 6
Skin permeation and deposition profile of drug *via* different formulations.

Parameters	Plain drug solution	Plain patch	Microneedle patch
Steady state flux (Jss, µg/cm^2/h)	0.623	0.885	1.608
Permeation enhancement ratio (PER)	–	1.42	2.58
Drug permeation across skin at 24 h (%)	13.34	15.07	26.30
Drug deposition within skin at 24 h (%)	21.67	18.48	63.37
Drug retained on skin surface at 24 h (%)	56.38	58.64	3.08

3.4. Histopathology study

The hematoxylin and eosin stained sections of pig ear skin treated with developed formulation was minutely examined under microscope for any pathological changes and compared with negative and positive control to study the safety aspect of using microneedle patch. The

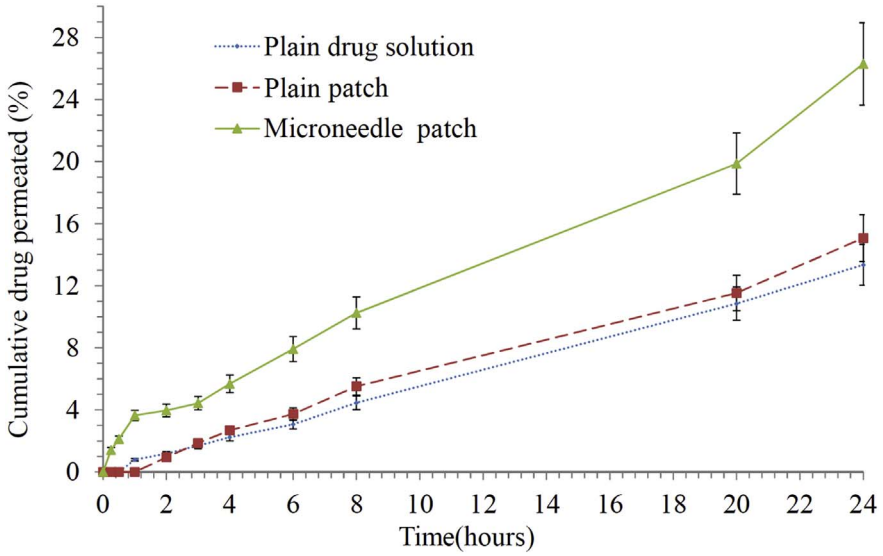

Fig. 7. Cumulative amount of drug permeated across full thickness rat skin *via* different formulations (n = 3).

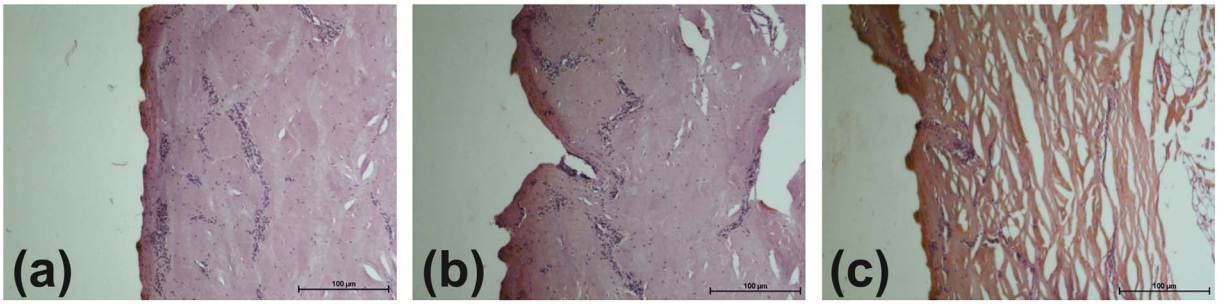

Fig. 8. Histopathological sections of pig ear skin treated with (a) negative control, (b) optimized microneedle patch and (c) positive control at 10 × magnification.

microscopic images have been shown in Fig. 8. The section of formulation treated skin showed almost similar cellular integrity as compared to skin treated with phosphate buffer saline (pH 7.4) as negative control with no sign of inflammation. The section of skin treated with isopropyl alcohol as positive control showed considerable damage to skin layers as an indication of irritation and toxicity.

3.5. In vivo pharmacodynamic study

The percent inhibition of inflammation in different treatment groups as compared to model control group was calculated and presented in Table 7. The inhibition was found to be maximum in standard control group (52.72%) that received oral suspension of marketed formulation. However, the group treated with microneedle patch showed slightly less but comparable percent inhibition (46.36%) as compared to standard control indicating a reasonable effectiveness of the developed microneedle patch to its existing oral marketed formulation. The result reflected a better systemic availability of meloxicam *in vivo* where the availability of larger epidermal space, as compared to *ex vivo* skin samples, could have caused meloxicam distribution to these spaces *via* lateral transport leading to a better partitioning and thereby a higher permeation to improve plasma drug levels. An improvement in percent inhibition can be seen in animals received microneedle patches as compared to animals received patches without microneedles (34.54%). This is in accordance with the *ex vivo* study and demonstrated the permeation enhancement through the microchannels created in skin by microneedles. The group treated with placebo microneedle patch showed no significant difference in the percent inhibition of inflammation (2.93%) as compared to model control group. The result eliminated the possibility of polymer contribution in pharmacological response of developed patches.

3.6. Stability study

Effect of storage condition on stability indicating parameters viz., axial needle fracture force and percent drug content are presented in Table 8. After 3 months of storage at 30 ± 2 °C and 65 ± 5% RH, an insignificant decrease was observed in percent drug content (98.17% to 95.67%) indicating the stability of drug in developed formulation. A significant change in axial needle fracture force was observed during storage which was decreased from an initial value of 0.9 N to 0.56 N in three months. However, the value was still sufficiently high to pierce the skin as suggested in literatures (Akhtar, 2014). Such a decrease in axial needle fracture force might be due to the moisture gain by the highly hygroscopic polymers sensitive to even trace amount of moisture. This problem can be solved by appropriate packaging of the product and use of suitable desiccant. It was found in literatures that silica gel works more efficiently at high moisture levels while desiccants such as calcium oxides work efficiently at low moisture levels (Chime et al., 2013).

Table 7
Percent inhibition of inflammation in different animal groups as per the treatment plan described in Table 2.

Time (hours)	% Inhibition*			
	Group II (Vehicle control)	Group III (Test group-I)	Group IV (Test group-II)	Group V (Standard control)
0.5	0.58 ± 0.13	6.84 ± 1.37	12.32 ± 2.51	8.21 ± 1.66
1	−0.19 ± 0.06	11.68 ± 2.31	16.88 ± 3.38	12.98 ± 2.57
2	0.39 ± 0.11	12.98 ± 2.62	20.77 ± 4.18	16.88 ± 3.41
3	0.95 ± 0.27	12.98 ± 2.61	17.48 ± 3.93	18.18 ± 3.60
4	1.17 ± 0.32	17.28 ± 3.43	20.80 ± 4.97	22.22 ± 4.43
6	0.73 ± 0.24	18.51 ± 3.75	22.70 ± 4.96	24.70 ± 4.89
8	1.31 ± 0.61	18.29 ± 3.68	25.60 ± 5.13	29.26 ± 5.88
24	2.93 ± 0.54	34.54 ± 6.93	46.36 ± 7.94	52.72 ± 9.89

* Mean ± SD (n = 6).

Table 8
Stability data of optimized microneedle patches stored at 30 ± 2 °C / 65 ± 5%RH.

Sampling time	Axial needle fracture force* (N)	Drug content* (%)
Immediately after preparation	0.90 ± 0.21	98.17 ± 0.41
After 1 month	0.77 ± 0.21	97.45 ± 0.27
After 2 months	0.64 ± 0.19	96.70 ± 0.24
After 3 months	0.56 ± 0.17	95.67 ± 0.23

* Mean ± SD (n = 3).

4. Conclusion

An attempt was made to develop meloxicam loaded fast dissolving microneedle patch to avoid gastric side effect associated with approved marketed oral dosage forms and to potentiate the transdermal transport of meloxicam to meet the therapeutic need for management of arthritis. Tailoring the proportion of polyvinyl alcohol to polyvinylpyrrolidone and solid content of matrix solution using combined d-optimal mixture design resulted in optimized microneedle patch with sufficiently high axial needle fracture force to pierce the skin. The formulation was found to be fast dissolving and the drug release was almost 100% in 60 min principally governed by the dissolution of the polymer matrix. The *ex vivo* permeation across rat skin was also found to improve by 2.58 folds along with significantly high skin deposition as compared to plain drug solution. The safety, efficacy and stability of optimized microneedle patch were also found satisfactory *via* histopthological, pharmacodynamic and stability evaluations, respectively signifying its potential for transdermal application. However, the significantly high skin deposition seen with microneedle patch might be helpful in further improving the effectiveness of the formulations on direct application to affected site. Hence, a further study in higher animals with local application of developed patches could be useful to demonstrate the utility of higher skin deposition of drug as found during *ex vivo* study.

Conflict of interest

Authors declare no conflict of interest.

Acknowledgements

Authors are thankful to Bharat Parenteral Limited, India for providing meloxicam as a generous gift. Authors are also thankful to 3M, USA for providing gift samples of transdermal patch components including double coated adhesive tape, release liner and impervious backing.

References

Akhtar, N., 2014. Microneedles: an innovative approach to transdermal delivery-a review. Int. J. Pharm. Pharm. Sci. 6, 18–25.
Bediz, B., Korkmaz, E., Khilwani, R., Donahue, C., Erdos, G., Falo Jr., L.D., Ozdoganlar, O.B., 2014. Dissolvable microneedle arrays for intradermal delivery of biologics: fabrication and application. Pharm. Res. 31, 117–135.
Bharkatiya, M., Nema, R., 2009. Skin penetration enhancement techniques. J. Young Pharm. 1, 110–115.
Brady, A.J., Donnelly, R.F., 2016. Clinical impact and patient safety: the potential of microneedles in changing the form and perception of transdermal drug delivery. In: Hamblin, M.R., Avci, P., Prow, T. (Eds.), Nanoscience in Dermatology. Mica Haley, London, pp. 47–56.
Brough, C., Miller, D.A., Keen, J.M., Kucera, S.A., Lubda, D., Williams III, R.O., 2016. Use of polyvinyl alcohol as a solubility-enhancing polymer for poorly water soluble drug delivery (part 1). AAPS PharmSciTech 17, 167–179.
Buckwalter, J.A., Martin, J.A., 2006. Osteoarthritis. Adv. Drug Deliv. Rev. 58, 150–167.
Chime, S., Onunkwo, G., Onyishi, I., 2013. Kinetics and mechanisms of drug release from swellable and non swellable matrices: a review. Res. J. Pharm. Biol. Chem. Sci. 4, 97–103.
Chu, L.Y., Choi, S.O., Prausnitz, M.R., 2010. Fabrication of dissolving polymer microneedles for controlled drug encapsulation and delivery: bubble and pedestal microneedle designs. J. Pharm. Sci. 99, 4228–4238.
Demir, Y.K., Akan, Z., Kerimoglu, O., 2013. Characterization of polymeric microneedle arrays for transdermal drug delivery. PLoS One 8, e77289.
Donnelly, R.F., McCrudden, M.T., Alkilani, A.Z., Larrañeta, E., McAlister, E., Courtenay, A.J., Kearney, M.-C., Singh, T.R.R., McCarthy, H.O., Kett, V.L., 2014. Hydrogel-forming microneedles prepared from “super swelling” polymers combined with lyophilised wafers for transdermal drug delivery. PLoS One 9, e111547.
Dowd, F.J., Johnson, B., Mariotti, A., 2016. Pharmacology and Therapeutics for Dentistry. Elsevier Health Sciencespp. 342.
Hong, X., Wei, L., Wu, F., Wu, Z., Chen, L., Liu, Z., Yuan, W., 2013. Dissolving and biodegradable microneedle technologies for transdermal sustained delivery of drug and vaccine. Drug Des. Dev. Ther. 7, 945–952.
Jain, D., Pathak, K., 2010. Design, characterization, and evaluation of meloxicam gel prepared by suspension and solution polymerization using solubility parameter as the basis for development. AAPS PharmSciTech 11, 133–142.
Khan, I.N., Khan, M.I., Mazumder, K., Ajrin, M., Sen, N., Rashid, A., Bhuiya, A., 2012. Characterization and ex-vivo skin permeation study of domperidone maleate transdermal patch. Bull. Pharm. Res. 2, 15–21.
Kolli, C.S., 2015. Microneedles: bench to bedside. Ther. Deliv. 6, 1081–1088.
Lee, I.C., He, J.S., Tsai, M.T., Lin, K.C., 2015. Fabrication of a novel partially dissolving polymer microneedle patch for transdermal drug delivery. J. Mater. Chem. B 3, 276–285.
McCrudden, M.T., Alkilani, A.Z., Courtenay, A.J., McCrudden, C.M., McCloskey, B., Walker, C., Alshraiedeh, N., Lutton, R.E., Gilmore, B.F., Woolfson, A.D., Donnelly, R.F., 2015. Considerations in the sterile manufacture of polymeric microneedle arrays. Drug Deliv. Transl. Res. 5, 3–14.
Pamornpathomkul, B., Duangjit, S., Laohapatarapant, S., Rojanarata, T., Opanasopit, P., Ngawhirunpat, T., 2015. Transdermal delivery of fluorescein isothiocyanate-dextrans using the combination of microneedles and low-frequency sonophoresis. Asian J. Pharm. Sci. 10, 415–424.
Patel, D., Kumar, P., Thakkar, H.P., 2015. Lopinavir metered-dose transdermal spray through microporated skin: permeation enhancement to achieve therapeutic needs. J. Drug Deliv. Sci. Technol. 29, 173–180.
Prausnitz, M.R., 1996. The effects of electric current applied to skin: a review for transdermal drug delivery. Adv. Drug Deliv. Rev. 18, 395–425.
Prevention, C.f.D.C.a, 2013. Prevalence of doctor-diagnosed arthritis and arthritis-attributable activity limitation. Morb. Mortal. Wkly Rep. 62, 869–873.
Quinn, H.L., Bonham, L., Hughes, C.M., Donnelly, R.F., 2015. Design of a dissolving microneedle platform for transdermal delivery of a fixed-dose combination of cardiovascular drugs. J. Pharm. Sci. 104, 3490–3500.
Ranade, V.V., Cannon, J.B., 2011. Drug Delivery Systems, Third Edition, third ed. CRC Press, Boca Raton, pp. 243–304.
Saad, M.N., Mabrouk, M.S., Eldeib, A.M., Shaker, O.G., 2016. Identification of rheumatoid arthritis biomarkers based on single nucleotide polymorphisms and haplotype blocks: a systematic review and meta-analysis. J. Adv. Res. 7, 1–16.
Siepmann, J., Peppas, N.A., 2001. Modeling of drug release from delivery systems based on hydroxypropyl methylcellulose (HPMC). Adv. Drug Deliv. Rev. 48, 139–157.
Silva, C.L., Topgaard, D., Kocherbitov, V., Sousa, J., Pais, A.A., Sparr, E., 2007. Stratum corneum hydration: phase transformations and mobility in stratum corneum, extracted lipids and isolated corneocytes. Biochim. Biophys. Acta Biomembr. 1768, 2647–2659.
Singh, A., Yadav, S., 2016. Microneedling: advances and widening horizons. Indian Dermatol. Online J. 7, 244–254.
Singh, M., Kumar, V., Singh, I., Gauttam, V., Kalia, A.N., 2010. Anti-inflammatory activity of aqueous extract of *Mirabilis jalapa* Linn. leaves. Pharmacogn. Res. 2, 364–367.
Thakkar, H.P., Savsani, H., Kumar, P., 2016. Ethosomal hydrogel of RaloxifeneHCl: statistical optimization & ex vivo permeability evaluation across Microporated pig ear skin. Curr. Drug Deliv. 13, 1111–1122.
USFDA, 2005. Guidance for Industry: Estimating the Maximum Safe Starting Dose in Initial Clinical Trials for Therapeutics in Adult Healthy Volunteers. U.S. Food and Drug Administration, Center for Drug Evaluation and Research.
USFDA, 2007. Medication Guide for Non-Steroidal Anti-Inflammatory Drugs (NSAIDs). U.S. Food and Drug Administration, Center for Drug Evaluation and Research.
Wishart, D.S., Knox, C., Guo, A.C., Shrivastava, S., Hassanali, M., Stothard, P., Chang, Z., Woolsey, J., 2005. Meloxicam. DrugBank, Canada.

Accepted Manuscript

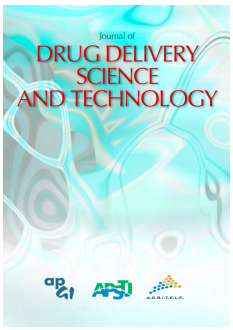

Lopinavir metered-dose transdermal spray through microporated skin: Permeation enhancement to achieve therapeutic needs

Dhruval Patel, Praveen Kumar, Dr. Hetal P. Thakkar

PII: S1773-2247(15)00120-3

DOI: 10.1016/j.jddst.2015.07.004

Reference: JDDST 64

To appear in: *Journal of Drug Delivery Science and Technology*

Received Date: 27 January 2015

Revised Date: 22 May 2015

Accepted Date: 7 July 2015

Please cite this article as: D. Patel, P. Kumar, H.P. Thakkar, Lopinavir metered-dose transdermal spray through microporated skin: Permeation enhancement to achieve therapeutic needs, Journal of Drug Delivery Science and Technology (2015), doi: 10.1016/j.jddst.2015.07.004.

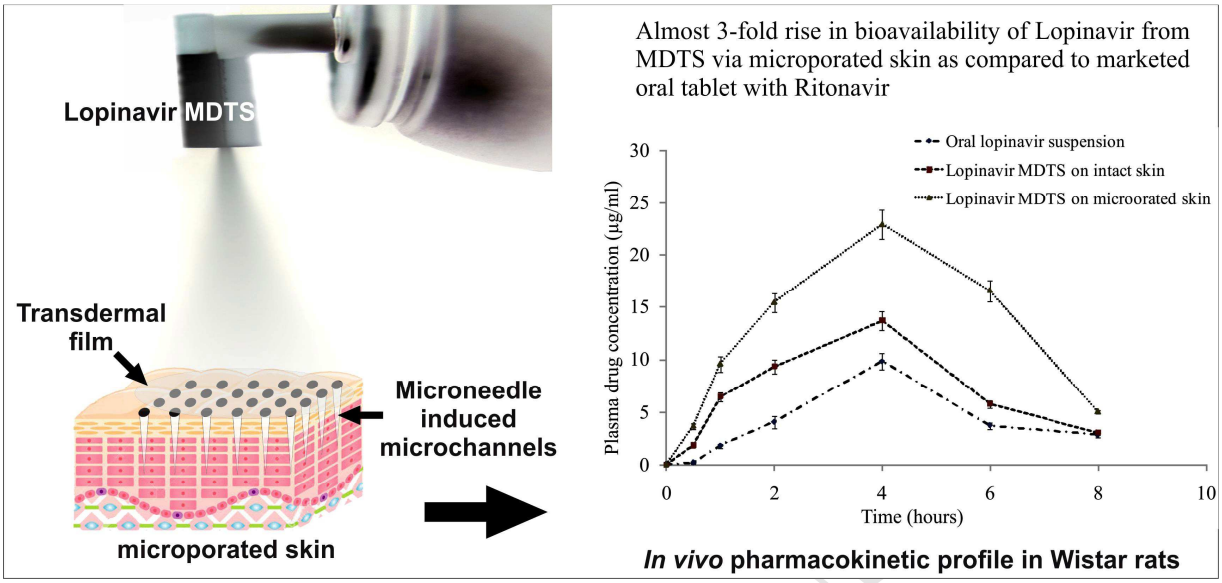

Date: 24.01.2015

To,

The Editor-in-Chief,
Journal of Drug Delivery Science & Technology.

COVER LETTER FOR SUBMISSION OF MANUSCRIPT

I am enclosing herewith a **research article** entitled "**Lopinavir metered-dose transdermal spray through microporated skin: Permeation enhancement to achieve therapeutic needs**" for publication in your esteemed journal for possible evaluation.

Encouraging relative bioavailability improvement in Wistar rats *in vivo* when compared to marketed formulation suggested the potential of the concept used in this study. This could be a milestone in reducing the well known problem of bioavailability associated with Lopinavir that imposes the burden of including Ritonavir in the regimen having its own side effects.

With the submission of this manuscript I would like to undertake that:

- All authors of this research paper have directly participated in the planning, execution, or analysis of this study;
- All authors of this paper have read and approved the final version submitted;
- The contents of this manuscript have not been copyrighted or published previously;
- The contents of this manuscript are not under consideration for publication elsewhere;
- The authors declare no competing interest;
- There are no directly related manuscripts or abstracts, published or unpublished, by any authors of this paper.

Yours truly

Dr. Hetal P. Thakkar,
Asst. Prof. (Pharmaceutics),
Pharmacy Department,
Faculty of Tech. & Engg.,
The M. S. University of Baroda,
Vadodara-390 001 (Guj.). INDIA

Lopinavir metered-dose transdermal spray through microporated skin: Permeation enhancement to achieve therapeutic needs

Dhruval Patel, Praveen Kumar, Hetal P. Thakkar[1]*

TIFAC CORE in NDDS, Pharmacy Department, Faculty of Technology & Engineering, The M.S. University of Baroda, Vadodara-390 001, INDIA.

*Correspondence: hetal_thakkar11@yahoo.com

[1] *Address for Correspondence:* Dr. Hetal P. Thakkar, Pharmacy Department, Faculty of Technology & Engineering, The M.S. University of Baroda, Kalabhawan, Vadodara 390 001, Gujarat, INDIA. Tel: +91-265-2434187. E-mail: hetal_thakkar11@yahoo.com

Abstract

A user friendly metered-dose transdermal spray (MDTS) of Lopinavir was developed and a combination of chemical and physical penetration enhancement techniques was utilized to enhance overall drug permeation across skin. Formulation was optimized varying Kollidon® VA 64 level while optimized batch was exhaustively characterized for *in vitro* drug release, *ex vivo* skin permeation and *in vivo* bioavailability. Safety and stability were also ascertained. Formulation containing 5 %w/v of Kollidon® had best sprayability and volatilization property. A significantly high permeation enhancement ratio (1.77) and steady state transdermal flux (52.5 µg/cm^2/h) through microporated pig ear skin *ex vivo* indicated the permeation enhancement potential of the techniques applied. A remarkable 3-fold rise in relative bioavailability via transdermal route ($F_{\text{MDTS via microporated skin}}$ = 291.15%) as compared to oral suspension of marketed tablet ($AUC_{0-\infty}$ = 45.94 h*µg/ml) further confirmed the validity of our hypothesis. The outcomes of *in vitro*, *ex vivo* and *in vivo* characterization of Lopinavir MDTS represented the system as safe, effective and stable which seems promising for their extended clinical evaluation.

Keywords: Metered-dose transdermal spray, Lopinavir, Microneedles, Skin microportion, Permeation enhancement, Kollidon® VA 64.

Acquired immune deficiency syndrome (AIDS), caused by human immune deficiency virus (HIV) infection, is one of the most serious infectious diseases that challenges public health globally [1]. As per the UNAIDS report 2013, even with a 33 % decrease since 2001, new HIV infections reported in 2012 being significantly high (about 2.3 million) with approximately 35.3 million people suffering from HIV worldwide [2]. Due to lack of efficacy of vaccines and macromolecular entry inhibitors, there is a growing consensus on the use of drugs with proven antiretroviral activity for prophylaxis of HIV. It is anticipated that the presence of sufficient concentrations of antiretroviral drugs at the site would help to prevent HIV infection. Hence, drugs which act on HIV entry, HIV fusion, HIV reverse transcriptase and HIV integrase are being explored for the HIV prophylaxis [3]. Current optimal highly active antiretroviral therapy (HAART) regimens consist of two nucleoside analogue reverse transcriptase inhibitors (NARTIs or NRTIs) along with either a protease inhibitor or a non-nucleoside reverse transcriptase inhibitor (NNRTI). Use of antiretroviral drug combination is a commonly employed strategy for HIV therapy to increase efficacy and reduce resistance and side effects. One of the classes of anti-HIV drugs that inhibit growth of virus is retroviral protease enzyme inhibitor which has been highly beneficial to many HIV-infected individuals since its introduction in 1996, when the protease inhibitor-based highly active antiretroviral therapy (HAART) initially became available. Lopinavir is a potent protease inhibitor indicated for the treatment of the HIV infection [4]. However, the oral administration of Lopinavir is limited by its poor bioavailability (~20%) due to its low aqueous solubility (0.01 mg/ml), poor dissolution, extensive first pass metabolism primarily mediated by cytochrome P450 3A4 and cytochrome P450 3A5 isoenzymes and high efflux by P-glycoprotein efflux system. Currently, it is co-administered with subtherapeutic dose of Ritonavir, a pharmacokinetic enhancer of Lopinavir. Ritonavir is a potent inhibitor of cytochrome P450 3A4 in liver microsomes. However, even in presence of Ritonavir, oral

bioavailability of lopinavir is only around 36 % [5]. Moreover, this combination is reported to cause several adverse effects including Diarrhea; headache; mild stomach pain or upset; nausea; tiredness; vomiting and weakness.

Transdermal delivery, an attractive alternative to oral delivery is associated with a number of advantages, particularly, avoidance of hepatic first-pass metabolism that can prematurely metabolize drugs. Metered dose transdermal spray (MDTS) formulations are gaining significant industrial attention because of their easy scalability and potential to overcome the limitations with other existing transdermal drug delivery systems. For example, problems with irritation and adhesion are often encountered with transdermal patches [6]; conventional gels must be applied over large surface areas and the possibility of passive transfer to clothing, or to another person, must be considered [7]. MDTS, on the other hand, is user friendly and permits a metered dose to be administered to a fixed skin area [8-9]. Being a solution based formulation, MDTS consists of drug and film forming polymer (with or without chemical penetration enhancer) dissolved in a volatile solvent. Once applied, the volatile components rapidly evaporate leaving behind a thin, uniform transdermal film with drug at high thermodynamic activity that is rapidly taken up into the skin [10]. However, overall transdermal flux remains limited by the extremely tough barrier property of stratum corneum. Achievement of desirable plasma concentration without the aid of a penetration enhancer is usually difficult. Isopropyl myristate (IPM) was selected as a chemical penetration enhancer that reversibly affect the bilayer architecture of the SC lipids by introducing phase separation and by direct perturbation of a proper lamellar arrangement [11]. Microneedle roller was also chosen as a physical way to facilitate the permeation that utilizes sub-millimeter sized microneedles designed to pierce the skin's stratum corneum barrier in a painless manner and create microchannels therein. Microneedle rollers have been

used to treat large areas of skin for cosmetic purposes and to increase skin permeability for drug delivery [12-13].

Thus, the present investigation aimed at development of metered dose transdermal spray of Lopinavir and to study its permeation through microporated skin. The various formulation parameters were optimized to obtain a spray formulation with the desired drug loading, spray pattern etc. The optimum formulation was evaluated for the *in vitro* drug release, *ex vivo* permeation through pig ear skin. *In vivo* pharmacokinetic studies were also performed using Wistar rats and comparison of the pharmacokinetic parameters was done with the oral suspension of marketed Lopinavir tablet.

I. EXPERIMENTAL

1. Materials

Lopinavir was obtained as a gift sample from Aurobindo Pharma Ltd., Hyderabad. Kollidon® VA 64 was procured from BASF, Mumbai. Isopropyl myristate and cellophane membrane (12kD) were purchased from HiMedia Labs, Mumbai. Metered dose spray containers were purchased from Valois India Pvt. Ltd., Mumbai. Microneedle rollers (CTS-150, Clinicares) were procured from Coherent Medical Systems, Mumbai. All other reagents used were of analytical grade.

2. Preparation of Metered dose transdermal spray

Accurately measured quantities of Kollidon® VA 64 (Table 1) and isopropyl myristate (0.15ml) were dissolved in 30 ml of acetone:ethanol (1:1). 600 mg of Lopinavir was uniformly mixed into it using bath sonication for 3 minutes followed by mechanical stirring for 10 minutes. Resulting formulations were then filled in metered dose spray containers and characterized for different parameters as discussed in subsequent sections.

3. Characterization of metered dose transdermal spray

3.1. Viscosity of spray solutions

The viscosity of the spray solutions was measured at 25±1°C using Ostwald viscometer.

3.2. Film drying time and its coverage area

Formulations were sprayed through the MDTS onto a glass plate from a distance of 3.0 cm. The time required for complete evaporation of solvent and the average diameter of the fully dried film formed (d) was observed. The area covered by the film was then calculated from its diameter using equation 1.

$$\text{Area covered by film} = \frac{\pi d^2}{4} \quad \ldots\ldots (1)$$

3.3. Drug content per spray and content uniformity

The drug content per metered dose was determined by actuating the pump five times in a beaker containing measured volume of Acetonitrile. The sprayed content was allowed to dissolve under mild agitation and the drug content per spray was quantified using first derivative UV spectroscopy as described elsewhere [14]. The content uniformity was also evaluated by quantifying the drug emitted in 1^{st}, 5^{th}, 10^{th}, 15^{th} and 30^{th} actuation.

3.4. Percent solid content per spray

The initial weights (W_1) of the MDTS containers were recorded. The containers were then actuated for five times (n) and their final weights (W_2) were recorded. The average solid content per spray ($SC_{avg/spray}$) was calculated using equation (2) and was divided by theoretically calculated solid content per spray ($SC_{T/spray}$) as given in equation (3) to get percent solid content per spray ($SC_{\%/spray}$).

$$SC_{avg/spray} = \frac{W_1 - W_2}{n} \quad \ldots\ldots (2)$$

$$SC_{\%/spray} = \frac{SC_{avg/spray}}{SC_{T/spray}} \quad \ldots\ldots (3)$$

3.5. Spray pattern

The spray pattern was assessed by delivering the spray through the MDTS onto a paper held at a distance (L) of 3.0 cm. The resulting wet region on paper was outlined and the average radius (r) was measured. Spray angle was then calculated using equation (4).

$$\text{Spray angle } (\theta; \text{radian}) = 2 \times \tan^{-1} \frac{(r)}{(L)} \quad \ldots\ldots (4)$$

3.6. Pump seal efficiency test

The initial weights (W_1) of the MDTS containers under test were recorded and then placed in the upright position at 30° for 3 days. The final weight (W_2) of containers were measured and the leakage rate was calculated using equation (5).

$$\text{Leakage rate} = \frac{W_1 - W_2}{W_1} \quad \ldots\ldots (5)$$

3.7. pH and clarity of spray solution

The pH of the spray solution was determined by spraying them on pH paper while the clarity was observed visually.

4. *In vitro* drug release study

The *in vitro* release study was done using specially designed Franz type diffusion cells with 1.13 cm^2 of effective permeation area and 8 mL of receptor chamber volume. Pre-activated dialysis membrane (MWCO, 12 kD) was used as permeation barrier and mounted between donor and receptor chambers of diffusion cell with the help of parafilm. The receptor chamber was filled with phosphate buffer pH 6.8: acetonitrile (7:3) solution as a diffusion medium. The formulations, viz. batch F_1 (without Kollidon) and optimized batch (F_{11}) containing 5 mg of Lopinavir were sprayed from MDTS onto the membrane. The diffusion medium was continuously stirred using a magnetic stirrer. Samples (1 ml) were withdrawn from the receptor compartment at predetermined time intervals, and the cell was replenished

with equal volume of fresh diffusion medium. Withdrawn samples were analyzed for the drug release by first derivative UV spectroscopy. The kinetics of drug release was investigated by fitting the data in various release models viz., Zero order, First order, Higuchi, Hixson-Crowell and Korsmeyer-Peppas models. Approximation accuracy of each model was decided based on its correlation coefficient (R^2) value ($R^2 \geq 0.970$ was considered as an acceptable correlation).

5. *Ex vivo* drug permeation and skin deposition study

Ex-vivo study was carried out using the similar experimental setup as used for *in vitro* drug release study. The only difference was the use of full thickness pig ear skin as a permeation barrier instead of dialysis membrane. The subcutaneous fat was carefully removed and the skin was mounted between donor and receptor chambers with the stratum corneum facing the donor side. The receptor chamber was filled with diffusion medium and the skin was allowed to equilibrate for 30 minutes before applying the formulation. The lopinavir solution in acetone:ethanol (1:1) and optimized lopinavir MDTS batch were selected as control and test group, respectively. Formulations containing 5 mg of lopinavir were applied on to the skin. Samples (1ml) were withdrawn from the receptor compartment at predetermined time intervals and replenished each time with same volume of fresh diffusion medium. The amount of Lopinavir in the samples was determined by HPLC method as described elsewhere [14]. At the end of permeation experiments (24 hrs), the drug retained on the skin surface was estimated by washing the skin with diffusion medium, passing the washings through 0.22µm membrane filter and estimating the amount of drug in the filtrate by HPLC method. For estimation of the drug deposited within the skin, the washed skin was cut into small pieces using a chopper, suspended in methanol and subjected to homogenization under cold conditions for 5 minutes followed by bath sonication for 15 minutes. The extracted Lopinavir

was separated by centrifugation at 5000 rpm and 25°C for 10 min and was quantified by HPLC method.

For determination of skin permeation through microporated skin, similar procedure was repeated using microporated skin instead of intact skin. For skin microporaton, microneedle rollers (Derma roller®; 2 mm long needles; figure 1A and 1B) were mildly rolled 10 times vertically, horizontally and obliquely at the same intensity covering the same area as depicted in figure 1C. The transdermal steady-state flux ($J_{SS;}$ µg/cm^2/h) was calculated from the slope of terminal linear portion of the cumulative amounts of drug permeated per unit area versus time plot. Permeation enhancement ratio (PER) was then calculated using equation (6):

$$PER = \frac{J_{SS}^{Test}}{J_{SS}^{Control}} \quad \ldots\ldots (6)$$

6. Histopathological study

The experimental protocol was approved by institutional animal ethics committee (protocol no.MSU/PHARM/IAEC/2013/23) & the experiments were conducted in accordance with CPCSEA guidelines. The abdominal hairs of six Wistar rats were trimmed off and Lopinavir MDTS (F_{11}) was actuated over it. On completion of six hours, the rat was euthanized and its abdominal skin was excised, dipped in 10% buffered formalin and transferred in gradually increasing concentrations of ethanol for dehydration followed by immersion in xylene. The processed skin was then embedded in paraffin block and longitudinally sectioned in to 5-µm thick portions using microtome. These skin sections were placed on glass slides to remove paraffin wax by gently warming the slide and washing the molten wax with xylene. Sections were then washed with absolute alcohol followed by water and stained with hematoxylin and eosin to determine gross histopathology and collagen deposition, respectively. Commercial glycerol's mounting fluid was used to finally mount the stained sections. Negative control and positive control slides were also prepared by treating rat skin with phosphate buffer

solution pH 6.8 and isopropyl alcohol (IPA), respectively using the procedure described above. The slides were observed at 10-fold magnification using optical microscope

7. *In vivo* pharmacokinetic study

The experimental protocol was approved by institutional animal ethics committee (protocol no.MSU/PHARM/IAEC/2013/23) & the experiments were conducted in accordance with CPCSEA guidelines. Precisely, eighteen healthy male Wistar rats weighing around 180-250 g were procured and housed under regulated environmental conditions with free access to food and water. Animals were randomly allocated into three treatment groups of six animals in each group and received formulations (an equivalent amount containing 10.27 mg of lopinavir) as described in table 2. Hairs from abdominal area of animals receiving transdermal formulation were removed using electrical clipper. Skin microporation in group III animals was done in similar way as described in earlier section. At predetermined time intervals, 0.5 ml of blood samples were withdrawn from the retro-orbital plexus in to heparinized vials and centrifuged at 4,000 rpm and 4°C for 15 min to separate plasma (supernatant). Separated plasma samples were then deproteinated using 1.5 ml acetonitrile, mixture was vortexed for 2 min and centrifuged for 5 min at 5000 rpm and 4°C. The supernatant was filtered through 0.2 μm syringe filter and the amount of Lopinavir present in it was determined using previously developed HPLC method [14]. Various pharmacokinetic parameters were obtained using Thermo Kinetica software (version 5.0, Thermo Fisher Scientific) and the relative bioavailability (F; %) was calculated using equation (7):

$$F\ (\%) = \frac{AUC_{0\text{-}\infty\ (\text{F-11 MDTS})}}{AUC_{0\text{-}\infty\ (\text{Oral suspension})}} \times 100 \qquad \ldots\ldots\ (7)$$

8. Stability study

Effect of storage on physical and chemical attributes of optimized transdermal spray was ascertained as an indicator of stability in accordance with ICH guidelines. The formulation was divided into six portions of 20mL each and packed in metered dose containers. Three containers were kept at 30 ± 2 °C / 65 ± 5 %RH while other three were kept at 4 ± 2 °C / ambient RH. On day 0, 15 and 30, each container was evaluated for spray pattern, pH, film appearance, drying time and percent drug content per spray.

9. Statistical Analysis

Wherever indicated, the experiments were performed in triplicate, the data were analyzed using Microsoft Excel (version 2007) and the results are expressed as mean ± standard deviation. GraphPad InStat software (version 5.00) was used for statistical analysis of the data. The one way ANOVA followed by Tukey's multiple comparison test was applied and $P < 0.05$ was considered as a minimal level of significance.

II. RESULTS AND DISCUSSION

Metered-dose transdermal spray system consists of a film forming polymer and the drug dissolved in a single phase of organic solvent(s) which upon application to the skin, rapidly evaporates leading to the formation of a thin supersaturated film [15]. Kollidon® VA 64, a vinyl pyrrolidone/vinyl acetate (VP/VA) copolymer, was selected based on its good film forming properties viz., high plasticity, low hygroscopicity, bioadhesiveness, luster and hardness. It has also reported to inhibit crystallization of susceptible drugs [16]. Different solvents were screened for preparation of a single phase solution dissolving all the ingredients and evaporate quickly. Blending acetone with ethanol facilitated a faster film formation where ethanol-acetone mixture (1:1) was found to perform best in fulfilling the need and hence selected as a solvent for spray. Warren and Reed also designated acetone and

primary alcohols as preferred solvents for topical solutions at a concentration range of 40-65 % [17].

1. Characterization of metered dose transdermal spray

The composition and characteristics of the different batches with varying amounts of Kollidon® have been shown in table 1. All the formulations were found to be clear and transparent indicating that the drug, polymer and the penetration enhancer were soluble in the solvent system and were homogenously present as a molecular dispersion in the spray. Quick drying films are desirable in order to avoid loss of drug through draining or transfer to other surfaces. The drying time of the formulation was reduced as the amount of Kollidon® was increased up to a level of 5% (Batch F_{11}) beyond which a further increase in Kollidon® increased the drying time. The reason may reside in the fact that with increase in the total solid content of the formulation; its viscosity, surface tension and solvent available for evaporation change that ultimately govern the physical traits of the spray viz., sprayability and volatilization upon skin contact. The reduction in drying time from F_1 to F_{11} batches may be attributed to reduction in solvent volume to be evaporated. However, from batch F_{12} to F_{15}, the viscosity seems to play a crucial role in reducing the solvent evaporation rate and increasing the drying time [18]. Lowest drying time was obtained for batch F_{11}, which consisted of 5 %w/v of Kollidon®.

The uniformity of the spray pattern of prepared batches was found to improve with increasing amount of Kollidon® that may be due to the flexible and cohesive film forming nature of Kollidon® used [16]. The film coverage area and spray angle was also narrowed down from batch F_1 to F_{11} which is desirable for less loss of the dose during application. The results support the fact that more viscous vehicle shows narrow spray angle [18]. Though, batches from F_{12} to F_{15} showed irregular spray pattern as an indication of poor sprayability of the

formulations owing to their unfavorable surface tension and viscosity. The maximum drug content per spray (1.02 mg) as well as percent solid content per spray (99.49 %) also reflected the optimum sprayability and volatilization characteristics of Batch F_{11}. All the containers passed pump seal efficiency test as almost negligible leakage (leakage rate varied from 0.001-0.002 / 3 days) was observed from any of the containers.

2. *In vitro* drug release study

The *in vitro* drug release from optimized formulation F_{11} was evaluated across dialysis membrane (MWCO, 12kD) and its kinetics was established by fitting the data in various drug release models. As evident in Table 3, among all the models applied, Higuchi's model showed highest linearity (R^2 = 0.994) and thus, expressed a diffusion controlled drug release kinetics from the transdermal film. The Korsmeyer-Peppas model with a good linearity (R^2 = 0.994) and an release exponent (*n*) value of 0.557 further confirmed a non-fickian type of diffusion (anomalous transport) [19], i.e. the release is governed by both diffusion of the drug and dissolution of the film forming polymer.

3. *Ex vivo* drug permeation and skin deposition study

To understand the permeation behavior of Lopinavir from spray-deposited transdermal film, *ex vivo* permeation study was conducted through intact as well as microporated pig ear skin and compared with plain drug solution (Figure 2). Pig ear skin was selected as its histological and biochemical properties had been shown significant resemblance to human skin [20-21]. The steady state transdermal flux obtained for plain drug solution (J_{SS}; 29.62 µg/cm^2/h) could be attributed to the high thermodynamic energy of drug resulting from rapid evaporation of the solvent mix [22]. In addition, ethanol could have also contributed to some extent in permeation of drug [23]. As evident in results (Table 4), the overall skin permeation of Lopinavir across intact pig ear skin was better via F_{11} where about 47.85 % drug entered the

skin in 24 hours out of which 28.00 % reached the receptor side. Such an improvement over drug permeation via plain drug solution, where only 29.39 % drug could successfully made to enter skin, reinforces the usefulness of IPM as a penetration enhancer (PER, 1.28). This finding is in good agreement with Hadgraft's concept of IPM deposition within skin and formation of 'patchless drug reservior' [24]. The microporation of skin with microneedle roller further aided in drug permeation (PER, 1.77) and significantly improved the overall drug permeation via F_{11} (54.37 %) when compared to its permeation across intact skin (47.85 %). The drug deposition level in intact skin was found to be higher (19.85 %) as compared to microporated skin (13.45 %) which could just be an indicative of less restricted permeation of drug through micropores resulting in a smaller fraction being deposited within skin while a larger fraction was being permeated across the skin.

4. Histopathological study

While selecting the formulation components, their recommended safe levels as per USFDA inactive ingredient guide limits were considered for preparing the batches. The histopathological studies were further performed to establish the safety of the optimized F_{11} batch. The F_{11} treated skin sections were carefully examined under optical microscope for epidermal or subepidermal cellular damage and presence of prominent blood vessels as a sign of irritation or toxicity and compared with sections of skin treated with phosphate buffer saline (pH 7.4) as negative control and isopropyl alcohol as positive control. Figure 3 represents the images of skin sections as observed under optical microscope at 10x magnification. As substantiated from the figure, no sign of pathological changes have been observed on section of F_{11} treated skin indicating the formulation as safe for transdermal application. Such results reflect the non-toxic and non-irritant nature of the ingredients used.

5. *In vivo* pharmacokinetic study

In vivo animal study is vital to predict the clinical usefulness of the newly developed F_{11} formulation via expression of its potential of achieving and maintaining the plasma drug concentration within therapeutic range for stipulated time period. Despite of thinner stratum corneum and higher hair follicle density than human skin, rats were successfully utilized to predict human skin permeability with low inter-individual variations and similar permeating rate with a two-fold difference [25]. Three groups of six male Wistar rats were used to compare the overall bioavailability attained from orally administered Lopinavir suspension and transdermally applied F_{11} over intact as well as microporated abdominal skin. The plasma drug concentration versus time plot was constructed (Figure 4) and various pharmacokinetic parameters viz., peak plasma concentration (C_{max}), peak time (T_{max}), mean residence time ($MRT_{0-\infty}$) and area under plasma drug concentration-time curve ($AUC_{0-\infty}$) were obtained (Table 5) using Thermo Kinetica software and the relative bioavailability via MDTS was calculated. The $AUC_{0-\infty}$ of standard control group was about 45.94 h*µg/ml which was found to increase by almost 1.5 fold via F_{11} batch applied on intact skin ($AUC_{0-\infty}$ = 69.29 h*µg/ml; F = 153.63 %). The data are in accordance with *ex vivo* skin permeation experiment and similarly reflect the permeation enhancement potential of IPM used in the formulation. The $AUC_{0-\infty}$ for F_{11} batch applied on microporated skin ($AUC_{0-\infty}$ = 131.30 h*µg/ml; F = 291.15 %) showed a surprising 3 fold increment when compared to standard control group. Such a significant rise could be attributed to the avoidance of presystemic metabolism through transdermal route and also the synergistic effect of using chemical as well as physical penetration enhancement techniques together to improve overall bioavailability through transdermal route.

6. Stability study

The short term stability data of F_{11} stored under two different environmental conditions has been shown in Table 6. Some of the stability indicating parameters remained unchanged viz., pH of spray solution, its spray pattern from MDTS container and appearance of the film formed. However, an insignificant change in other parameters was observed viz., the film drying time was slightly increased and the percent drug content per meter dose spray was slightly decreased on storage. Hence, it can be stated that formulation in MDTS containers are sufficiently stable at both the environmental conditions. This further indicates absence of any evaporative loss of volatile spray solvents in hermetically sealed / MDTS containers.

III. CONCLUSION

Metered dose transdermal sprays always seem promising due to simple, fewer and easily scalable production steps; capability of patient friendly, discreet and convenient dosing via the skin and greatly reduced skin-irritation owing to their non-occlusive nature. Kollidon® VA 64 and isopropyl myristate were used as film forming polymer and chemical permeation enhancer, respectively. Microneedle roller was used as a physical mode to breach the stratum corneum. Among all batches, F_{11}, containing 5 %w/v of Kollidon®, was found to possess most favorable sprayability and volatilization characteristics. *In vitro* drug release study showed non-fickian diffusion as a principle release mechanism. *Ex vivo* skin permeation and deposition studies revealed a significant rise in steady state transdermal flux across microporated pig ear skin when compared to plain drug solution (PER, 1.77). Histopathological skin sections did not show any sign of irritation and also the formulation retained its desirable properties during one month of stability testing. *In vivo* bioavailability study in male Wistar rats demonstrated significant improvement over orally administered Lopinavir suspension ($F_{\text{MDTS via microporated skin}}$, 291.15%). These outcomes of *in vitro*, *ex vivo* and *in vivo* characterization of Lopinavir MDTS represented the system as safe, effective and

stable. These findings appear encouraging, however; oblige a cautious clinical evaluation and long term stability testing before reaching the market.

REFERENCES

[1] E. Ojewole, I. Mackraj, P. Naidoo, T. Govender, Exploring the use of novel drug delivery systems for antiretroviral drugs, Eur J Pharm Biopharm 70 (2008) 697-710.
[2] UNAIDS, AIDS by the numbers UNAIDS, Geneva, 2013, http://www.unaids.org/sites/default/files/media_asset/JC2571_AIDS_by_the_numbers_en_1.pdf, Accessed 31 December 2014.
[3] R. Teply, M. Goodman, C. J. Destache, Lopinavir/Ritonavir: A Review for 2011, Clinical Medicine Insights: Therapeutics 3 (2011) 93-102. doi:10.4137/cmt.s2018.
[4] A. Chandwani, J. Shuter, Lopinavir/ritonavir in the treatment of HIV-1 infection: a review, Ther Clin Risk Manag 4 (2008) 1023-33.
[5] K. W. Garren, S. Rahim, K. Marsh, J. B. Morris, Bioavailability of generic ritonavir and lopinavir/ritonavir tablet products in a dog model, J Pharm Sci 99 (2010) 626-31. doi:10.1002/jps.21712.
[6] A. W. Meikle, A permeation-enhanced nonscrotal testosterone transdermal system for the treatment of male hypogonadism., in: Nieschlag E, Behre HM, (Ed.).^(Eds.), Testosterone-action, deficiency, substitution, 2nd ed, Springer-Verlag, Berlin, 1998, pp. 389-422.
[7] G. Schaison, B. Couzinet, H. M. Behre, Percutaneous dihydrotestosterone treatment, in: Nieschlag E, (Ed.).^(Eds.), Testosterone- action, deficiency, substitution, 2nd ed, Springer-Verlag, Berlin, 1998, pp. 329-48.
[8] M. L. Leichtnam, H. Rolland, P. Wuthrich, R. H. Guy, Identification of penetration enhancers for testosterone transdermal delivery from spray formulations, J Control Release 113 (2006) 57-62. doi:S0168-3659(06)00108-8 [pii]
10.1016/j.jconrel.2006.03.008.
[9] A. Bakshi, A. Bajaj, G. Malhotra, M. Madan, N. Amrutiya, A novel metered dose transdermal spray formulation for oxybutynin, Indian J Pharm Sci 70 (2008) 733-9. doi:10.4103/0250-474X.49094.
[10] A. Lulla, G. Malhotra, inventors; Waterlead Limited, assignee, Transdermal Pharmaceutical Spray Formulations Comprising a Vp/Va Copolymer and a Non-Aquous Vehicle, United States2007.
[11] T. N. Engelbrecht, B. Deme, B. Dobner, R. H. Neubert, Study of the influence of the penetration enhancer isopropyl myristate on the nanostructure of stratum corneum lipid model membranes using neutron diffraction and deuterium labelling, Skin Pharmacol Physiol 25 (2012) 200-7. doi:000338538 [pii]
10.1159/000338538.
[12] A. K. Banga, Microporation applications for enhancing drug delivery, Expert Opin Drug Deliv 6 (2009) 343-54. doi:10.1517/17425240902841935.
[13] M. R. Prausnitz, Microneedles for transdermal drug delivery, Adv Drug Deliv Rev 56 (2004) 581-7. doi:10.1016/j.addr.2003.10.023
S0169409X03002394 [pii].
[14] K. K. Patel, P. Kumar, H. P. Thakkar, Formulation of niosomal gel for enhanced transdermal lopinavir delivery and its comparative evaluation with ethosomal gel, AAPS PharmSciTech 13 (2012) 1502-10. doi:10.1208/s12249-012-9871-7.

[15] M. L. Reid, M. B. Brown, S. A. Jones, Manipulation of corticosteroid release from a transiently supersaturated topical metered dose aerosol using a residual miscible co-solvent, Pharm Res 25 (2008) 2573-80. doi:10.1007/s11095-008-9675-3.
[16] V. Buhler, Kollidon® Polyvinylpyrrolidone escipients for the pharmaceutical industry, BASF SE Pharma Ingredients & Services, Ludwigshafen, Germany, 2008, http://www.kollidon.com/Documents/ENP/Brochure/EN/G-EMPMD256_Kollidon_Polyvinylpyrrolidone_excipients_for_the_pharmaceutical_industry.pdf, Accessed November 01, 2014.
[17] R. Warren, J. C. Reed, inventors; PROCTER & GAMBLE (US), assignee, Topical tanning compositions, patent EP0302147 A1. 1989.
[18] M. L. Leichtnam, H. Rolland, P. Wuthrich, R. H. Guy, Formulation and evaluation of a testosterone transdermal spray, J Pharm Sci 95 (2006) 1693-702. doi:10.1002/jps.20641.
[19] J. Siepmanna, N. A. Peppas, Modeling of drug release from delivery systems based on hydroxypropyl methylcellulose (HPMC), Adv Drug Deliv Rev 48 (2001) 139-57.
[20] I. P. Dick, R. C. Scott, Pig ear skin as an in-vitro model for human skin permeability, J Pharm Pharmacol 44 (1992) 640-5.
[21] U. Jacobi, M. Kaiser, R. Toll, S. Mangelsdorf, H. Audring, N. Otberg et al., Porcine ear skin: an in vitro model for human skin, Skin Res Technol 13 (2007) 19-24. doi:SRT179 [pii] 10.1111/j.1600-0846.2006.00179.x.
[22] K. Moser, K. Kriwet, Y. N. Kalia, R. H. Guy, Enhanced skin permeation of a lipophilic drug using supersaturated formulations, J Control Release 73 (2001) 245-53. doi:S0168365901002905 [pii].
[23] G. Oliveira, A. E. Beezer, J. Hadgraft, M. E. Lane, Alcohol enhanced permeation in model membranes. Part II. Thermodynamic analysis of membrane partitioning, Int J Pharm 420 (2011) 216-22. doi:S0378-5173(11)00799-X [pii] 10.1016/j.ijpharm.2011.08.037.
[24] P. Santos, A. C. Watkinson, J. Hadgraft, M. E. Lane, Influence of penetration enhancer on drug permeation from volatile formulations, Int J Pharm 439 (2012) 260-8. doi:S0378-5173(12)00905-2 [pii] 10.1016/j.ijpharm.2012.09.031.
[25] K. McCormack, Non-steroidal anti-inflammatory drugs and spinal nociceptive processing, Pain 59 (1994) 9-43. doi:0304-3959(94)90045-0 [pii].

ACKNOWLEDGEMENT

This work was financially supported by grants from All India Council of Technical Education (AICTE), a statutory body of Government of India.

Table 1. Composition of various batches of MDTS and their characteristics

Batch	Kollidon® VA 64 (%w/v)	Viscosity# (mPa*s)	Film drying time# (sec)	Area covered by film# (cm^2)	Drug content per spray# (mg)	Percent solid content per spray# (%)	Spray angle (°)	Leakage rate / 3 days
F_1	0.0	0.71 ± 0.041	82.33 ± 2.51	5.96 ± 0.62	0.97 ± 0.02	100.98 ± 2.65	49.33	0.001
F_2	0.5	1.12 ± 0.083	74.33 ± 1.52	5.72 ± 0.42	0.94 ± 0.02	99.40 ± 1.32	48.45	0.001
F_3	1.0	1.47 ± 0.077	71.00 ± 2.64	5.45 ± 0.63	0.96 ± 0.02	98.46 ± 1.02	47.42	0.002
F_4	1.5	1.95 ± 0.101	68.66 ± 1.52	5.31 ± 0.40	0.93 ± 0.04	98.77 ± 2.14	46.87	0.001
F_5	2.0	2.29 ± 0.106	66.33 ± 1.52	5.18 ± 0.61	0.96 ± 0.02	97.98 ± 1.67	46.35	0.002
F_6	2.5	2.63 ± 0.092	64.33 ± 1.52	4.90 ± 0.39	0.95 ± 0.03	98.26 ± 1.39	45.21	0.002
F_7	3.0	2.91 ± 0.061	63.33 ± 1.15	4.53 ± 0.37	0.98 ± 0.01	99.53 ± 2.18	43.64	0.001
F_8	3.5	3.34 ± 0.126	60.33 ± 1.15	4.41 ± 0.57	0.91 ± 0.04	97.74 ± 1.63	43.11	0.002
F_9	4.0	3.79 ± 0.099	58.33 ± 1.53	4.15 ± 0.36	0.91 ± 0.02	98.24 ± 0.98	41.93	0.002
F_{10}	4.5	4.12 ± 0.154	56.66 ± 1.15	3.92 ± 0.54	0.94 ± 0.03	99.25 ± 1.53	40.85	0.001
F_{11}	**5.0**	**4.51 ± 0.138**	**53.33 ± 0.57**	**3.39 ± 0.23**	**1.02 ± 0.02**	**99.49 ± 0.82**	**38.21**	**0.001**
F_{12}	7.0	6.17 ± 0.192	58.33 ± 1.00	3.35 ± 0.38	0.89 ± 0.06	97.07 ± 3.46	38.00	0.002
F_{13}	10.0	8.74 ± 0.214	59.66 ± 1.52	3.31 ± 0.34	0.87 ± 0.07	96.21 ± 4.79	37.79	0.002
F_{14}	12.0	10.88 ± 0.412	61.00 ± 1.15	3.26 ± 0.44	0.84 ± 0.08	94.86 ± 6.21	37.52	0.002
F_{15}	15.0	14.74 ± 0.375	62.66 ± 2.08	3.18 ± 0.29	0.82 ± 0.07	93.76 ± 8.17	37.09	0.001

data presented as mean ± SD (n=3)

Table 2. Treatment plan for *in vivo* study

Group	Treatment
Standard control	Per oral suspension of marketed Lopinavir tablets in distilled water
Treatment-I	Transdermal Lopinavir spray on intact skin (without microneedle treatment)
Treatment-II	Transdermal Lopinavir spray on microporated skin (with microneedle treatment)

Table 3. Correlation coefficient of various *in vitro* release models applied and interpretation of release mechanism based on release exponent value

Release models	R^2	Release exponent (n)
Zero order	0.922	-
First order	0.946	-
Higuchi	**0.994**	-
Hixson-crowell	0.938	-
Korsmeyer-Peppas	**0.994**	**0.557**

'n' values	Mechanism of drug release
n = 0.5	Fickian diffusion
0.5 < n < 1.0	**Non-fickian (anomalous) diffusion**
n = 1.0	Case II (zero order) transport

Table 4. *Ex vivo* permeation and deposition profile of Lopinavir through pig ear skin

Parameters	Plain drug solution on intact skin	Lopinavir MDTS on intact skin	Lopinavir MDTS on microporated skin
Transdermal flux (J_{SS}, µg/cm^2/h)	29.62	37.78	52.5
Permeation enhancement ratio (PER)	-	1.28	1.77
Percent drug permeated through skin[#]	20.89 ± 0.70	28.00 ± 1.13	40.92 ± 1.21
Percent drug deposited within skin[#]	8.5 ± 0.46	19.85 ± 0.91	13.45 ± 1.03
Percent drug retained on skin surface[#]	61.41 ± 1.69	44.71 ± 1.09	39.37 ± 1.91

[#] data presented as mean ± SD (n=3)

Table 5. *In vivo* pharmacokinetic parameters

Pharmacokinetic parameters	Formulations		
	Marketed Lopinavir oral suspension	**Lopinavir MDTS through intact skin**	**Lopinavir MDTS through microporated skin**
C_{max} (µg/ml)	9.80 ± 0.76	13.68 ± 1.14	22.91± 1.79
T_{max} (h)	4.00 ± 0.00	4.00 ± 0.00	4.00 ± 0.00
$MRT_{0\rightarrow8}$ (h)	5.47 ± 0.421	4.58 ± 0.536	4.86 ± 0.374
$AUC_{0\rightarrow8}$ (h*µg/ml)	37.19 ± 2.49	61.64 ± 5.38	116.05 ± 9.36
$AUC_{0\rightarrow\infty}$ (h*µg/ml)	45.94 ± 4.53	69.29 ± 7.01	131.30 ± 8.97
F (%)	-	153.63 ± 12.32	291.15 ± 23.57

[#] data presented as mean ± SD (n=6)

Table 6. One month stability data of Lopinavir MDTS

Parameters	Sampling time (in days)	Storage conditions	
		30 ± 2 °C / 65 ± 5 %RH	**4 ± 2 °C / ambient RH**
Spray pattern	0	Uniform	Uniform
	15	Uniform	Uniform
	30	Uniform	Uniform
pH	0	6	6
	15	6	6
	30	6	6
Drying time (seconds)	0	53.12 ± 1.15	53.41 ± 1.00
	15	53.25 ± 0.55	53.57 ± 1.15
	30	55.00 ± 1.52	56.13 ± 2.08
Film appearance	0	Clear, transparent	Clear, transparent
	15	Clear, transparent	Clear, transparent
	30	Clear, transparent	Clear, transparent
Percent drug content per meter dose spray	0	100.00 ± 0.00	100.00 ± 0.00
	15	99.19 ± 0.35	100.00 ± 0.19
	30	98.79 ± 0.91	98.99 ± 0.34

FIGURE CAPTIONS

Figure 1. Microneedle roller and its rolling pattern
CTS-150 microneedle roller photograph (A); microscopic image of its microneedle at 4x magnification (B) and the vertico-horizontal (i) as well as oblique (ii) rolling pattern followed for skin microporation (C).

Figure 2. *Ex vivo* skin permeation profile of different Lopinavir formulations

Figure 3. Histopathological rat skin sections
Histopathological sections of rat skin treated with Phosphate buffer saline (A); Lopinavir MDTS (B) and Isopropyl alcohol (C) at 10x magnification.

Figure 4. *In vivo* pharmacokinetic profile
In vivo plasma drug concentration-time profile of Lopinavir from various formulations.

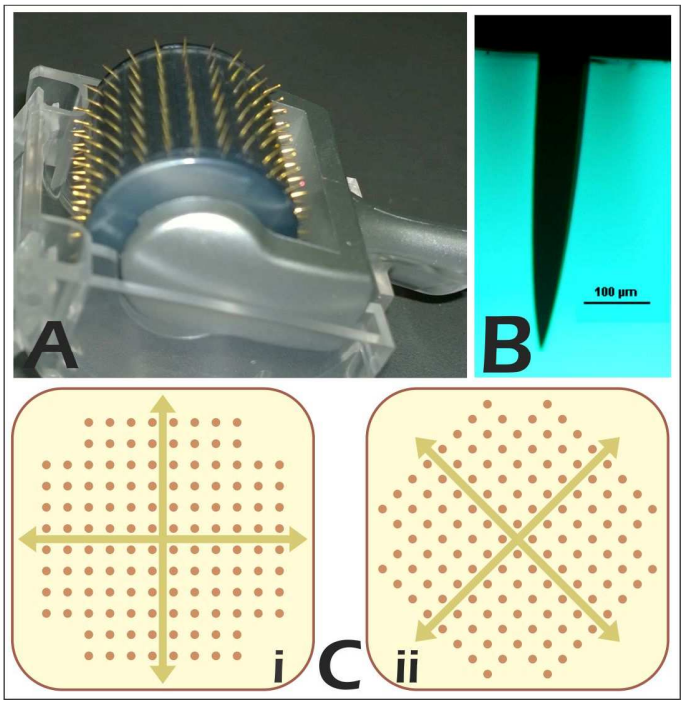

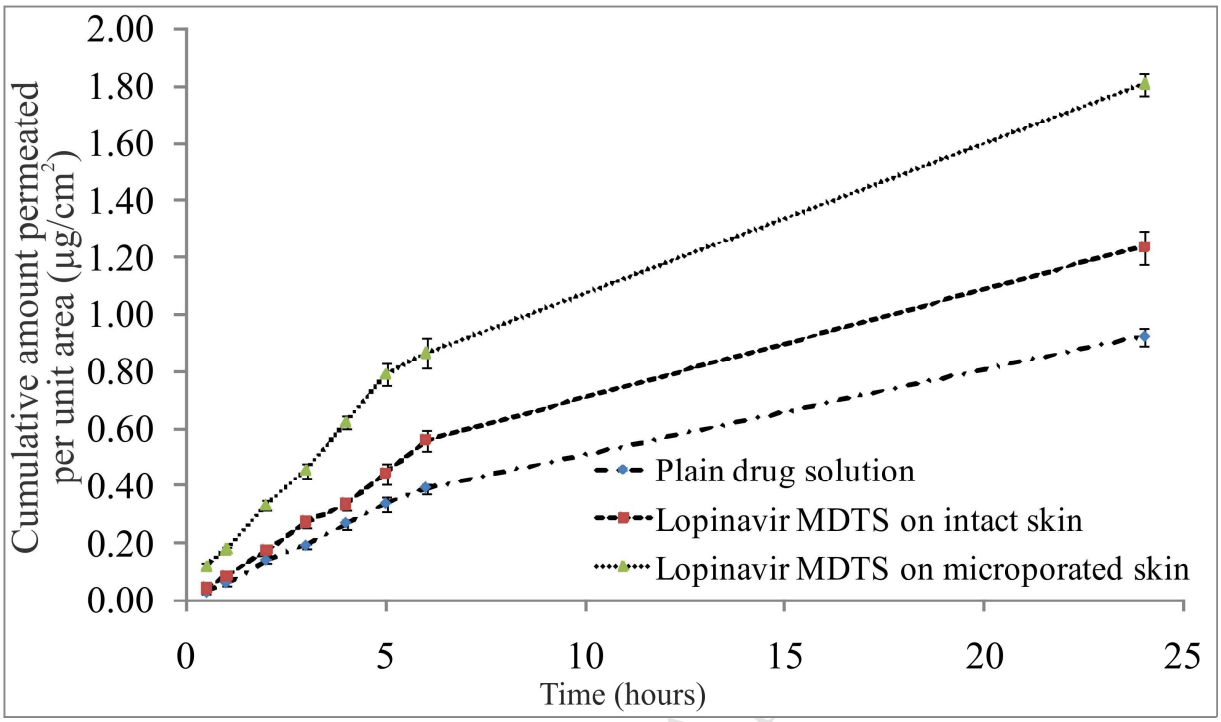

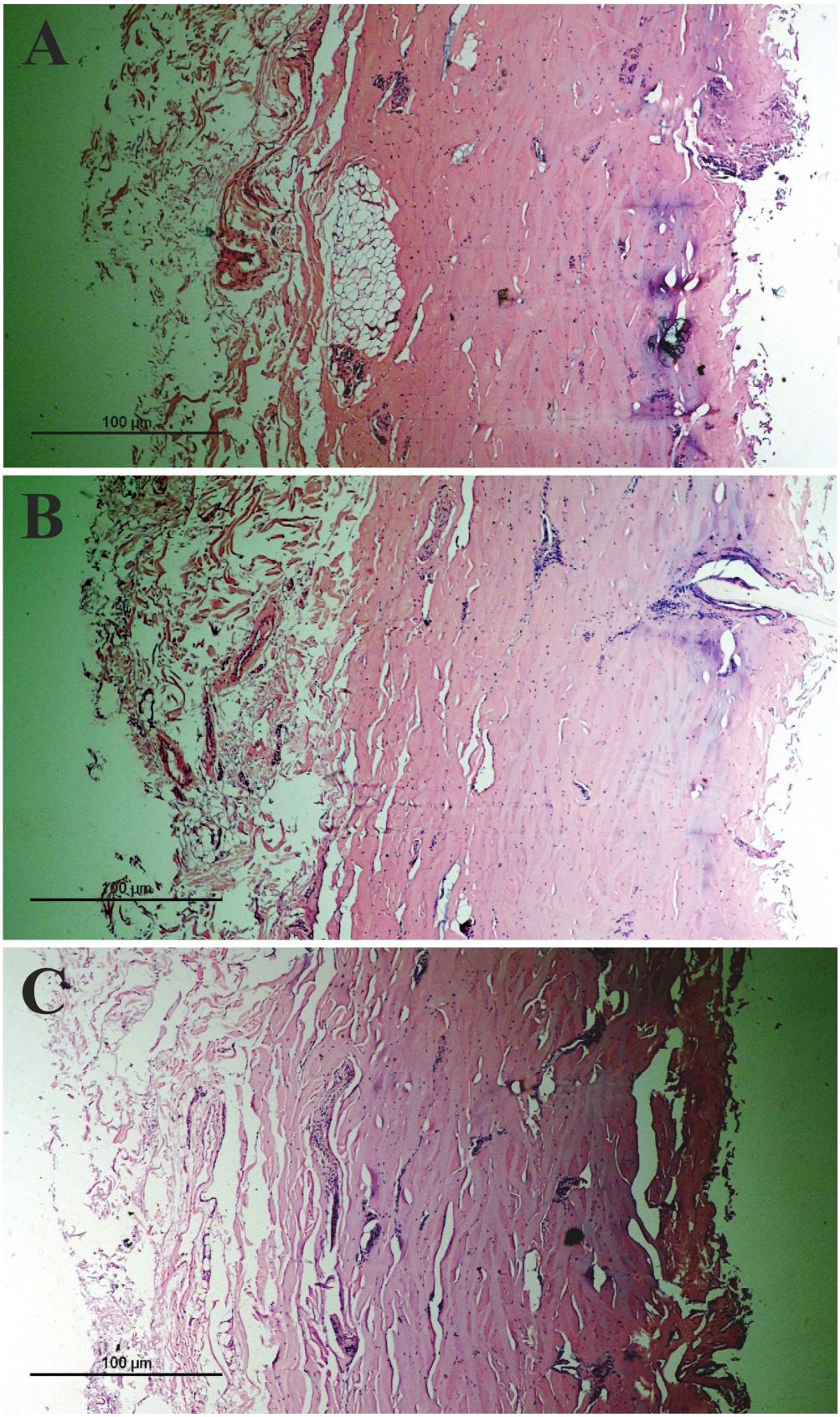
A
100 µm
B
100 µm
C
100 µm

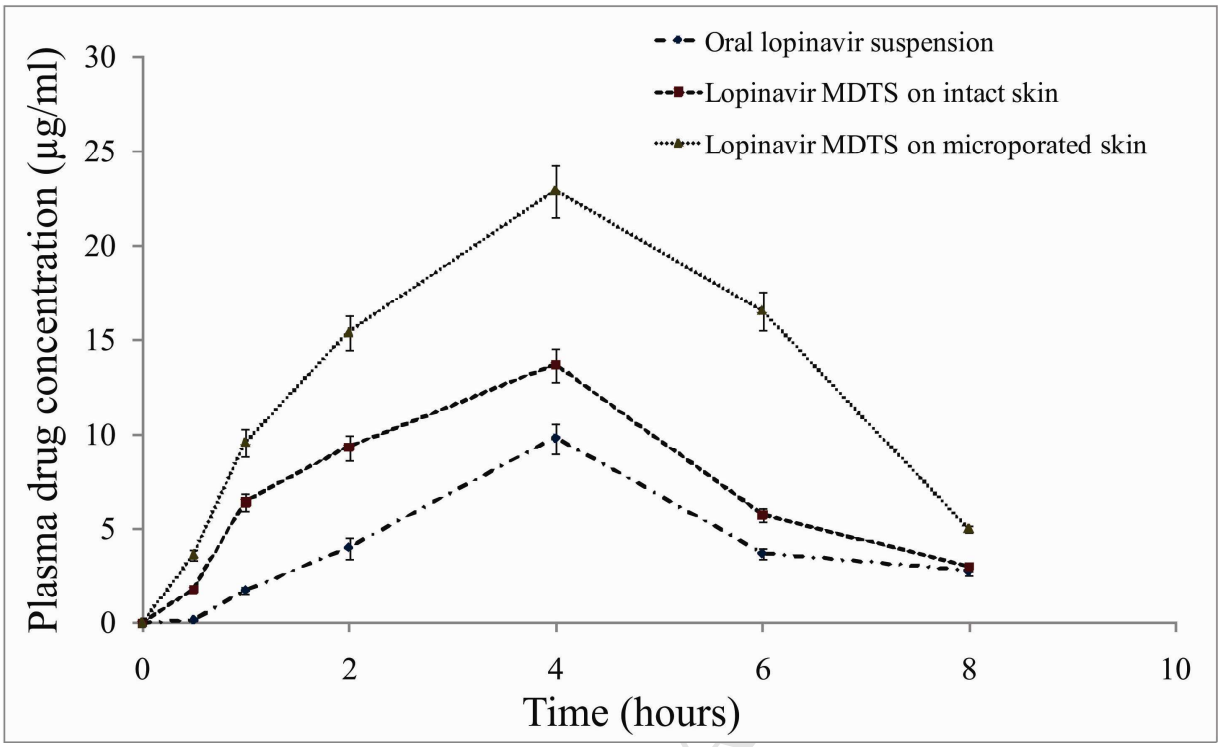

Send Orders for Reprints to reprints@benthamscience.ae

Current Drug Delivery, 2016, *13*, 000-000

Ethosomal Hydrogel of Raloxifene HCl: Statistical Optimization & *Ex Vivo* Permeability Evaluation Across Microporated Pig Ear Skin

Hetal P. Thakkar*, Hitesh Savsani and Praveen Kumar

Pharmacy Department, Faculty of Technology & Engineering, The M.S. University of Baroda, Vadodara-390001, India


H.P. Thakkar

Abstract: ***Background***: The oral bioavailability of Raloxifene hydrochloride, an FDA approved selective estrogen receptor modulator, is severely limited due to its poor aqueous solubility and extensive first pass metabolism. The Present work focuses on the development of ethosomal hydrogel for transdermal delivery of Raloxifene HCl as an alternate way to solve aforementioned problem. The physical breaching of stratum corneum, the principal barrier, by microneedle treatment was also employed to potentiate its transdermal permeation.

Methods: The influence of lipid and ethanol concentration on vesicle size and entrapment efficiency was extensively investigated using response surface methodology based on central composite design. The software based optimization was done and validated using check point analysis. Optimized batch was extensively evaluated for its safety, efficacy and stability.

Results: The optimized ethosomal batch possessed 403 nm size and 74.25% drug entrapment. Its zeta potential and in vitro drug release were also found favorable for transdermal permeation. The ex vivo skin permeation study revealed a transdermal flux of 4.621 µg/cm2/h through the intact pig ear skin which was further enhanced through the microporated skin (transdermal flux, 6.194 µg/cm2/h) with a 3.87 fold rise when compared to drug permeation from plain solution applied over intact skin (transdermal flux, 1.6 µg/cm2/h). Histopathological skin sections showed the non-irritant nature of the ethosomal hydrogel and microneedle treatment. The formulation was found stable under both refrigeration and room temperature conditions for 6 weeks.

Conclusion: In a nutshell, the developed system was found efficient, safe and stable and seems promising for transdermal use.

Keywords: Experimental design, central composite design, Raloxifene, microneedles, skin microporation, ethosomal hydrogel, transdermal permeation.

Received: August 05, 2015 **Revised: November 05, 2015** **Accepted: January 20, 2016**

1. INTRODUCTION

Postmenopausal osteoporosis is a highly prevalent and serious socio-economic health concern in older women arising due to a quick drop in estrogen levels after menopause. It is characterized by low bone mass, microarchitectural disruption, and skeletal fragility, resulting in decreased bone strength and an increased risk of fracture. Initiation of hormone replacement therapy (HRT) at the onset of menopause manage to decrease the risk of osteoporotic vertebral and non-vertebral fractures in women [1]. However, potential risk of developing breast cancer associated with this medication [2] restricts the drug in reserve class and recommended to be used for the shortest time possible. Selective Estrogen Receptor Modulators or SERM have been developed as non-hormonal compounds capable of reproducing the beneficial effects of estrogens on the skeletal system (estrogen agonist effect), without the negative effects on the breast and endometrium (estrogen antagonist effect) to overcome the limitations of HRT.

Raloxifene HCl, an FDA approved nonsteroidal benzothiophene derivative of this class, is widely being used to treat post-menopausal osteoporosis. In addition to preventing postmenopausal bone loss at all skeletal sites and reducing markers of bone turnover to premenopausal concentrations, Raloxifene HCl also presents beneficial effects on lipid metabolism as it is capable of lowering LDL-cholesterol levels and increasing HDL-cholesterol ones [3] and reduces the risk of invasive breast cancer [4].

However, oral absorption of Raloxifene is dissolution rate limited due to its poor aqueous solubility (0.25 mg/litre, BCS class II drug) and only 60% of dose administered could get absorbed orally. Moreover, before reaching the systemic circulation, an extensive first-pass metabolism occurs by

*Address correspondence to this author at Pharmacy Department, Faculty of Technology & Engineering, The M. S. University of Baroda, Kalabhawan, Vadodara-390001, Gujarat, India; Tel/Fax: +91, +0-000-000-0000;
E-mail: hetal_thakkar11@yahoo.com

1567-2018/16 $58.00+.00

glucuronide conjugation which severely limits the absolute oral bioavailability of Raloxifene to approximately 2% [5].

Added advantages of first pass metabolism avoidance and better patient compliance has emerged transdermal route as an alternative for drugs which may not be given orally due to variety of reasons. Though, the barrier nature of skin's outermost stratum corneum layer poses a serious challenge for drug permeation through this route. In order to enhance the permeation, several physical, chemical and formulation based approaches have been successfully explored. Present investigation incorporates a combination of two approaches together to maximize the overall drug permeation through skin. Firstly, ethosomal nanocarrier system was selected since its high ethanol content is known to improve transdermal permeation by fluidizing the intercellular lipids of skin layer and also by imparting flexibility as well as stability to liposomal membrane through its interdigitation effect [6]. Further, Zhang, et al., 2014 reported a great reduction in ethanol mediated cytotoxicity when incorporated in to lipid vesicles [7]. Secondly, microneedles were utilized as a minimally invasive and relatively safe tool to create microchannels within the skin in a painless, precisely controlled and convenient manner [8] which further seemed to support the permeation of ethosomal nanocarriers. In addition, for ease of handling and providing an occlusive condition which is known to keep the microchannels open for prolonged duration [9], ethosomal dispersion was incorporated in carbopol hydrogel.

Development of the ethosomal system with optimal properties always remains challenging to formulation scientists as a number of process and formulation variables potentially influence its quality characteristics [10]. Conventional method of optimization, where single factor is varied at a time while keeping all other factors fixed at a particular level, is tedious and inefficient in determining the interaction among variables. Response surface methods of experimental design have emerged as a powerful statistical and mathematical tool for designing experiments, generating models, analyzing the influence of several factors together and deciding the optimum conditions to produce the best combination of several desirable responses [11]. In the present work, central composite design capable of providing information on direct effects, pairwise interaction effects and curvilinear variable effects were applied to derive the functional relationship between key formulation variables and selected responses.

Hence, the current work includes the formulation and optimization of Raloxifene HCl loaded ethosomal hydrogel and investigation of its transdermal drug delivery potential through both normal healthy as well as microneedle treated excised pig ear skin.

2. MATERIALS & METHODS

2.1. Materials

Raloxifene HCl and hydrogenated soya phosphatidylcholine (HSPC) were generous gifts from Aarti Drugs Ltd., India and Lipoid GmbH, Germany, respectively. DermaStamp® was purchased from Coherent medical systems, India. Absolute ethyl alcohol and dialysis membrane-70 (MWCO, 12kD) were purchased from Changshu Yangyuan Chemical Co. Ltd., China and HiMedia Pvt. Ltd., India, respectively. All other reagents used were of analytical grade.

2.2. Preparation of RH Loaded Ethosomal Dispersion

RH loaded ethosomes of HSPC were prepared by the Cold method [12]. Briefly, 1.5 mg of RH and varying quantities of HSPC (Tables **1** and **2**) were added into covered glass bottles containing different quantities of ethanol (Tables **1** and **2**) at room temperature. The contents were dissolved by vigorous stirring while intermittently adding the propylene glycol (10% v/v of ethanol). The temperature of the mixture was then raised to 55°C (Tg of HSPC) in a water bath. The distilled water, previously maintained at 55°C, was slowly added to the mixture with gentle stirring to make up the volume to 6 ml. The stirring was continued for another 30 minutes to obtain ethosomal dispersion.

2.3. Formulation Optimization Using Central Composite Design

Optimization of various process and formulation variables was done by studying the effect of changing levels of these variables on the desirable characteristics of the ethosomal carriers. The vesicular size (Y_1; nm) and percent entrapment efficiency (Y_2; %) of ethosomes were selected as the two response variables. Preliminary experiments were performed to identify the key variables significantly affecting the vesicular size and percent entrapment efficiency of the formulation while establishing the optimum level of other process variables. Lipid concentration (X_1; mM) and ethanol concentration (X_2; % v/v), the two identified key factors, were optimized using central composite design (CCD). Other process variables such as stirring time, stirring speed, processing temperature, final batch volume, etc. were kept at their optimum level as established during preliminary trials (data not shown).

Table 1. Independent factors and their coded levels for optimization of RH loaded ethosomal dispersions.

Factors	Levels				
	-1.41 (-α)	**-1**	**0**	**+1**	**+1.41 (+α)**
Lipid concentration; X_1 (mM)	2.38	3	4.5	6	6.62
Ethanol concentration; X_2 (% v/v)	15.86	20	30	40	44.14

Table 2. Randomized central composite design matrix with experimentally determined values of response variables.

Run order	Formulation code	Factors		Response Variables	
		X_1	X_2	VS[#] (nm)	%EE[#] (%)
3	F_{01}	-1	-1	561 ± 13	43.4 ± 2.75
1	F_{02}	1	-1	540 ± 21	73.2 ± 3.82
8	F_{03}	-1	1	567 ± 28	42.7 ± 1.93
4	F_{04}	1	1	395 ± 11	74.3 ± 4.17
6	F_{05}	-1.41	0	601 ± 33	39.8 ± 2.45
13	F_{06}	1.41	0	540 ± 16	73.3 ± 3.46
9	F_{07}	0	-1.41	492 ± 22	60.4 ± 2.91
2	F_{08}	0	1.41	485 ± 13	61.5 ± 3.29
10	F_{09}	0	0	501 ± 27	60.4 ± 4.25
5	F_{10}	0	0	521 ± 30	64.8 ± 2.76
12	F_{11}	0	0	555 ± 15	60.8 ± 3.05
7	F_{12}	0	0	517 ± 24	60.4 ± 1.79
11	F_{13}	0	0	520 ± 12	61.9 ± 2.55

[#]Values represented as mean±SD (n=3); VS, vesicular size; %EE, percent entrapment efficiency.

2.3.1. Response Variables

Vesicular size: Ethosomal samples were suitably diluted with pre-filtered distilled water (through 0.22μm membrane filter). The vesicular size (VS, average diameter based on volume distribution) and polydispersity index (PDI) were measured using a Zeta size particle analyzer (Microtrac Inc., USA) working on the principle of dynamic light scattering. The instrument divides measuring range into fixed "channel" or particle sizes and generates a table in Microtrac FLEX software where volume percent of smaller sized particles at each channel is given as % passing while the difference in % passing at any particular channel and the adjacent channel (of smaller particle size) is represented as % channel (volume percent-in-channel) [13].

Percent Entrapment Efficiency: The unentrapped drug fraction was removed from ethosomal dispersion using the dialysis method. Briefly, 2 ml of formulation was filled into a dialysis bag (MWCO, 12 KD) in a leakproof manner and dialyzed for 3 hours in a closed container having 50 ml of 30% hydroethanolic solution as a dialysis medium. Later, samples from dialysis bag and dialysis medium were withdrawn for estimation of entrapped and unentrapped drug fraction, respectively. These samples were suitably diluted with methanol and the absorbances were recorded at 287nm using UV-1700 spectrophotometer (Shimadzu, Japan). Mass balance was ascertained and percent entrapment efficiency (% EE) was calculated using equation **1**:

$$\%\,EE = \left(\frac{\text{Drug entrapped within ethosomal carrier}}{\text{Total drug taken}} \right) \times 100 \qquad (1)$$

2.3.2. The Central Composite Design

Different levels of the two independent variables, X_1 and X_2 along with their coded values are presented in Table **1**. Design-Expert v7.0.1 software (Stat-Ease Inc., Minneapolis, MN) was used for experiment design, statistical analysis of data and optimization of RH loaded ethosomes. Briefly, a total of 13 batches of ethosomal dispersions were prepared based on the randomized design matrix (Table **2**) and evaluated for vesicular size and percent entrapment efficiency. Multiple linear regression analysis (MLRA) was applied to generate second order polynomial equations **2** and **3** including interaction and quadratic terms for both the response variables

$$Y_1 = \beta_0 + \beta_1 X_1 + \beta_2 X_2 + \beta_{12} X_1 X_2 + \beta_1^2 X_1^2 + \beta_2^2 X_2^2 \qquad (2)$$

$$Y_2 = \beta_0 + \beta_1 X_1 + \beta_2 X_2 + \beta_{12} X_1 X_2 + \beta_1^2 X_1^2 + \beta_2^2 X_2^2 \qquad (3)$$

Where, β_0 is the intercept while β_1, β_2; β_1^2, β_2^2; and β_{12}, are regression coefficient of simple linear; quadratic and interaction effects, respectively. Analysis of variance (ANOVA) followed by F-test was used to ascertain the significance of the model as well as model terms. Two dimensional contour plots and three dimensional response surface plots demonstrating the relationship between independent and response variables were generated. Simplified reduced model (RM) equations including only the significant model terms were generated and ANOVA followed by F-test was applied to justify the exclusion of insignificant model terms [14] $F_{calculated}$ was obtained for the purpose using the equation **4**:

$$F_{calculated} = \frac{(SS_{E2} - SS_{E1})/N}{MS_{E1}} \qquad (4)$$

Where, SS = sum of square, MS = mean sum of square, E1 = residual of full model; E2 = residual of reduced model, N = no. of parameters omitted.

Optimization solution based on preselected desirability criteria (minimum vesicular size and maximum percent entrapment efficiency) was obtained from the software. The check point analysis was performed to ensure the utility of the model equations by randomly selecting the three different combinations of X_1 and X_2 within the design space for preparation of RH loaded ethosomes and the predicted and experimental value of Y_1 and Y_2 for these batches were compared using t-test. Normalized error (NE) was also calculated using following equation **5** to further confirm the quantitative relationship between variables.

$$NE = \sqrt{\sum \left\{ \frac{\left(Y_{Pre} - Y_{Exp}\right)}{Y_{Exp}} \right\}^2} \quad (5)$$

2.4. Hydrogel Preparation

Hydrogels of optimized ethosomal dispersion was prepared by adding them to overnight soaked 2 % w/v carbopol 940 followed by the addition of 10 % v/v propylene glycol and stirred gently for uniform mixing. Finally, the pH was adjusted to 6.8 using 0.07 % v/v triethanolamine to effect hydrogel formation. Plain RH hydrogel was also prepared using the same procedure by replacing optimized ethosomal dispersion for hydroethanolic solution (15% v/v) of RH.

2.5. *In vitro* Characterization of Optimized Ethosomal Dispersion and its Hydrogel

2.5.1. Zeta Potential

Samples from optimized ethosomal dispersion were suitably diluted with pre-filtered distilled water (through 0.22µm membrane filter) and analyzed for the zeta potential using Zetasizer (Zetatrac Inc., Particle Metrix GmbH).

2.5.2. In vitro Drug Release Study

Drug release from plain RH solution (RH dissolved in 15% v/v hydroethanolic solution), plain RH hydrogel and ethosomal hydrogel was studied *in vitro* through the dialysis membrane (MWCO, 12 kD; Himedia Pvt. Ltd, Mumbai). The activated membrane was mounted between the donor and receptor chambers of a modified Franz-type diffusion cell (effective permeation area, 1.13 cm^2) containing 8 ml of 10 % v/v methanol solution in phosphate buffer (pH, 7.4) as a diffusion medium. The assembly was kept under mild stirring for equilibration. After half an hour, formulation containing 0.5 mg RH was applied over the membrane and sampling was done at predetermined time points over 24 hours. 2 ml of sample was withdrawn at each time point and replaced with an equal volume of fresh diffusion medium. The drug present in withdrawn samples was quantified using UV-1700 spectrophotometer (Shimadzu, Japan) at 287 nm. Drug release data were fitted in various mathematical models viz., Zero order, First order, Higuchi and Hixson-Crowell models as an empirical approach to determine the kinetics of drug release and their correlation coefficient (R^2) values were compared. Korsmeyer-Peppas model was further applied to confirm the release mechanism.

2.6. *Ex vivo* Characterization

2.6.1. Microneedle Mediated Skin Microporation

Microneedle stamp (Dermastamp®) containing 6 titanium needles of 2 mm length and about 200µm base diameter was used for skin microporation. Available online literatures suggested the safety of microneedles with 2.0mm needle length if used only once every five weeks on the same skin area with a proper knowledge to judge which part of the skin is thick enough to safely use them [15]. Full thickness pig ear skin was procured from Polar Genetics India Pvt. Ltd., Punjab. After careful removal of adherent fats, the skin was bathed with 10% glycerol solution in phosphate buffer saline (pH, 7.4), wrapped in aluminum foils and preserved in a deep refrigerator at -70°C until used. Prior to use, the skin was thawed at room temperature and placed on a tissue paper stack to simulate *in situ* mechanical support. Microneedles stamp was fixed on the upper plunger of CT3 texture analyzer (Brookfield) and was programmed to pierce the skin with a force of 20 N, remain in place for 5 seconds and retract. A pre-marked circular area of 1cm diameter on the skin was microporated by repeating the procedure 10 times while changing the piercing point on each occasion.

2.6.2. Drug Permeation and Deposition Study

Permeation of RH from optimized ethosomal hydrogel was studied across intact as well as microporated full thickness pig ear skin and compared with its permeation from plain solution as well as plain hydrogel. The skin was fastened between the donor and receptor chambers of a modified Franz-type diffusion cell (effective permeation area, 1.13 cm^2) with *stratum corneum* facing the donor side. Receptor chamber was filled with 8 ml of 10 % v/v methanol solution in phosphate buffer (pH, 7.4) as diffusion media. The whole assembly was kept under controlled temperature and stirring conditions. After 30 minutes of skin equilibration, the test formulations containing 0.5 mg RH were applied to the skin. Two ml of samples were withdrawn from the receptor compartment at predetermined time intervals over 24 hr and each time an equal volume of fresh diffusion media was replaced. The drug present in withdrawn samples was quantified using UV spectrophotometry at 287 nm absorption maximum. Cumulative amounts of drug permeated per unit area were plotted against time and the slope of its terminal linear portion was used to calculate transdermal steady-state flux (J_{SS}, µg/cm^2/h). In order to compare the permeability of drug from different formulations, permeation enhancement ratio (PER) was calculated from steady-state flux [16] obtained for ethosomal (J_{SS}^{test}) and plain drug hydrogel ($J_{SS}^{control}$) using equation **6**.

$$PER = \frac{J_{SS}^{test}}{J_{SS}^{control}} \quad (6)$$

Percent drug retained on the skin and percent drug deposited within the skin was estimated at the end of permeation

experiments (24 hours). To collect the drug retained on the skin surface, the surface was washed three times with diffusion medium (15 ml x 3). These washings were combined and the drug present in it was quantified spectrophotometrically as mentioned above. The washed skin was minced using a chopper and then collected in 20 ml methanol to extract out the drug deposited within it. The mix was subjected to bath sonication for 3 cycles of 5 minutes each followed by homogenization for 5 minutes under cold condition. The extracted out the drug was then separated by centrifugation at 4000 rpm for 10 min. The supernatant was collected and the drug present in it was analyzed spectrophotometrically using above method.

2.6.3. Histopathological Studies

Ethosomal hydrogel containing 0.5 mg RH was applied on the shaved abdominal skin of three male Wistar rats. After six hours, rats were euthanized; their abdominal skins were separated out and immediately preserved in 10% neutral buffered formalin as fixative. Skin was processed through gradually increasing concentrations of ethanol as dehydrating agent followed by xylene as clearing agent and finally embedded in paraffin. The 5-µm thick sections of skin were cut from these paraffin blocks using microtome and placed on glass slides. De-waxing was done by gently warming the slide and washing the molten wax with xylene. Sections were then rehydrated using gradually decreasing concentrations of ethanol followed by water and stained with hematoxylin and eosin to demonstrate gross histopathology and collagen deposition. After staining, sections were again dehydrated and cleared using the same method as described above and mounted using commercial glycerol's mounting fluid. Negative control and positive control slides were also prepared from the abdominal skin of Wistar rats treated with phosphate buffer solution pH 7.4 and isopropyl alcohol (IPA), respectively. The slides were analyzed at 10-fold magnification using optical microscope (Magnus MLX).

2.7. Stability Study

The short term stability study was conducted in accordance with ICH guidelines for a period of twelve weeks. Eighteen out of thirty six hermetically sealed vials, each containing 2ml of optimized ethosomal dispersion, were stored at 4 ± 2°C with ambient relative humidity while another eighteen were stored at 30 ± 2°C with 60 ± 5% relative humidity. Likewise, two groups, each of eighteen hermetically sealed tubes filled with optimized ethosomal hydrogel were stored under different environmental conditions as mentioned above. Three vials and three tubes from each environment were withdrawn fortnightly and evaluated for vesicular size and percent drug retained, respectively, to demonstrate the stability of batches at selected environment conditions.

2.8. Statistical Analysis

Excluding the formulation optimization, mean and standard deviation for every experiment, conduced in triplicate, was obtained using Microsoft Excel (version 2007). Statistical analysis was performed using GraphPad InStat software (version 5.00) using one way ANOVA followed by Tukey's multiple comparison test with $P < 0.05$ as a minimal level of significance.

3. RESULTS & DISCUSSION

Ethosomes have been successfully developed for transdermal delivery of a number of drugs like Tamoxifene, Ropinirole etc [17]. In present investigation, a total of 13 batches; representing 4 factorial (batch F_{01}-F_{04}), 4 axial (batch F_{05}-F_{08}) and 5 center points (batch F_{09}-F_{13}); were prepared and evaluated for the two most desirable characteristics viz., vesicular size and percent entrapment efficiency (data presented in Table **2**). Software based analysis of variance (ANOVA) for response surface quadratic model (Table **3**) revealed the significance of this model [p-value; 0.0154 (VS), < 0.0001 (PDE)] with an insignificant lack of fit [p-value; 0.1370 (VS), < 0.2089 (PDE)] relative to the pure error for both the response variables. The adequacy of developed model was further ensured on the basis of correlation coefficients (R) and determination coefficients (R^2) values (Table **4**). An excellent correlation among independent variables was represented by high correlation coefficients (VS, 0.9054; PDE, 0.9876) while the determination coefficients

Table 3. Regression Coefficients and their P-values for vesicular size and percent entrapment efficiency.

Source	VS		%EE	
	Coefficients	P-value	Coefficients	P-value
Model	-	*0.0154*	-	*< 0.0001*
Intercept	*522.80*	*1.16E-09*	*61.66*	*1.1E-10*
X_1	*-34.78*	*0.009701*	*13.59*	*7.8E-07*
X_2	-18.74	0.099606	0.2382	0.7827
X_1X_2	*-37.50*	*0.031314*	0.4375	0.7208
X_1^2	-20.35	0.096122	*-2. 6456*	*0.0209*
X_2^2	-20.65	0.092195	-0.4456	0.6324
Residual: Lack of fit	-	0.1370	-	0.2089

*Significant terms having P-value < 0.05 were represented in italics.

Table 4. Analysis of variance of full and reduced model for both characteristics of RH loaded ethosomal dispersion.

		df	SS	MS	F-value	p-value	R	R^2	Adj. R^2
Vesicular Size									
Regression	FM	5	24837.08	4967.415	6.366	0.0154	0.9054	0.8197	0.6910
	RM	2	15304.07	7652.034	5.103	0.0297	0.7107	0.5051	0.4061
Residual (Error)	FM	7	5462.00	780.286		0.1370			
	RM	10	14995.01	1499.501		0.0561			
$F_{calculated} = 4.07$; $F_{tabulated} = 4.35$									
Percent drug entrapment									
Regression	FM	5	1527.654	305.531	55.285	<0.0001	0.9876	0.9753	0.9577
	RM	2	1525.053	762.527	184.694	<0.0001	0.9867	0.9736	0.9684
Residual (Error)	FM	7	38.685	5.526		0.2089			
	RM	10	41.286	4.129		0.4104			
$F_{calculated} = 0.16$; $F_{tabulated} = 4.35$									

(VS, 0.8197; PDE, 0.9753) indicated that 82% of the total variations for VS and 97% of the total variations for PDE were explained by the model. A multiple linear regression analysis by the software provided the following second order polynomial equations **7** and **8** for VS and PDE, respectively, including all the model terms (full model, FM).

$$VS = 522.80 - 34.78\ X_1 - 18.74\ X_2 - 37.50\ X_1X_2 + 20.35\ X^2_1 - 20.65\ X^2_2 \quad (7)$$

$$PDE = 61.66 + 13.59\ X_1 + 0.24\ X_2 + 0.44\ X_1X_2 - 2.65\ X^2_1 - 0.45\ X^2_2 \quad (8)$$

The significance of each model term was ascertained using p-value which was obtained from the software (Table **3**). For vesicular size (Y_1), the quadratic main effect of lipid concentration (X_1) and interactive effect of lipid and ethanol concentration (X_1X_2) possessed a p-value less than 0.05 indicating their significant influence over Y_1. Though, quadratic main effect of ethanol concentration (X_2) and the second order main effect of lipid concentration (X^2_1) and ethanol concentration (X^2_2) were expected to alter Y_1 insignificantly (p-value greater than 0.05). Similarly for percent drug entrapment (Y_2), X_1 and X^2_1 were considered significant owing to their p-value below 0.05 while X_2, (X^2_2) and X_1X_2 were considered insignificant owing to their p-value above 0.05. As evident in equation 6 and 7, significant model terms had higher coefficient values and non-significant model terms had lower coefficient values. This further reflected the extent to which each model term contributes to that particular response. To further simplify the equation, the non-significant model terms were excluded and following new equations **9** and **10** were generated (reduced model, RM) using the software

$$VS = 522.62 - 34.78\ X_1\ \ 37.50\ X_1X_2 \quad (9)$$

$$PDE = 61.35 + 13.59\ X_1 - 2.59\ X^2_1 \quad (10)$$

The ANOVA and F-test for full and reduced model resulted in $F_{calculated} < F_{tabulated}$ for both VS and PDE (Table **4**) representing an insignificant difference in full and reduced model. This confirmed the predictability of VS and PDE even with a reduced model as omitted terms were seemed to contribute insignificantly. However, this omission also reduced the R^2 value owing to the fact that as the number of factors increased, the R^2 value increases and *vice versa*.

In order to explain the relationship between independent and dependent variables, the values were diagrammatically represented as two-dimensional contour plots (Fig. **1Ax** and **Ay**). The contour plot for vesicular size showed a decrease in size as the lipid concentration (X_1) was increased. This influence of X_1 was found to increase with increasing levels of ethanol concentration (X_2). At mid X_1 level, the X_2 seemed to have negligible influence over VS. However, the increase in X_2 at low X_1 level increased the VS while at the high X_1 level it behaved oppositely and a reduction in VS was observed. Overall, the highest VS was obtained for low X_1 and high X_2 whereas the lowest VS was obtained for high X_1 and high X_2. The contour plot for percent drug entrapment revealed a negligible influence of ethanol concentration on PDE at all levels of X_1. Though, a linear increase in PDE is apparent with increasing levels of X_1 confirming the significant influence of lipid concentration on PDE. Consequently, to obtain Minimum VS and maximum PDE, lipid as well as ethanol concentrations must be at their high levels.

The three dimensional response surface plots (Fig. **1Bx** and **By**) were further utilized to demonstrate main and interaction effects of the independent variables. A reduction in vesicular size and increase in percent drug entrapment was evident as the amount of bilayer forming lipid was increased. The reduction in size could be a result of an improved packing of drug and lipid within the bilayer while the increase in

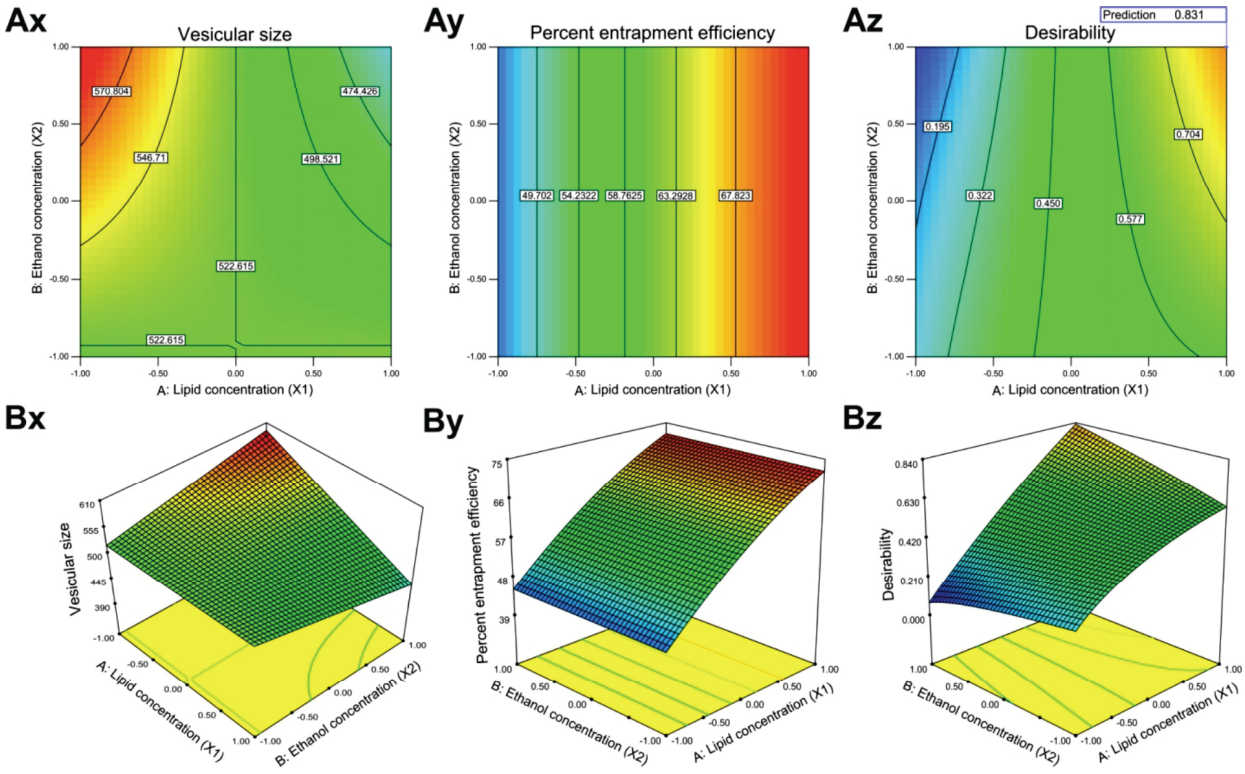

Fig. (1). Design-Expert® software-generated 2-d contour (**A**) and 3-d response surface (**B**) plots showing influence of lipid and ethanol concentration on vesicular size (x), percent entrapment efficiency (y) and desirability (z) for optimization of ethosomal dispersion.

entrapment might owe to a more bilayer space available for drug incorporation [12]. The size reduction with increasing lipid concentration was more significant at higher ethanol concentrations which might be due to the fluidity imparted to lipid bilayer by ethanol [18]. An insignificant change in vesicular size on increasing the ethanol concentration at lower lipid concentration reflected the importance of bilayer packing over its fluidity for vesicular size reduction. The effect of ethanol concentration on percent drug entrapment was found insignificant. Ethanol increases the solubility of the drug in dispersion medium which could have both positive as well as negative effect on entrapment efficiency of ethosomes. In one hand, the increase in drug solubility increases the amount of drug in encapsulated aqueous core and thus should have increased the entrapment. However, this increment could have been nullified due to simultaneous increase in partitioning of the drug from lipid bilayer, which is rendered leaky by excessively high ethanol levels [12], to external dispersion medium.

To obtain the optimum levels of independent variables, desirability criteria was set to minimize the vesicular size and maximize the percent entrapment efficiency while keeping the quantities of independent variables in range (Table **5**). The numerical optimization provided by the design expert software indicated that the formulation containing 6 mM concentration of lipid and 40 % v/v concentration of ethanol might possess minimum possible vesicular size (450.332nm) without compromising the percent entrapment efficiency (72.35%). A desirability of 0.831 (Fig. **1Az** and **Bz**) indicated the suitability of the model applied. Further, three check point batches were prepared and their predicted vesicular size and percent entrapment efficiency values were compared with experimentally observed values. Analysis of result using student's t test revealed that there was no statistically significant difference ($p < 0.05$) between experimentally obtained values and predicted values (Table **6**). A lower value of normalized error (0.131423 for vesicular size and 0.06431 for percent entrapment efficiency) also indicated that measured responses were accurately predicted by reduced model. The optimized batch was then incorporated in the loose network of carbopol hydrogel matrix which does not seem to affect the vesicular size of ethosomes. Moreover, literatures involving incorporation of nanocarriers in carbopol hydrogel does not report such issue [19].

3.1. Characterization of Optimized Formulation

3.1.1. Zeta Potential

Zeta potential was measured to demonstrate the tendency of dispersed nanocarriers towards aggregation. The zeta potential of optimized batch was found 35.20 mV which appeared strong enough to hinder agglomeration and to provide stability to the formulation [20].

3.1.2. In vitro Drug Release Study

As illustrated in Fig. (**2**), percent drug released in 24 hours from plain drug solution, plain drug hydrogel and ethosomal hydrogel were 35.3%, 32.0% and 32.4 %, respectively. These difference were found insignificant ($p < 0.05$) suggesting that incorporation of drug or formulation in 2%

Table 5. Numerical optimization by Design-Expert® software.

	X_1	X_2	VS	% EE	Desirability
Goal	in range	in range	minimize	maximize	1.000
Solution	6 mM	40 % v/v	450.332 nm	72.35 %	0.831

Table 6. Check point analysis to validate the model reduction.

Batch	X_1 (mM)	X_2 (% v/v)	VS (nm)		PDE (%)	
			Observed	Predicted	Observed	Predicted
CP_1	6	40	403	450.34	74.25	72.35
CP_2	6	20	537	525.34	73.2	72.35
CP_3	3	40	564	594.9	42.7	45.17
T test	$T_{calculated}$		0.334051		0.949952	
	$T_{tabulated}$		4.302653		4.302653	
Normalized error			0.131423		0.06431	

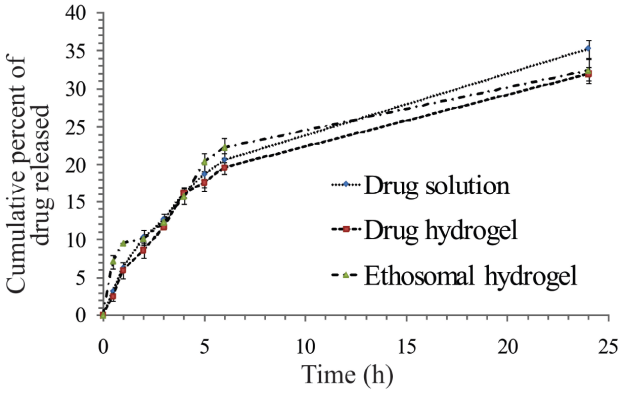

Fig. (2). Graphical representation of cumulative percent of drug released *in vitro* at different time points from its plain solution, plain hydrogel and optimized ethosomal hydrogel.

w/v carbopol hydrogel and ethosomal carriers did not affect the drug release considerably. There might be two possible reasons behind such finding. Firstly, the fluidity imparted to the ethosomal lipid bilayer membrane by high ethanol concentration could have aided in release via rapid equilibration of drug concentration between bilayer and outer dispersion medium. Secondly, with occlusive nature and water holding capacity, carbopol hydrogel could have maintained sufficiently large aqueous channels causing minimal hindrance to the movement of drug molecule as well as ethosomal carrier. The correlation coefficient (R^2) values obtained for various release models are summarized in Table **7**. The highest R^2 values for Higuchi model in all three cases suggested diffusion as a principle mechanism for drug release. The release exponent (n) of Korsmeyer-Peppas model further confirmed that the drug release from ethosomal hydrogel followed fickian diffusion (n = 0.416).

3.2. *Ex vivo* Drug Permeation and Deposition Study

Cumulative amount of drug released per cm^2 of intact as well as microporated full thickness pig ear skin is demonstrated in Fig. (**3A**) and the steady state transdermal flux (J_{SS}) along with permeation enhancement ratio (PER) is given in Table **8**. The flux for Plain RH solution through intact skin was 1.60µg/cm^2/h while the flux for RH loaded plain hydrogel through intact skin was 2.581µg/cm^2/h. The occlusive environment and presence of ethanol in hydrogel preparation might have contributed to this 1.6 fold enhancement via decreasing the phase-transition temperature of the stratum corneum lipid bilayer and thereby inducing phase separation and crystal-phase transition of solid and liquid lipids within the lipid bilayer to reversibly alter their dense molecular arrangement [21]. The flux was significantly ($p < 0.05$) improved for ethosomal hydrogel applied on intact skin (J_{SS}, 4.621µg/cm^2/h; PER, 2.9). This may be attributed to the flexibility and fluidity imparted to the ethosomal lipid bilayer by the high ethanol concentration which renders the vesicle deformable. These deformable vesicles permeate through smaller gaps created by loosened lipid bilayer arrangement to reach the deeper skin layers [21]. A significant enhancement in transdermal flux is further evident in results when ethosomal hydrogel was applied on microporated skin (J_{SS}, 6.194µg/cm^2/h; PER, 3.87). This result is in good agreement with other studies [22] which have shown that microneedles can effectively breach the cornified layer and create aqueous microchannels. These microchannels provide an extra residing space for drug carriers from where lateral diffusion of released drug into the underlying tissues becomes easier. For similar reason, the RH loaded plain hydrogel might have shown an improved flux through microporated skin (3.407 µg/cm^2/h) as compared to its flux though intact skin (Table **8**). An earlier reported nanotransfersomes of Raloxifene HCl also showed a comparable transdermal

Table 7. Correlation coefficients of various *in vitro* drug release models.

Release models	Values	Plain drug solution	Plain drug gel	Ethosomal gel
Zero order	R^2	0.820	0.788	0.751
First order		0.873	0.837	0.801
Higuchi		**0.979**	**0.962**	**0.944**
Hixson-Crowell		0.856	0.821	0.784
Korsmeyer-Peppas	R^2	-	-	0.939
	n value	-	-	0.416
	Release mechanism	-		Fickian diffusion

Table 8. *Ex vivo* transdermal permeation indicating parameters.

Parameters	Plain drug solution through intact skin	Plain hydrogel		Ethosomal hydrogel	
		Intact skin	Microporated skin	Intact skin	Microporated skin
J_{SS} (μg/cm^2/h)	1.600	2.581	3.407	4.621	6.194
PER	-	1.613	2.129	2.888	3.871

J_{SS}, steady state transdermal flux; PER, permeation enhancement ratio.

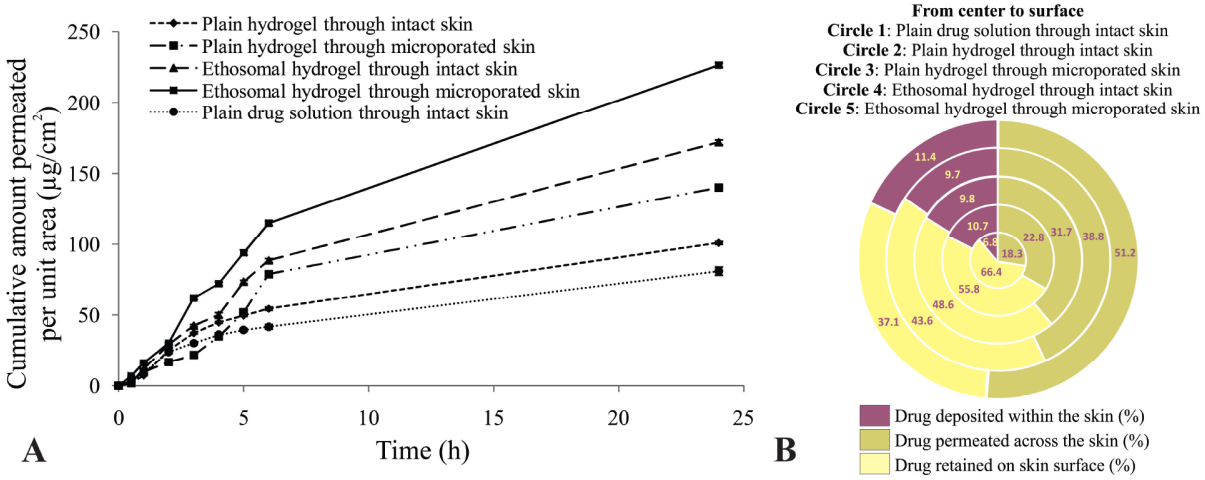

Fig. (3). *Ex vivo* profile of drug permeation across (**A**) and drug deposition within (**B**) full thickness intact as well as microporated pig ear skin from plain as well as optimized ethosomal hydrogel.

flux of 6.5±1.1 μg/cm^2/hour across rat skin [23]. However, present study utilized pig ear skin for penetration experiments that shows greater resemblance and similar permeability to human skin as compared to rat skin which is generally more permeable than human skin [24].

Fig. (**3B**) depicts the drug permeation and deposition pattern from plain and ethosomal hydrogels across intact as well as microporated pig ear skin at 24 hours. When applied on intact pig ear skin, drug retention on surface was significantly reduced while drug permeation through it was significantly increased for ethosomal hydrogel (43.6 and 38.8 %, respectively) as compared to plain hydrogel (55.8 and 22.8 %, respectively) which advocates the permeation enhancement potential of ethanol and also supports the fact that use of more viscous and more hygroscopic propylene glycol enhances drug's affinity towards hydrophilic dermal region and thereby contribute to the enhanced permeation [25]. Similarly, Skin microporation further improved the drug permeation (51.2 %) supporting the aforementioned theory of adapting lateral diffusion pathway by released drug. The percent

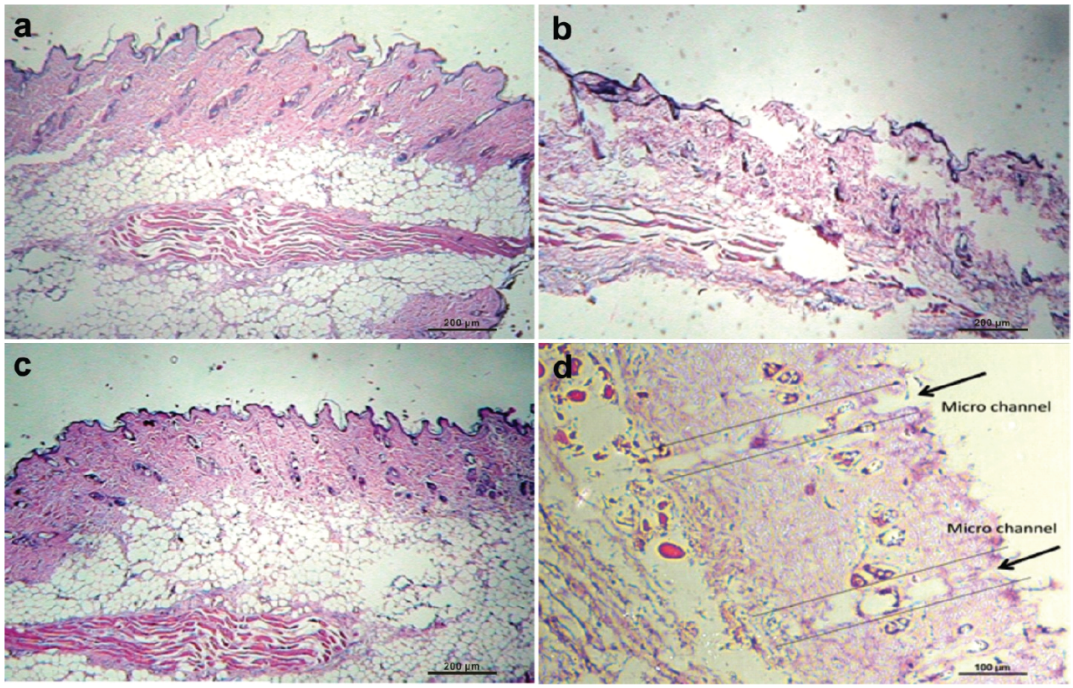

Fig. (4). Photomicrograph showing hematoxylin-eosin stained histopathological sections of intact rat abdominal skin treated with PBS pH 7.4 as negative control (**A**), isopropyl alcohol as positive control (**B**), ethosomal hydrogel (**C**) and microporated rat abdominal skin treated with ethosomal hydrogel (**D**).

Table 9. Stability study data of RH loaded ethosomal dispersion and gel.

Time (weeks)	Vesicular size of ethosomes in dispersion (nm)		Percent drug retained in ethosomal gel (%)	
	4 ± 2°C ambient humidity	30 ± 2°C 60 ± 5% rel. hum.	4 ± 2°C ambient humidity	30 ± 2°C 60 ± 5% rel. hum.
0	395 ± 11.2	395 ± 11.2	100.0 ± 0.00	100.0 ± 0.00
2	395 ± 19.4	401 ± 13.7	99.6 ± 0.04	99.3 ± 0.28
4	397 ± 23.4	409 ± 18.4	99.2 ± 0.18	98.4 ± 0.64
6	400 ± 22.7	416 ± 25.3	98.6 ± 0.35	97.3 ± 0.63
8	404 ± 26.3	422 ± 31.2	98.3 ± 0.27	96.4 ± 0.56
10	410 ± 38.2	429 ± 34.7	98.0 ± 0.19	95.7 ± 0.67
12	414 ± 29.5	438 ± 29.4	97.8 ± 0.23	94.9 ± 0.72

of drug deposited within the skin seems to be same in all three cases Fig. (**3B**). However, the same was found higher for plain hydrogel as compared to ethosomal hydrogel when the percent drug deposited was calculated considering the amount of drug that crossed the stratum corneum as 100%. This also reflects a better permeation profile of ethosomal system.

3.3. Histopathology Study

Being one of the major concerns of transdermal delivery, safety to the skin from developed system was ascertained using histopathology study. HE stained sections of treated rat skin portions were observed under optical microscope (Olympus BX40). As shown in Fig. (**4**), skin sections treated with isopropyl alcohol as a positive control showed considerable damage to the epidermal and sub epidermal regions together with infiltration of inflammatory cells while no such damage or infiltration was evident in skin sections treated with phosphate buffer (pH 7.4) as negative control. Sections of intact skin treated with ethosomal hydrogel did not show any pathological change in the skin anatomy indicating the non-irritant nature of the system. Even with the sections of microporated skin treated with ethosomal hydrogel, an insignificant disruption, damage and edema in the epidermal and sub epidermal regions was evident. These results concur with other reports supporting the non-toxic and non irritant nature of ethosomal systems [26] while less and short lasting irritation by microneedle treatment [27].

3.4. Stability of Optimized Ethosomal Formulation

Effect of two different storage conditions on vesicular size of ethosomes in dispersion and percent drug retained by ethosomal hydrogel are presented in Table **9**. After 12 weeks, at 4 ± 2°C and ambient humidity, an insignificant change in vesicular size (395nm to 414nm) and percent drug retained (100% to 97.8%) was observed. Formulations stored at 30 ± 2°C and 60 ± 5% relative humidity showed a greater increase in vesicular size (395nm to 438nm) as well as a greater decrease in percent drug retained (100% to 94.9%) after 12 weeks as compared to formulations stored under refrigeration conditions. However, the same was found insignificant suggesting the suitability of both the environmental conditions for storage of ethosomal system. Such a good stability at both the storage conditions could be attributed to the use of HSPC having moderately high phase transition temperature (Tm; about 55°C) that might have remained in gel phase with tightly packed lipid chains at selected storage conditions and thus reduced the drug leakage [28]. An insignificant rise in vesicular size may also be attributed to the sufficiently positive zeta potential on vesicles' surface maintaining ample repulsion among vesicles and thus, avoiding their aggregation [20]. In addition, incorporation of the nano-dispersion in carbopol hydrogel might have also retarded their aggregation and thus improved the stability. The use of propylene glycol with ethanol had also been reported to improve the stability of ethosomal vesicles [29].

4. CONCLUSIONS

With an aim to enhance the penetration of Raloxifene HCl through transdermal route, its ethosomal hydrogel were successfully developed and optimized using central composite design. The analysis of variance revealed that reduced quadratic model including significant model terms were adequate to optimize lipid and ethanol concentrations for minimizing the vesicular size and maximizing the percent entrapment efficiency of ethosomes. The check point analysis showed that ethosomal batch having 6mM HSPC and 40 % v/v ethanol was accurately predicted as optimum by the model and was found to possess 403 nm size and 74.25% drug entrapment. As confirmed by *ex vivo* skin permeation studies, the drug carrying potential of developed ethosomal hydrogel (J_{SS} 4.621 J_{SS}, μg/cm^2/h; PER 1.79) was well augmented via microneedle mediated skin microporation (J_{SS} 6.194 J_{SS}, μg/cm^2/h; PER 2.40). Histopathology and stability study also demonstrated the system as safe and stable. However, an extension of research involving the complete characterization of microneedles and in vivo studies could further be needed to decide its clinical utility.

CONFLICT OF INTEREST

The author(s) confirm that this article content has no conflict of interest.

ACKNOWLEDGEMENTS

Authors extend their sincere thanks to Aarti Drugs Ltd., India; Lipoid GmbH, Germany and Polar Genetics, Jalandhar, India for providing gift samples of Raloxifene HCl, hydrogenated soya phosphatidylcholine and pig ears, respectively.

PATIENT CONSENT

Declared none.

REFERENCES

[1] Landa, M. C., [Role of hormone replacement therapy in the prevention and treatment of menopausal osteoporosis]. *An. Sist. Sanit. Navar.* **2003,** *26 Suppl 3*, 99-105.

[2] Beral, V., Breast cancer and hormone-replacement therapy in the Million Women Study. *Lancet* **2003,** *362* (9382), 419-27.

[3] Delmas, P. D.; Genant, H. K.; Crans, G. G.; Stock, J. L.; Wong, M.; Siris, E.; Adachi, J. D., Severity of prevalent vertebral fractures and the risk of subsequent vertebral and nonvertebral fractures: results from the MORE trial. *Bone* **2003,** *33* (4), 522-32.

[4] Vogel, V. G.; Costantino, J. P.; Wickerham, D. L.; Cronin, W. M.; Cecchini, R. S.; Atkins, J. N.; Bevers, T. B.; Fehrenbacher, L.; Pajon, E. R., Jr.; Wade, J. L., 3rd; Robidoux, A.; Margolese, R. G.; James, J.; Lippman, S. M.; Runowicz, C. D.; Ganz, P. A.; Reis, S. E.; McCaskill-Stevens, W.; Ford, L. G.; Jordan, V. C.; Wolmark, N., Effects of tamoxifen vs raloxifene on the risk of developing invasive breast cancer and other disease outcomes: the NSABP Study of Tamoxifen and Raloxifene (STAR) P-2 trial. *JAMA* **2006,** *295* (23), 2727-41.

[5] Gluck, O.; Maricic, M., Skeletal and nonskeletal effects of raloxifene. *Curr. Osteoporos. Rep.* **2003,** *1* (3), 123-8.

[6] Elsayed, M. M. A.; Abdallah, O. Y.; Naggar, V. F.; Khalafallah, N. M., Deformable liposomes and ethosomes: Mechanism of enhanced skin delivery. *Int. J. Pharm.* **2006,** *322* (1–2), 60-66.

[7] Zhang, Y.-T.; Shen, L.-N.; Wu, Z.-H.; Zhao, J.-H.; Feng, N.-P., Comparison of ethosomes and liposomes for skin delivery of psoralen for psoriasis therapy. *Int. J. Pharm.* **2014,** *471* (1–2), 449-452.

[8] (a) Prausnitz, M. R., Microneedles for transdermal drug delivery. *Adv. Drug Deliv. Rev.* **2004,** *56* (5), 581-7; (b) McAllister, D. V.; Wang, P. M.; Davis, S. P.; Park, J. H.; Canatella, P. J.; Allen, M. G.; Prausnitz, M. R., Microfabricated needles for transdermal delivery of macromolecules and nanoparticles: fabrication methods and transport studies. *Proc. Natl. Acad. Sci. U. S. A.* **2003,** *100* (24), 13755-60; (c) Kaushik, S.; Hord, A. H.; Denson, D. D.; McAllister, D. V.; Smitra, S.; Allen, M. G.; Prausnitz, M. R., Lack of pain associated with microfabricated microneedles. *Anesth. Analg.* **2001,** *92* (2), 502-4; (d) Nalluri, B. N.; Sai Sri Anusha, V.; Sri Bramhini, R.; Amulya, J.; Ashraf Sultana, S. K.; Chandra Teja, U.; Das, D. B., In Vitro Skin Permeation Enhancement of Sumatriptan by Microneedle Application. *Curr Drug Deliv* **2015**.

[9] Kalluri, H.; Banga, A. K., Formation and closure of microchannels in skin following microporation. *Pharm. Res.* **2011,** *28* (1), 82-94.

[10] Nayak, A. K.; Pal, D., Development of pH-sensitive tamarind seed polysaccharide-alginate composite beads for controlled diclofenac sodium delivery using response surface methodology. *Int. J. Biol. Macromol.* **2011,** *49* (4), 784-93.

[11] Asadollahzadeh, M.; Tavakoli, H.; Torab-Mostaedi, M.; Hosseini, G.; Hemmati, A., Response surface methodology based on central composite design as a chemometric tool for optimization of dispersive-solidification liquid-liquid microextraction for speciation of inorganic arsenic in environmental water samples. *Talanta* **2014,** *123*, 25-31.

[12] Patel, K. K.; Kumar, P.; Thakkar, H. P., Formulation of niosomal gel for enhanced transdermal lopinavir delivery and its comparative evaluation with ethosomal gel. *AAPS PharmSciTech* **2012,** *13* (4), 1502-10.

[13] Plantz, P. E. Explanation of Data Reported by Microtrac Instruments 2008. http://www.microtrac.com/MTWP/wp-content/uploads/2012/10/Explanation-of-Data-Reported-by-Microtrac-Instruments.pdf.

[14] Kumar, A.; Sawant, K. K., Application of multiple regression analysis in optimization of anastrozole-loaded PLGA nanoparticles. *J. Microencapsulation* **2013,** *31* (2), 105-114.

[15] Vaughter, S. Dermaneedling instructions 2014. http://dermaroller.owndoc.com/dermaroller-instructions.pdf.

[16] (a) Ahad, A.; Aqil, M.; Kohli, K.; Sultana, Y.; Mujeeb, M., Enhanced transdermal delivery of an anti-hypertensive agent via nanoethosomes: statistical optimization, characterization and pharmacokinetic assessment. *Int. J. Pharm.* **2013,** *443* (1-2), 26-38;

(b) Patel, D.; Kumar, P.; Thakkar, H. P., Lopinavir metered-dose transdermal spray through microporated skin: Permeation enhancement to achieve therapeutic needs. *J. Drug Deliv. Sci. Tech*. **2015,** *29*, 173-180.

[17] (a) Mishra, A. D.; Patel, C. N.; Shah, D. R., Formulation and optimization of ethosomes for transdermal delivery of ropinirole hydrochloride. *Curr Drug Deliv* **2013,** *10* (5), 500-16; (b) Sarwa, K. K.; Suresh, P. K.; Debnath, M.; Ahmad, M. Z., Tamoxifen citrate loaded ethosomes for transdermal drug delivery system: preparation and characterization. *Curr Drug Deliv* **2013,** *10* (4), 466-76.

[18] Paolino, D.; Lucania, G.; Mardente, D.; Alhaique, F.; Fresta, M., Ethosomes for skin delivery of ammonium glycyrrhizinate: in vitro percutaneous permeation through human skin and in vivo anti-inflammatory activity on human volunteers. *J. Controlled Release* **2005,** *106* (1-2), 99-110.

[19] Garg, B. J.; Garg, N. K.; Beg, S.; Singh, B.; Katare, O. P., Nanosized ethosomes-based hydrogel formulations of methoxsalen for enhanced topical delivery against vitiligo: formulation optimization, in vitro evaluation and preclinical assessment. *Journal of Drug Targeting* **2015**, 1-14.

[20] Zeta potential: An introduction in 30 minutes. http://www3.nd.edu/~rroeder/ame60647/slides/zeta.pdf (accessed 21 july).

[21] Jain, S.; Tiwary, A. K.; Sapra, B.; Jain, N. K., Formulation and evaluation of ethosomes for transdermal delivery of lamivudine. *AAPS PharmSciTech* **2007,** *8* (4), 249-257.

[22] (a) Qiu, Y.; Gao, Y.; Hu, K.; Li, F., Enhancement of skin permeation of docetaxel: A novel approach combining microneedle and elastic liposomes. *J. Controlled Release* **2008,** *129* (2), 144-150; (b) Gomaa, Y. A.; El-Khordagui, L. K.; Garland, M. J.; Donnelly, R. F.; McInnes, F.; Meidan, V. M., Effect of microneedle treatment on the skin permeation of a nanoencapsulated dye. *J Pharm. Pharmacol.* **2012,** *64* (11), 1592-602.

[23] Mahmood, S.; Taher, M.; Mandal, U. K., Experimental design and optimization of raloxifene hydrochloride loaded nanotransfersomes for transdermal application. *Int J Nanomedicine* **2014,** *9*, 4331-46.

[24] Jung, E. C.; Maibach, H. I., Animal Models for Percutaneous Absorption. In *Topical Drug Bioavailability, Bioequivalence, and Penetration*, Second ed.; Shah, V.; Maibach, H. I.; Jenner, J., Eds. Springer: New York, 2014; pp 21-40.

[25] Elsayed, M. M.; Abdallah, O. Y.; Naggar, V. F.; Khalafallah, N. M., PG-liposomes: novel lipid vesicles for skin delivery of drugs. *J. Pharm. Pharmacol.* **2007,** *59* (10), 1447-50.

[26] Touitou, E.; Dayan, N.; Bergelson, L.; Godin, B.; Eliaz, M., Ethosomes - novel vesicular carriers for enhanced delivery: characterization and skin penetration properties. *J. Controlled Release* **2000,** *65* (3), 403-18.

[27] Bal, S. M.; Caussin, J.; Pavel, S.; Bouwstra, J. A., In vivo assessment of safety of microneedle arrays in human skin. *Eur. J. Pharm. Sci.* **2008,** *35* (3), 193-202.

[28] Chen, J.; Cheng, D.; Li, J.; Wang, Y.; Guo, J. X.; Chen, Z. P.; Cai, B. C.; Yang, T., Influence of lipid composition on the phase transition temperature of liposomes composed of both DPPC and HSPC. *Drug Dev. Ind. Pharm.* **2013,** *39* (2), 197-204.

[29] Manconi, M.; Mura, S.; Sinico, C.; Fadda, A. M.; Vila, A. O.; Molina, F., Development and characterization of liposomes containing glycols as carriers for diclofenac. *Colloids Surf., A* **2009,** *342* (1–3), 53-58.

AAPS PharmSciTech (© 2012)
DOI: 10.1208/s12249-012-9871-7

Research Article

Formulation of Niosomal Gel for Enhanced Transdermal Lopinavir Delivery and Its Comparative Evaluation with Ethosomal Gel

Ketul K. Patel,[1] Praveen Kumar,[1] and Hetal P. Thakkar[1,2]

Received 12 July 2012; accepted 3 October 2012

Abstract. The aim was to develop niosomal gel as a transdermal nanocarrier for improved systemic availability of lopinavir. Niosomes were prepared using thin-film hydration method and optimized for molar quantities of Span 40 and cholesterol to impart desirable characteristics. Comparative evaluation with ethosomes was performed using *ex vivo* skin permeation, fluorescence microscopy, and histopathology studies. Clinical utility via transdermal route was acknowledged using *in vivo* bioavailability study in male Wistar rats. The niosomal formulation containing lopinavir, Span 40, and cholesterol in a molar ratio of 1:0.9:0.6 possessed optimally high percentage of drug entrapment with minimum mean vesicular diameter. *Ex vivo* skin permeation studies of lopinavir as well as fluorescent probe coumarin revealed a better deposition of ethosomal carriers but a better release with niosomal carriers. Histopathological studies indicated the better safety profile of niosomes over ethosomes. *In vivo* bioavailability study in male Wistar rats showed a significantly higher extent of absorption ($AUC_{0\rightarrow\infty}$, 72.87 h×μg/ml) of lopinavir via transdermally applied niosomal gel as compared with its oral suspension. Taken together, these findings suggested that niosomal gel holds a great potential of being utilized as novel, nanosized drug delivery vehicle for transdermal lopinavir delivery.

KEY WORDS: ethosomes; lopinavir; niosomes; transdermal.

INTRODUCTION

Acquired immune deficiency syndrome (AIDS), the advanced stage of the disease caused by human immunodeficiency virus (HIV) infection, is one of the most serious infectious diseases that challenges public health globally (1). Interventions such as AIDS counseling, educational tools, and antiretroviral drug therapy have contributed to transforming HIV infection from a fatal to a manageable chronic infectious disease. However, as per the global report by UNAIDS in 2010 (2), the number of people receiving therapy has grown 13-fold since 2004, including more than five million people in low- and middle-income countries. Hence, despite available preventive measures, much remains to be accomplished as the number of newly reported HIV infections still remains unacceptably high.

Lopinavir, (2S)-*N*-[(2S,4S,5S)-5-[2-(2,6-dimethylphenoxy)-acetamido]-4-hydroxy-1,6-diphenylhexan-2-yl]-3-methyl-2-(2-oxo-1,3-diazinan-1-yl)-butanamide, a specific reversible inhibitors of the HIV protease, exerts its effect against HIV infection by blocking the ability of the protease to cleave the Gag-Pol polyprotein, resulting in the production of immature, noninfectious viral particles. However, the systemic availability of lopinavir via oral route is severely limited (3) by its sensitivity towards cytochrome P450 3A4, susceptibility for P-glycoprotein efflux transporters, poor aqueous solubility (~0.01 mg/ml), moderately high molecular weight (~628 Da), and high log P value (~4.56). Though the marketed tablet and capsule formulations of lopinavir are generally combined with Ritonavir, a potent inhibitor of cytochrome P450 3A4, to minimize presystemic metabolism of lopinavir (4), other challenges contributing to poor oral absorption remain unanswered. Hence, to overcome all the limitations associated with oral administration of lopinavir and to promote single drug administration, utilization of vesicular nanocarriers through transdermal route could prove to be effective, as the approach combines the inherent advantages of transdermal route and the drug carrying potential of vesicular nanocarriers across the tough and otherwise impervious skin barrier layer, i.e., stratum corneum (SC).

Among several nanovesicular carriers, niosome is selected here as a carrier of choice owing to its dominance over conventional liposomes with respect to stability and cost-effectiveness. Niosome contains several concentric bilayer membrane mainly composed of nonionic surfactants and cholesterol enclosing aqueous phase in the core. Niosomes are known to improve the solubility, bioavailability, and stability of some poorly soluble drugs (5–8) along with an ability to provide sustained release for prolonged drug action (9). Surfactants contribute to the overall penetration enhancement of compounds primarily by adsorption at interfaces, by interacting with biological membranes and by alteration of the barrier function of the SC, as a

[1] Centre for Research in Pharmaceutical Sciences, The M.S. University of Baroda, Shri G.H. Patel Pharmacy Building, Vadodara, 390002, India.
[2] To whom correspondence should be addressed. (e-mail: hetal_thakkar11@yahoo.com)

aaps
Published online: 27 October 2012

Table I. Composition and Characterization of Lopinavir-Loaded Niosomal Dispersions

S. No.	Formulation code	Composition (molar quantities)			Vesicular size[a] (nm)	PDI[a]	% entrapment efficiency[a]
		Lopinavir	Span 40	Cholesterol			
1	F1	1	0.5	–	354.94±9.16	0.228±0.012	45.3±1.87
2	F2	1	1.0	–	276.38±8.22	0.194±0.014	52.9±3.39
3	*F3*	*1*	*1.5*	–	*196.45±6.23*	*0.165±0.011*	*58.9±1.98*
4	F4	1	2.0	–	203.52±3.97	0.216±0.021	57.4±2.76
5	F3a	1	1.3	0.2	169.34±1.24	0.212±0.022	62.5±1.84
6	F3b	1	1.1	0.4	132.86±2.01	0.189±0.014	68.1±0.37
7	*F3c*	*1*	*0.9*	*0.6*	*105.22±1.96*	*0.127*±0.011	*75.5±0.50*
8	F3d	1	0.7	0.8	114.65±2.21	0.133±0.009	74.5±0.86

PDI polydispersity index
[a] Values represented as mean±SD (n=3)

result of reversible lipid modification (10). Ethosomes, soft, malleable lipid vesicles with high ethanol content tailored for enhanced transdermal delivery of active agents (11), are used for comparative study wherever required.

So, the aim of the present work was to develop lopinavir-loaded niosomal gel and characterize it for its usefulness as a transdermal nanocarrier in delivering therapeutically sufficient quantity of lopinavir to combat against AIDS. The work encompasses its comparative evaluation with lopinavir-loaded ethosomes for drug-carrying potential through full-thickness rat's abdominal skin *ex vivo* and the bioavailability assessment of lopinavir via both oral suspension (OS) as well as transdermal F3c gel *in vivo*.

MATERIALS AND METHODS

Materials

Lopinavir was received as a gift sample from Aurobindo Pharma Ltd. Phospholipid (Phospholipon 90 H) was a gift sample from Lipoid, GmbH, UK. Span 40, cholesterol, carbopol, coumarin, chloroform, and methanol were purchased from S. D. Fine Chemicals, India. Nuclepore polycarbonate membrane 0.2 μm 25 mm was purchased from Whattman, USA. Water (distilled) prepared in laboratory by distillation. All the chemicals and reagents used were of analytical grade.

Preparation of Lopinavir-Loaded Niosomes

Different niosomal formulations of lopinavir were prepared by changing the proportions of drug surfactant and surfactant cholesterol (Table I) using *thin-film hydration* technique as described by Agarwal *et al*. with slight modification (12). Briefly, the Span 40, cholesterol, and lopinavir were dissolved in a mixture of chloroform and methanol (ratio of 7:3, *v*/*v*) in a 250-ml round bottom flask. The solvent was evaporated in the rotary flash evaporator until thin, dry, and uniform film is formed. The thin dry lipid film thus formed was hydrated using phosphate-buffered saline (pH 7.4) at a temperature slightly above the Tg of Span 40 (49±1°C). The formed niosomal dispersion was first sonicated in an ice bath using probe sonicator (four cycles of 30 s each) to convert multilamellar vesicles into desired size unilamellar vesicles and then subjected to centrifugation at 4,000 rpm and 4°C for 15 min using laboratory centrifuge (Remi, India) to effect sedimentation of unentrapped drug as pellet at the bottom of the centrifugation tube (13). Niosomal dispersion (supernatant) was then decanted and characterized for vesicle size and percentage of drug entrapment (PDE) while the drug pellet (sediment) was used to measure unentrapped drug in order to ascertain mass balance. The formulation process parameters were optimized to achieve maximum possible drug entrapment with desirable size range (14).

Table II. Composition and Characterization of Lopinavir-Loaded Ethosomal Dispersions

S. No.	Formulation code	Composition (% *w*/*w*)			Vesicular size[a] (nm)	PDI[a]	% entrapment efficiency[a]
		Lopinavir	Soya PC	Ethanol			
1	E1	0.5	1	30	225.6±11.0	0.264±0.016	48.3±3.7
2	E2	0.5	1	45	157.2±07.5	0.212±0.027	63.4±4.1
3	E3	0.5	1	60	178.2±09.2	0.118±0.006	39.2±4.3
4	E4	0.5	2	30	176.7±18.6	0.146±0.013	61.7±3.8
5	*E5*	*0.5*	*2*	*45*	*112.8±12.4*	*0.131*±0.008	*79.6±4.1*
6	E6	0.5	2	60	132.7±07.6	0.223±0.017	43.6±4.7
7	E7	0.5	3	30	164.5±06.1	0.283±0.023	50.3±3.4
8	E8	0.5	3	45	105.3±03.9	0.244±0.018	70.7±4.4
9	E9	0.5	3	60	123.8±11.2	0.198±0.011	33.7±4.2

PDI polydispersity index, *PC* phosphatidylcholin
[a] Values represented as mean±SD (n=3)

Table III. *Ex vivo* Drug Release and Skin Deposition Profile of Lopinavir from Various Formulations

S. No.	Parameters	Plain gel	Niosomal dispersion	Niosomal gel	Ethosomal gel
1	% drug release[a]	6.43±0.21	18.32±0.18	21.24±0.23	11.15±0.15
2	% skin deposition[a]	10.21±0.22	22.65±0.35	24.45±0.64	54.63±0.29
3	% drug retained on the surface[a]	83.42±0.77	58.35±1.23	53.82±0.79	33.42±0.45

[a] Values represented as mean±SD (n=3)

Preparation of Lopinavir-Loaded Ethosomes

Ethosomes of lopinavir consisting of soya phosphatidylcholin (PC), propylene glycol and ethanol were prepared by cold method (15). Briefly, lopinavir with varying proportions of phospholipid were dissolved in varying amount of ethanol (Table II) in a covered vessel at room temperature by vigorous stirring. Propylene glycol was added during stirring. The mixture was then heated to 47°C in a water bath. The water, previously heated to 47°C in a separate vessel, was added slowly to the mixture till a white suspension was formed and stirred for 10 min. Resultant dispersion of ethosomes was then sonicated in an ice bath using probe sonicator (four cycles of 30 s each) to get desired sized unilamellar vesicles. Unentrapped drug was separated by centrifugation at 4,000 rpm and 4°C for 15 min using laboratory centrifuge (Remi, India) and estimated for drug content (same procedure as mentioned for niosomes).

Preparation of Gel

The gel of optimized niosomal (F3c) and ethosomal (E5) dispersions were prepared by dispersing 0.8% (*w*/*v*) carbopol 934 in it and allowing it to hydrate for 24 h. Finally, neutralization of gel was done by adding triethanolamine that made it transparent. Plain drug gel was also prepared by using same procedure with hydroethanolic solution (15% (*v*/*v*) ethanol) of lopinavir.

Characterization of Niosomes and Ethosomes

Vesicular Shape and Surface Morphology

Photomicrographs taken by Olympus BX 40 microscope (at ×40) were used for initial visualization of niosomes and ethosomes before sonication. Scanning electron microscope (JSM-5610LV, JEOL, Japan) was used later to determine

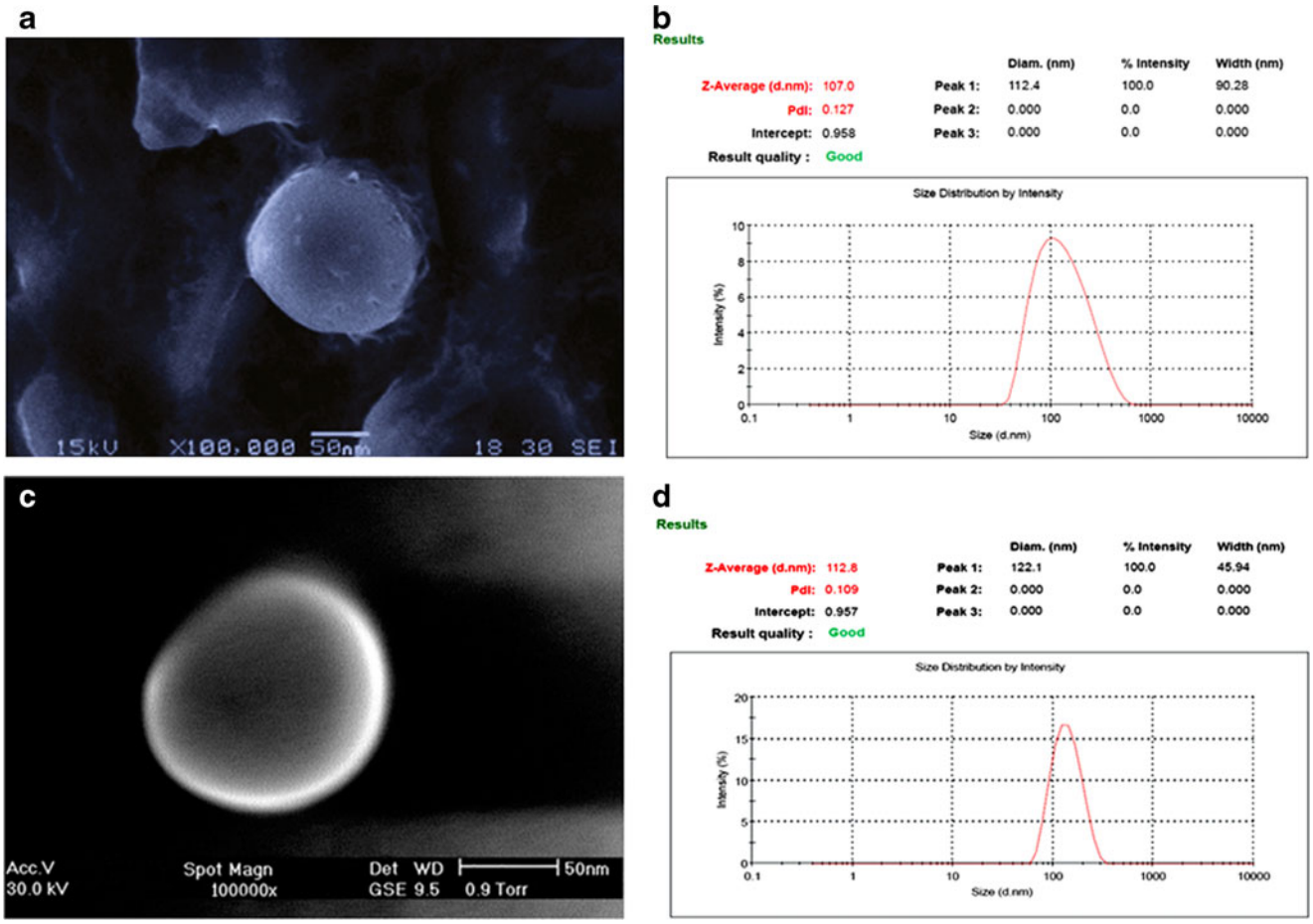

Fig. 1. Scanning electron photomicrograph and size distribution graph of lopinavir-loaded F3c (**a**, **b**) and E5 dispersion (**c**, **d**)

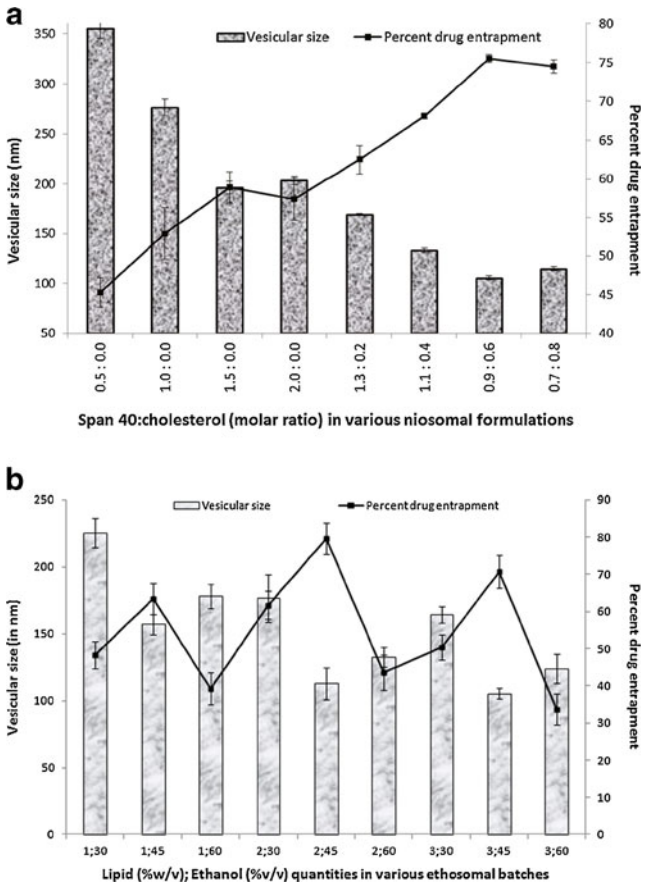

Fig. 2. Effect of **a** Span 40 and cholesterol; **b** soya PC and ethanol on vesicular size and PDE of lopinavir-loaded niosomal and ethosomal formulations, respectively

surface morphology of F3c and E5 dispersions. Samples were attached to sample stubs, silver coated, and then viewed using an accelerating voltage (15 kV) at the magnification of ×100,000.

Vesicular Size and Zeta Potential

Vesicular dispersions were diluted ten times with distilled water and then it was analyzed for vesicular size and zeta potential by Malvern Zetasizer Nanoseries-ZS (Malvern Instruments, Malvern, UK).

Percentage of Drug Entrapment

Amount of lopinavir entrapped within niosomes and ethosomes was estimated using first derivative UV–visible spectroscopic technique (UV-1700, Shimadzu). In brief, an appropriate quantity of drug-loaded formulation and unentrapped fraction (separation method is described earlier in preparation section) of lopinavir were dissolved separately in a mixture of aetonitrile/methanol (7:3 ratio) and absorbance difference ($dA/d\lambda$) were recorded at a wavelength of 219 nm. The corresponding concentrations were obtained from first derivative standard calibration curve of lopinavir prepared at 219 nm. The method was found to obey Beer's law between concentration range of 10 to 35 μg/ml with limit of detection (LOD) and limit of quantification (LOQ) values as 0.844 and 2.558 μg/ml, respectively. The PDE was finally calculated using the formula:

$$\% \text{ drug entrapment} = \frac{\text{Entrapped drug}}{\text{Total drug}} \times 100$$

Stability Study

The lopinavir-loaded F3c and E5 dispersions were stored in a sealed glass vials and subjected to stability study in triplicate. The vials were kept at two different storage conditions, i.e., 4±1°C with ambient humidity and 30±2°C with 65±5% RH, and the samples were withdrawn periodically at an interval of 1 month for 2 months, suitably diluted with water and analyzed for vesicular size and percent drug retention.

***Ex vivo* Studies**

Drug Release Study

Ex vivo study was carried out using full-thickness rat abdominal skin (16). Rat was killed by cervical dislocation method; the abdominal skin was removed and dipped into phosphate buffer solution (pH 6.8). Hairs were gently removed using electric clipper. The hairless skin was then dipped in hot water and subcutaneous fat was removed with scalpel. The skin was mounted on receptor compartment of the Franz diffusion cell (effective surface area, 3.14 cm^2) in such a way that the SC was facing upwards and then the donor chamber was clamped in place. The excess skin was trimmed off and the receptor compartment was filled with 24 ml of

Table IV. Stability Study of Optimized Niosomal (F3c) and Ethosomal (E5) Dispersions

S. No.	Formulation	Time (in months)	Vesicular size[a] (nm)		% drug retained[a]	
			2–8°C	30±2°C	2–8°C	30±2°C
1	F3c dispersion	0	105.76±1.24	105.76±1.24	100	100
2		1	109.24±2.16	138.18±3.75	96.23±0.458	54.43±0.538
3		2	115.31±1.87	186.51±2.66	91.18±0.759	39.32±0.346
4	E5 dispersion	0	113.3±5.43	113.3±5.43	100	100
5		1	143.6±1.09	198.72±2.13	85.79±2.983	43.12±5.789
6		2	178.2±6.83	301.68±7.69	69.52±4.191	23.73±2.443

[a] Values represented as mean±SD (n=3)

diffusion media consisting of phosphate buffer (pH 6.8)/ isopropyl alcohol mixture in a ratio of 3:1. The whole assembly was put on magnetic stirrer for gentle stirring and the temperature of the diffusion media was maintained at 32± 0.5°C. Various gel formulations selected for the study (Table III) were applied to the skin. The samples were collected over 24 h at predetermined time intervals and analyzed by HPLC method. Two milliliters of sample was withdrawn each time from the receptor compartment, and the volume was then maintained by adding 2 ml of fresh diffusion media. On completion of 24 h, the skin surface was washed thrice with diffusion medium and the washings were filtered under vacuum using 0.22 μm polycarbonate membrane filter. These filtered samples were then suitably diluted and analyzed for drug retained on skin surface. To extract out the drug deposited into the skin, the skin was chopped into small pieces using sharp knife and collected in diffusion medium. It was then subjected to bath sonication for three cycles each of 5 min, and the extracted drug was analyzed by HPLC method.

Fluorescence Microscopic Study

For the purpose of visualizing skin penetration behavior of F3c as well as E5 formulations, coumarin was added to the formulation as a fluorescent marker and the formulations were prepared using the same method as described earlier for F3c gel preparation by replacing the drug with coumarin. Hairs from the dorsal portion of rat's skin were gently removed using electrical clipper and the formulations were applied on hairless portion of skin. After 6 h, the rats were killed by cervical dislocation and the skin was wiped with cotton wool wetted with PBS to remove any formulation left onto the skin surface. The skin was then removed, embedded in paraffin block and 5-μm thick sections were cut using microtome. These sections were investigated by fluorescence microscopy at 40-fold magnification.

Histopathological Study

F3c and E5 gel were applied on hairless rat's abdominal skin obtained using the method as described in previous section. After 6 h, the rat was killed and the skin was excised. The excised skin was immediately immersed in 10% buffered formalin, dehydrated in graded concentrations of ethanol, immersed in xylene, and then embedded in paraffin block. The 5-μm thick sections of skin were cut using microtome and were mounted on slide using commercial glycerol's mounting fluid. The paraffin wax was removed by warming the slide gently, until the wax melted, and then was washed with xylene followed by washings with absolute alcohol and water. The sections were stained with hematoxylin–eosin to determine gross histopathology and collagen deposition, respectively. The slides were analyzed at 40-fold magnification using optical microscope. Phosphate-buffered saline was used as negative control.

In vivo Bioavailability Study

The experimental protocol of the study was approved by the Institutional Animal Ethics Committee of MS University of Baroda and was in accordance with the guidelines of Committee for Purpose of Control and Supervision of Experiments on Animals, Ministry of Social Justice and Empowerment, Government of India. Healthy male Wistar rats weighing around 240–270 g were selected for the study and divided into two groups of six animals each. One group served as control receiving oral lopinavir suspension while another group kept as test group receiving F3c gel topically. For the control group, after overnight fasting the animals were administered with 7.2 mg/ml of lopinavir suspension in distilled water (dose calculated as per USFDA guidelines). For the test group, hairs from abdominal area were removed using electrical clipper followed by application of F3c gel (an equivalent amount containing 7.2 mg of lopinavir) on abdominal skin of anaesthetized rat. Serial blood sampling (0.5 ml) was then done from the tail vein at predetermined time intervals. Plasma was separated by centrifugation at 3,000 rpm, 4°C, for 15 min and 4 ml methanol was added to 200 μl plasma samples for deproteination and for extraction of drug. The mixture was then vortexed for 2 min, followed by centrifugation for 5 min at 3,200 rpm using a tabletop centrifuge (Remi Instruments, Mumbai, India). The organic layer was separated and filtered using 0.2-μm membrane syringe filter. About 20 μl of the filtrate was injected into the HPLC for estimation of lopinavir concentrations. The pharmacokinetic parameters were calculated using Kinetica software (version 4.4).

HPLC Analysis of Lopinavir

For quantitative estimation of lopinavir in samples obtained from *ex vivo* and *in vivo* studies, a more sensitive Shimadzu HPLC system equipped with a LC 20AT pump, a SPD-20A UV visible detector, a Thermosil® C-18 column (250×4.6×10 μ) and a guard column (4.5 mm internal diameter) was used. 10 mM of ammonium acetate buffer (pH 6.0) mixed with acetonitrile in a ratio of 40:60 was used as mobile phase at a flow rate of 1.5 ml/min (for *ex vivo* study) and at 1.0 ml/min (for *in vivo* study). Column eluant was monitored at 220 nm as λ_{max} and concentrations of lopinavir were compared against a standard calibration curve of lopinavir in mobile phase. The method was found to obey Beer's law between concentration range of 100 ng/ml to 20 μg/ml with LOD and LOQ values as 10 and 50 ng/ml, respectively.

Statistical Analysis

Data analysis was carried out using Microsoft Excel (version 2007), and results are expressed as mean ± standard deviation (n=3 independent samples). Statistical analysis was performed using GraphPad InStat software (version 5.00) using one way ANOVA followed by Tukey's multiple comparison test with $P<0.05$ as a minimal level of significance.

RESULT AND DISCUSSION

Enormous surface area of skin and advantages such as noninvasive nature, bypassing first-pass metabolism, reduced dosing frequency, controlled delivery of medicament, improved patient compliance have established the transdermal route as a better alternative to drugs with limited oral bioavailability. Several investigations demonstrating the potential

of various nanoconstructs in combating the barrier nature of SC further raised the interest of researchers in exploring the newer ways to maximize the drug delivery through transdermal route. Among these nanocarriers, niosomes were selected in the present study for their better stability, less toxicity, and cost-effectiveness with an aim to enhance the systemic availability of lopinavir, and the results were compared with ethosomes, lipid vesicles containing a well-known penetration enhancer ethanol.

Formation of uniform, tiny and predominantly spherical systems was ascertained from photomicrographs taken using Olympus BX-40 microscope at a magnification of ×40 before ultrasonication. Scanning electron photomicrograph and polydispersity index of niosomal and ethosomal dispersions further confirmed the formation of smooth surfaced nanoconstructs possessing vesicular characteristics and uniformity in size distribution (Fig. 1a–d).

To decide the optimum amount of Span 40 and cholesterol in niosomal formulation, vesicular size and PDE was estimated. As shown in Table I and Fig. 2a, increase in molar fraction of Span 40 resulted in a decreased vesicular size and increased entrapment efficiency of niosomes. The result may be attributed to the saturation of Span 40 bilayers with drug at initial stages causing the precipitation of drug and poor entrapment efficiency (17) which later on improved as the amount of Span 40 was increased. F3c vesicles with a 1:1.5 molar ratio of lopinavir: Span 40 (formulation code, F3) possessed minimum size (196.45±6.23 nm) and maximum entrapment efficiency (58.9±1.98%). A further increase in Span 40 level adversely affected both the parameters. Hence, further optimization of cholesterol content was performed by replacing moles of Span 40 with similar moles of cholesterol while keeping the moles of lopinavir constant. It was observed that increasing the cholesterol level at first reduced the vesicle size and enhanced the drug entrapment capacity to their optimum level (105.22±1.96 nm and 75.5±0.5%, respectively) at a 0.9:0.6 molar ratio of Span 40/cholesterol indicating an improvement in overall bilayer-forming ability of Span 40. Unfavourable results beyond this point led us to consider 0.9:0.6 as an optimum ratio of surfactant-to-cholesterol (formulation code, F3c) to produce vesicles with desirable characteristics. An initial decrease in vesicular size could be an indicative of close packing of surfactant monomers by cholesterol molecule providing suitable molecular geometry and hydrophobicity for bilayer vesicle formation (18). Beyond Span 40/cholesterol molar ratio of 0.9:0.6, a further increase in cholesterol level resulted in increased vesicle size that may be due to disturbance imparted in the vesicular membrane by increased hydrophobicity and thereby formation of larger vesicles with more thermodynamic stability taken place (19). An improvement in entrapment efficiency of lopinavir with increasing cholesterol level may be attributed to a better lipophilic behavior and stability of lipid bilayer (20) with decreased permeability (21) in presence of higher cholesterol content. However, on higher cholesterol level a reduction in entrapment efficiency resulted probably due to the competition between cholesterol and drug for packing space within the bilayer (6).

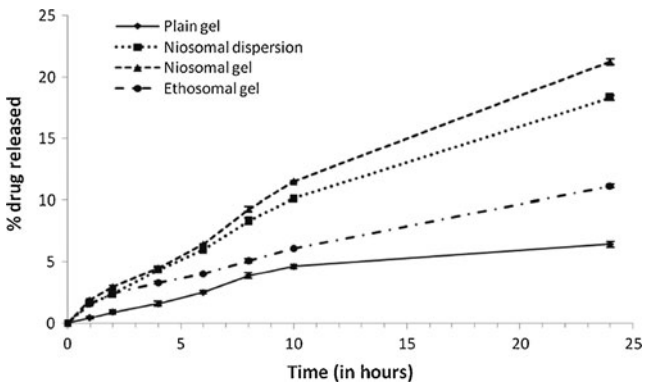

Fig. 3. Cumulative percentage of drug release via full-thickness rat abdominal skin *versus* time profile of various lopinavir formulations

As the amount of lipid and ethanol are known to affect vesicular size as well as PDE, the optimization of ethosomal system were based on these parameters and the results obtained are shown in Table II and Fig. 2b. On decreasing the drug-to-lipid ratio by increasing the lipid fraction of bilayer, the vesicular size was found to decrease while the PDE was found to increase probably due to a better packing of drug molecule within lipid bilayer improving the overall geometry and integrity of vesicle membrane. A decrease in PDE at 3% (*w*/*w*) lipid level could be a result of low drug-to-lipid ratio causing poor association of lopinavir with bilayer. Increasing concentrations of ethanol also contributed in size reduction as well as PDE enhancement may be owing to its ability to impart fluidity to bilayer (22). However, beyond optimum level, a further increase in ethanol concentration may have rendered the bilayer leaky causing a severe decrease in PDE while slightly increasing the vesicular size. Ethosomal formulation with 2% (*w*/*v*) of soya PC and 45% (*v*/*v*) of ethanol had maximum drug entrapment with desirable size and was considered to be the optimized composition.

The stability study of F3c and E5 dispersions were conducted by subjecting the formulations to aging for a period of 2 months at two different environmental conditions and observing the changes in vesicular size and drug retentive potential were selected as key indicators for stability. As shown in Table IV, the storage of F3c formulations at 4±1°C/ambient RH for 2 months did not affect the mean vesicular size (115.31±1.87 nm) as well as percent drug retention (91.18±0.759) significantly while the formulations stored at 30±2°C/65±5% RH have managed to retain only 39.32±0.346% of the drug with a significant rise in mean vesicular size (186.51±2.66 nm) at the end of 2 months. During 2 months of storage, a significant rise in mean vesicular size of ethosomes along with a significant fall in percentage of drug retained within these systems, even at 4±1°C/ambient RH, clearly indicated the poor stability of lipidic systems when compared with niosomal carriers. The results provided compelling evidence of better stability profile of niosomes over ethosomal systems and supported 4±1°C/ambient RH as an optimal storage condition for carriers under study as compared with storage condition of 30±2°C/65±5%RH.

In order to understand the ability of the F3c gel to aid in lopinavir permeation through the skin and also to study its skin deposition and toxicity, *ex vivo* studies were conducted and compared with the conventional plain drug gel, F3c dispersion and E5 gel.

Skin permeation profiles of lopinavir under nonocclusive condition was studied from plain gel, F3c dispersion, F3c gel,

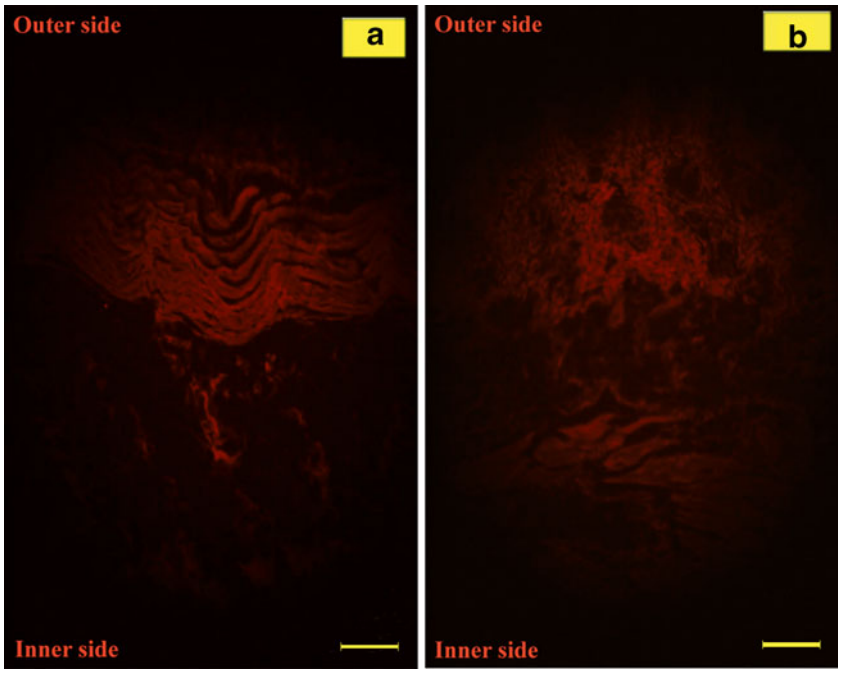

Fig. 4. Photomicrograph showing deposition of fluorescence probe coumarin within rat skin after 6 h via **a** E5 gel and **b** F3c gel. *Scale bar*, 100 μm

and E5 gel using rat's abdominal skin *ex vivo*. Interesting results were observed when *ex vivo* skin deposition and release pattern of lopinavir via F3c gel was compared with E5 gel (Fig. 3; Table III). In terms of overall skin permeation (including percent deposited within skin and percent released into diffusion media), E5 gel appeared to be more proficient than F3c gel (Table III). However, it is also evident that major fraction of lopinavir delivered via E5 gel remained deposited within the skin (54.63±0.29) while lopinavir in F3c gel efficiently delivered deeper into the skin and released 21.24± 0.23% of drug in 24 h, an amount significantly greater than that released via E5 gel (11.15±0.15%). A less skin deposition and better permeation of F3c carriers across more hydrophilic dermal region may be attributed to greater hydrophilicity of niosomes as compared with ethosomal carriers. The percent release and skin deposition of lopinavir obtained from F3c gel was better than that obtained from F3c dispersion (18.32± 0.18%). This may be due to sufficient porosity of gel matrix as well as the occlusive condition provided by the gel that helps in holding the water and thus keeping the hydration level of skin at a higher level for a longer duration as compared with dispersed system where water starts evaporating at

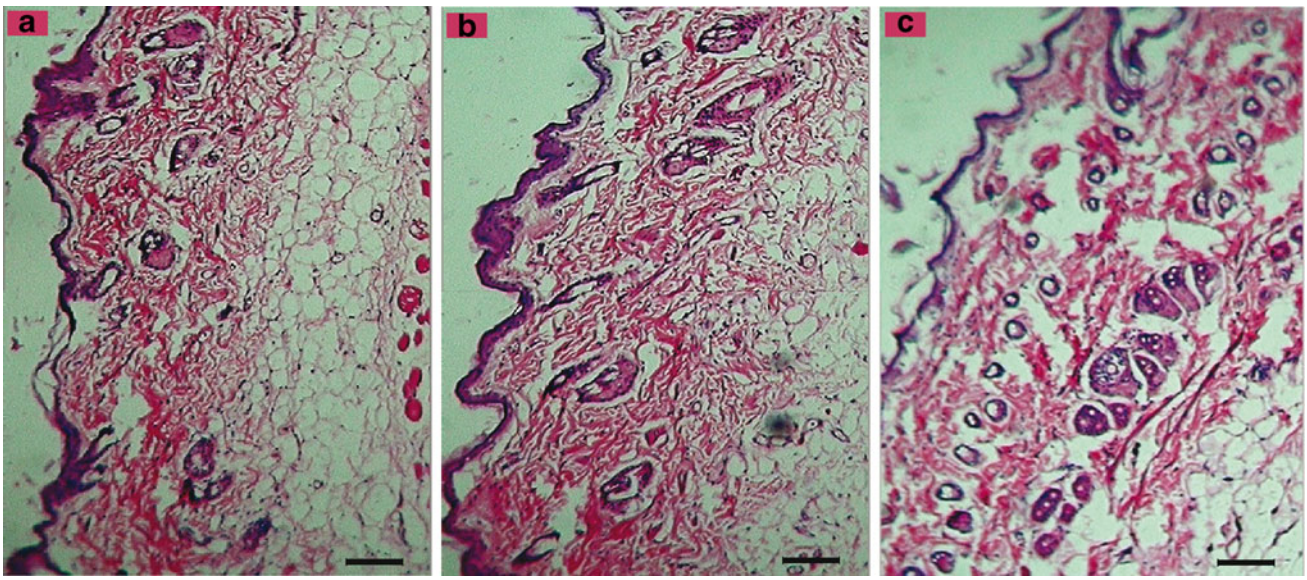

Fig. 5. Photomicrograph of hematoxylin–eosin stained rat skin for histopathological evaluation of **a** PBS as negative control, **b** F3c gel and **c** E5 gel. *Scale bar*, 50 μm

Table V. *In vivo* Pharmacokinetic Parameters of Lopinavir-Loaded Niosomal (F3c) Gel Compared with Its Oral Suspension (OS)

Formulations	Pharmacokinetic parameters			
	C_{max}[a] (μg/ml)	T_{max} (h)	$AUC_{0\rightarrow12}$ (h×μg/ml)	$AUC_{0\rightarrow\infty}$ (h×μg/ml)
OS	5.8±0.2	4	16.19	52.94
F3c gel	7.9±0.2	4	24.34	72.87

C_{max} peak plasma concentration, T_{max} peak time, $AUC_{0\rightarrow\infty}$ complete area under the PDC *versus* time curve
[a] Values represented as mean±SD (n=6)

a higher rate soon after applying the formulation (23). Highest amount of drug retained on the surface was observed in case of plain drug loaded gels (83.42±0.77) indicating the limited permeability of the drug alone across the SC layer that may be attributed to its moderately high molecular weight.

Figure 4a, b represents the fluorescence microscopic images of rat skin sections after 6 h application of coumarin-loaded E5 gel and F3c gel, respectively. Relatively high fluorescence intensity is evident in cases of ethosomes demonstrating a better skin permeation profile of ethosomes over niosomes. However, the presence of fluorescence at greater skin depths in case of niosomes suggests its potential as a better transdermal drug delivery module over ethosomes. The deeper penetration of niosomes than ethosomes could be because of the fact that sub-epidermal tissues contain a higher proportion of water supporting the permeation of more hydrophilic molecules across it while causing difficulty in passage of molecules with relatively high lipophilicity.

The clinical usefulness of prepared F3c gel was further examined by staining rat's skin, previously treated with formulations, using hematoxylin–eosin, and microscopic investigation was performed to observe any pathological changes as a sign of skin irritation or toxicity. The histopathological images were then compared with the images of skin treated with PBS used as negative control (Fig. 5). On comparing the extent of epidermal and subepidermal cellular damage or presence of prominent blood vessels, the formulations can be arranged in an order of PBS<F3c gel<E5 gel representing niosomes as a better drug delivery tool than ethosomes with respect to skin irritancy. Hence, it can be stated that the result provided an undeniable evidence of better safety profile of Span 40 over ethanol

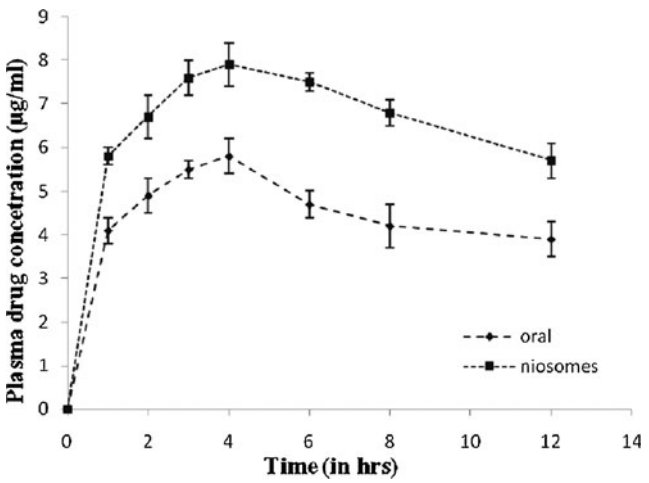

Fig. 6. PDC-time profile of lopinavir achieved via F3c gel and OS

To demonstrate the effect of route of administration as well as F3c gel on lopinavir bioavailability, *in vivo* bioavailability study in a group of six male Wistar rats after single transdermal application of F3c gel was performed and compared with orally administered lopinavir suspension to another group of six male Wistar rats. The plasma drug concentration (PDC) at various time points were estimated and various important pharmacokinetic parameters (such as peak plasma concentration (C_{max}), peak time (T_{max}), and complete area under the PDC *versus* time curve ($AUC_{0\rightarrow\infty}$)) useful in establishing the overall bioavailability of lopinavir from its formulation were calculated. As represented in Table V and Fig. 6, the significant differences in C_{max} (7.9 and 5.8 μg/ml, respectively) and $AUC_{0\rightarrow\infty}$ value (72.87 and 52.94 hμg/ml, respectively) of transdermally and orally administered lopinavir evidently advocate the enhanced bioavailability via F3c gel. The results were in accordance with the two facts that (a) extensive presystemic metabolism observed in oral drug administration can be bypassed by selecting transdermal route and (b) F3c carriers can efficiently carry the drug across skin layers.

CONCLUSIONS

Lopinavir, highly potent protease inhibitor used in the treatment of AIDS, needs to be co-administered with ritonavir because of its high presystemic metabolism resulting in poor systemic bioavailability. In the current study, an attempt was made to develop niosomal gel for improved systemic availability of lopinavir via transdermal route. As suggested by the results, niosomes with a 1:0.9:0.6 molar ratio of lopinavir, Span 40, and cholesterol, respectively possess optimum characteristics with respect to vesicular size and percentage of entrapment efficiency along with sufficient stability at 4±1°C/ambient RH. *Ex vivo* skin permeation studies showing 18.32±0.18% of drug release in 24 h suggested a better systemic availability of lopinavir via F3c gel as compared with E5 gel showing significantly less drug release in same duration (11.15±0.15%). Presence of fluorescence throughout the skin thickness as well as insignificant alteration in skin histopathology further aided in considering niosomes as better permeating and non-irritant transdermal drug delivery tool in comparison to ethosomes. Systemic availability of lopinavir at a better rate (C_{max}, 7.9 μg/ml) and to a greater extent ($AUC_{0\rightarrow\infty}$, 72.87 hμg/ml) was also observed with transdermally administered F3c gel during *in vivo* studies. Encouraging results of niosomal stability, skin penetrability, non-irritancy and ability to improve overall bioavailability of lopinavir have led us to conclude that niosomal gel holds a great potential as a novel transdermal nanocarriers in safely carrying lopinavir to systemic circulation and thus surmounting the need of adding Ritonavir in formulations to hoist the lopinavir bioavailability.

REFERENCES

1. Ojewole E, Mackraj I, Naidoo P, Govender T. Exploring the use of novel drug delivery systems for antiretroviral drugs. Eur J Pharm Biopharm. 2008;70(3):697–710.
2. WHO/UNAIDS. UNAIDS report on the global AIDS epidemic. Switzerland; 2010.
3. Abbott L. Clinical Pharmacology and Biopharmaceutics review of Kaletra oral solution (NDA#021251). U.S. Food and Drug Administration (updated 20 November 2001). Available from: http://www.accessdata.fda.gov/drugsatfda_docs/nda/2000/21-226_Kaletra_biopharmr_P1.pdf. Accessed 23 August 2012
4. ter Heine R, Van Waterschoot RA, Keizer RJ, Beijnen JH, Schinkel AH, Huitema AD. An integrated pharmacokinetic model for the influence of CYP3A4 expression on the *in vivo* disposition of lopinavir and its modulation by ritonavir. J Pharm Sci. 2011;100(6):2508–15.
5. Attia IA, El-Gizawy SA, Fouda MA, Donia AM. Influence of a niosomal formulation on the oral bioavailability of acyclovir in rabbits. AAPS PharmSciTech. 2007;8(4):E106.
6. Balakrishnan P, Shanmugam S, Lee WS, Lee WM, Kim JO, Oh DH, *et al*. Formulation and *in vitro* assessment of minoxidil niosomes for enhanced skin delivery. Int J Pharm. 2009;377(1–2):1–8.
7. Cable C. An examination of the effects of surface modifications on the physicochemical and biological properties of non-ionic surfactant vesicles. Ph.D. thesis, Glasgow University of Strathclyde; 1989.
8. Jadon PS, Gajbhiye V, Jadon RS, Gajbhiye KR, Ganesh N. Enhanced oral bioavailability of griseofulvin via niosomes. AAPS PharmSciTech. 2009;10(4):1186–92.
9. Solanki AB, Parikh JR, Parikh RH, Patel MR. Evaluation of different compositions of niosomes to optimize aceclofenac transdermal delivery. Asian J Pharm Sci. 2010;5(3):87–95.
10. Kushla GP, Zatz JL, Mills Jr OH, Berger RS. Noninvasive assessment of anesthetic activity of topical lidocaine formulations. J Pharm Sci. 1993;82(11):1118–22.
11. Godin B, Touitou E. Ethosomes: new prospects in transdermal delivery. Crit Rev Ther Drug Carrier Syst. 2003;20 (1):63–102.
12. Agarwal R, Katare OP, Vyas SP. Preparation and *in vitro* evaluation of liposomal/niosomal delivery systems for antipsoriatic drug dithranol. Int J Pharm. 2001;228(1–2):43–52.
13. Karki R, Mamatha GC, Subramanya G, Udupa N. Preparation, characterization and tissue disposition of niosomes containing isoniazid. Rasayan J Chem. 2008;1(2):224–7.
14. Verma DD, Verma S, Blume G, Fahr A. Particle size of liposomes influences dermal delivery of substances into skin. Int J Pharm. 2003;258(1–2):141–51.
15. Touitou E, Dayan N, Bergelson L, Godin B, Eliaz M. Ethosomes—novel vesicular carriers for enhanced delivery: characterization and skin penetration properties. J Control Release. 2000;65(3):403–18.
16. Bhalaria MK, Naik S, Misra AN. Ethosomes: a novel delivery system for antifungal drugs in the treatment of topical fungal diseases. Indian J Exp Biol. 2009;47(5):368–75.
17. Mokhtar M, Sammour OA, Hammad MA, Megrab NA. Effect of some formulation parameters on flurbiprofen encapsulation and release rates of niosomes prepared from proniosomes. Int J Pharm. 2008;361(1–2):104–11.
18. Manosroi A, Wongtrakul P, Manosroi J, Sakai H, Sugawara F, Yuasa M, *et al*. Characterization of vesicles prepared with various non-ionic surfactants mixed with cholesterol. Colloids Surf B. 2003;30(1):129–38.
19. Essa EA. Effect of formulation and processing variables on the particle size of sorbitan monopalmitate niosomes. Asian J Pharm. 2010;4(4):227–33.
20. Bernsdorff C, Wolf A, Winter R, Gratton E. Effect of hydrostatic pressure on water penetration and rotational dynamics in phospholipid–cholesterol bilayers. Biophys J. 1997;72(3):1264–77.
21. Kirby C, Clarke J, Gregoriadis G. Effect of the cholesterol content of small unilamellar liposomes on their stability *in vivo* and *in vitro*. Biochem J. 1980;186(2):591–8.
22. Paolino D, Lucania G, Mardente D, Alhaique F, Fresta M. Ethosomes for skin delivery of ammonium glycyrrhizinate: *in vitro* percutaneous permeation through human skin and *in vivo* anti-inflammatory activity on human volunteers. J Control Release. 2005;106:99–110.
23. Morgan CJ, Renwick AG, Friedmann PS. The role of stratum corneum and dermal microvascular perfusion in penetration and tissue levels of water-soluble drugs investigated by microdialysis. Br J Dermatol. 2003;148(3):434–43.

Journal of Molecular Liquids 242 (2017) 1156–1168

Contents lists available at ScienceDirect

Journal of Molecular Liquids

journal homepage: www.elsevier.com/locate/molliq

Development of dual drug loaded solid self microemulsifying drug delivery system: Exploring interfacial interactions using QbD coupled risk based approach

Aamin M. Vohra, Chintankumar V. Patel, Praveen Kumar, Hetal P. Thakkar *

Shri G. H. Patel Pharmacy Building, Faculty of Pharmacy, The Maharaja Sayajirao University of Baroda, Fatehgunj, Vadodara 390 002, Gujarat, India

ARTICLE INFO

Article history:
Received 24 May 2017
Received in revised form 31 July 2017
Accepted 1 August 2017
Available online 03 August 2017

Keywords:
Febuxostat
Aceclofenac
Solid SMEDDS
Quality by design (QbD)
Failure mode and effects analysis (FMEA)

ABSTRACT

Aceclofenac is widely prescribed with Febuxostat, the drug of choice in gout management, to eliminate the risk of gout flare. Though, no attempts have been made till date to combine them in single formulation. Hence, present research envisaged to develop dual drug loaded solid self microemulsifying drug delivery system addressing the associated formulation challenges. Quality by design approach was utilized to thoroughly understand various material attributes and process parameters playing vital role in formulation development. Quality Target Product Profile was laid down and failure mode and effects analysis was performed for better identification of the risks, ways to mitigate them and to put forward a control strategy. The amount of oil, surfactant and co-surfactant were identified as high risk variables, and their influence on product quality was studied using D-Optimal Mixture design considering globule size and % transmittance as dependent variables. Neusilin® US2 was selected as an adsorbent after screening of various silicates. The morphology of the oil globules in microemulsion was observed using transmission electron microscopy. Febuxostat and Aceclofenac loaded solid self microemulsifying drug delivery system also exhibited 1.87 and 4.19 fold increase in the oral bioavailability, respectively and remained stable during three months stability testing. Final risk assessment revealed that the risk associated with all the failure modes was significantly reduced after implementation of control strategy. Results collectively signified successful development of dual drug loaded solid self microemulsifying drug delivery system.

1. Introduction

Gout is a metabolic disorder resulting from excessive production or reduced excretion of uric acid, a by-product of purines metabolism, that leads to hyperuricemia followed by deposition of sodium urate crystals typically in kidneys, cartilage of joints and ears [1]. In gouty arthritis, the sodium urate crystals irritate the cartilage, causing inflammation, swelling and acute pain. If untreated, the crystals destroy all the joint tissues, the ends of articulating bones fuse and the joint becomes immovable [2].

Xanthine oxidase inhibitors (e.g. Allopurinol and Febuxostat) are the drugs of choice for chronic gout conditions [3]. Febuxostat (FBX) has been reported to be more effective in lowering and maintaining serum urate levels than allopurinol [4]. It is potent and more selective than allopurinol, and can be used safely in patients with hypersensitivity reactions to allopurinol [5,6]. However, FBX has a side effect known as gout flare, characterized by development of inflammatory condition at the initiation of the therapy [7]. Aceclofenac (ACL) is frequently prescribed with FBX due to its high therapeutic potential in arthritic pain [8,9] and also in controlling the symptoms of Gout flare [10]. Hence present work focuses on combining FBX and ACL in single dosage form in order to improve patient compliance. Furthermore, being Biopharmaceutics Classification System (BCS) class II (low solubility and high permeability) drugs with almost similar physicochemical characteristics, FBX and ACL carry similar delivery challenges that can be addressed through a common formulation strategy.

The oral bioavailability of FBX is hampered by its low (<5 μg/ml) aqueous solubility [11] and extensive enzymatic degradation in intestine and liver. Furthermore, FBX peak plasma concentration (C_{max}) reduced by 38–49% in presence of food [12]. Also, the oral bioavailability

Abbreviations: FBX, Febuxostat; ACL, Aceclofenac; BCS, Biopharmaceutics Classification System; SMEDDS, Self-Microemulsifying Drug Delivery System; L-SMEDDS, Liquid Self-Microemulsifying Drug Delivery System; S-SMEDDS, Solid Self-Microemulsifying Drug Delivery System; QbD, Quality by Design; FMEA, Failure Mode and Effects Analysis; QTPP, Quality Target Product Profile; ICH, International Council of Harmonization; CQA, Critical Quality Attributes; RPN, Risk Priority Number; USP, United States Pharmacopoeia; FTIR, Fourier Transform Infra Red; DSC, Differential Scanning Calorimetry; S_{mix}, surfactant:co-surfactant mixture; % T, % Transmittance; ANOVA, Analysis of Variance; GI, Gastrointestinal; o/w, Oil in water; C_{max}, Peak plasma concentration; T_{max}, Time to achieve C_{max}; AUC, Area Under the Curve; MRT, Mean Residence Time; TEM, Transmission Electron Microscopy; HDPE, High Density Polyethylene.; NSAIDS, Nonsteroidal Anti-Inflammatory Drug.

* Corresponding author at: Pharmacy Department, Faculty of Pharmacy, The Maharaja Sayajirao University of Baroda, Kalabhavan Campus, Vadodara 390001, Gujarat, India.
E-mail address: hetal.thakkar-pharmacy@msubaroda.ac.in (H.P. Thakkar).

http://dx.doi.org/10.1016/j.molliq.2017.08.002
0167-7322/

of ACL is limited owing to its very less aqueous solubility (<15 μg/ml) and extensive hepatic metabolism [13].

The review of related literatures showed various approaches like cyclodextrin complexes [14,15], nanosuspension [16,17], co-crystallization [18,19] and solid dispersion [20,21] to improve solubility and bioavailability of either drug. However, use of costly and sophisticated instruments and specially designed materials for the development of such formulations reduce manufacturing ease and ultimately lacks commercialization prospects.

In the recent years, much attention has been given to self-microemulsifying drug delivery system (SMEDDS) for their advantages like thermodynamic stability, improved solubilization of poorly water soluble drugs, spontaneous microemulsification, drug protection from gut environment, targeting gastrointestinal (GI) absorption window, ease of manufacturing and scale up etc. [22]. SMEDDS are isotropic mixtures of oil, surfactant, co-surfactant and solubilized drug/s; which spontaneously forms oil in water (o/w) nanodispersion of oil globules in aqueous environment of GI tract. Solid SMEDDS (S-SMEDDS) are considered as an advancement to the liquid-SMEDDS (L-SMEDDS) formulations due to their salient features like ease of handling, good portability, improved stability and better patient compliance [23]. In the present study, combined S-SMEDDS formulation of FBX and ACL is developed which is expected to improve oral bioavailability and ultimately reduce the cost of the therapy.

Use of Quality by Design (QbD) approach involving statistical design of experiment (DoE) for systematic optimization of microemulsion preconcentrates has been reported to minimize expenditure in terms of time, money and efforts when compared to conventional OFAT (one factor at a time) approach [24]. QbD based product development has gained significant attention as it is recommended by most regulatory bodies all over the world [25]. QbD approach involves defining quality target product profile (QTPP) which describes desired product criteria structuring the basis for determining the critical quality attributes (CQAs). Risk management by FMEA (failure mode and effects analysis) serves quantitative method to evaluate the risk associated with individual CQAs which are governed by material attributes or process parameters. QbD coupled with risk management ensures continuous improvement in product quality through real time adaptive control strategies to generate design space which renders manufacturing process robust [26]. The selection of different values of the parameters from the approved design space in order to achieve desired outcome is acceptable by most regulatory bodies all over the world. It is considered that the product quality will remain unaffected by these changes hence qualifies waiver from post approval change process [27]. Hence, in the present work, a stepwise systematic QbD approach was utilized to develop FBX and ACL dual drug loaded S-SMEDDS formulation. Since the formulation of isotropic systems involves complex interfacial phenomena, it was essentially required to thoroughly understand and quantify the magnitude and the nature of effect i.e. synergistic or antagonistic. The present investigation aimed at a) formulation development using QbD approach b) application of principles of FMEA and risk assessment c) implementation of D-Optimal mixture experimental design for formulation optimization, hence describing full picture of the effects of material attributes and process parameters on the response variables.

2. Material and methods

2.1. Materials

FBX was obtained as a generous gift from Ami Drugs and Speciality Chemicals Pvt. Ltd., India. ACL was obtained as kind gift from Centurion Lab., India. Olive oil, linseed oil, cottonseed oil and Propylene Glycol were obtained from S.D. Fine Chemicals, India. Caprol MPGO and Caprol glycol PEG-860 were purchased from Abitec Corporation, USA. Corn oil, oleic acid, sunflower oil and castor oil were purchased from Triveni Interchem Pvt. Ltd., India. Isopropyl Myristate was obtained from Haxon Laboratory Pvt. Ltd., India. Maisine 35, Peceol, Lauroglycol 90, Labrafil M2125 were kindly provided by Gattefosse, France. Cremophore EL and Transcutol HP were purchased from Sigma Aldrich, India. Span 20, Span 60, Tween 20, Tween 60, Tween 80, PEG-200, PEG-400, PEG-600, Methanol and Acetonitrile (AR and HPLC Grades) were procured from Spectrochem, India. Cremophor RH 40 was obtained from BASF, India. Olive oil, linseed oil, cottonseed oil, corn oil, sunflower oil and castor oil used were of highly refined grade. All other chemicals used were of analytical grade.

2.2. Establishment of QTPP and CQAs of FBX and ACL S-SMEDDS

As per ICH guidelines Q8(R2) recommendations the target product profile of proposed formulation was established utilizing prior knowledge and experimental assessment about the formulation. In order to meet the QTPP, the CQAs were selected from various quality attributes (QAs) like globule size, % transmittance (% T), self-emulsification time, drug content and drug release.

2.3. Risk assessment by FMEA

In the present study, overall risk assessment of the process and formulation parameters was performed using FMEA. The critical quality attributes were selected from many possible alternatives like formulation type, its design, method of manufacturing etc. Using FMEA method, the failure modes which are not meeting the QTPP and those which could have highest influence on product performance and greatest chance of causing product failure were identified. Failure modes can be prioritized for risk management conferring according to the seriousness of their effects, frequency of their occurrence and with what ease it can be detected [28,29]. The risk priority number (RPN) was given to each process/formulation variable according to the relative risk they presents [30]. The RPN was calculated using Eq. 1.

$$\mathrm{RPN} = \mathrm{Severity\ (S)} \times \mathrm{Occurrence\ (O)} \times \mathrm{Detectability\ (D)} \quad (1)$$

Where, O represents occurrence probability or the likelihood of an event to occur. It was ranked as 5- frequent; 4- probable; 3- occasional; 2- remote and 1- improbable to occur. The severity of the parameter i.e. the extent of damage to the quality of the product upon failure mode is denoted by S. It was ranked as 5- catastrophic; 4- critical; 3- serious; 2- minor and 1- negligible or no effect on product quality. The last parameter D was the detectability which means how easily the failure mode can be detectable. As the detectability of the failure mode increases, the associated risk with product quality decreases. Accordingly, D was ranked 1-easily detectable or absolute certain; 2- high detectable; 3- moderately detectable; 4- low or remote detectable and 5 as hard to detect or absolute uncertain [31].

2.4. Preformulation studies

2.4.1. Screening of formulation components based on saturation solubility studies

The solubility of each drug (FBX and ACL) was analysed in different formulation components viz. oils, surfactants and co-surfactants as a measure to maximize drug loading. An excess amount of each drug was added to 1 ml of each solvents (oils, surfactants and co-surfactants) in microcentrifuge tubes. The tubes were click locked and shaken for 24 h at 50 strokes per minute using a mechanical shaker. After 24 h, each tube was centrifuged at 10,000 rpm for 10 min to settle down excess insoluble drug. The clear supernatant was isolated and the concentration of FBX and ACL were determined after suitable dilution with methanol using UV spectrophotometry at λ_{max} of 315 and 277 nm respectively.

2.4.2. Selection of surfactant: co-surfactant (S_{mix}) ratio based on pseudoternary phase diagram

The water titration method was used to build pseudoternary phase diagram between oil, S_{mix} and water. The weight ratio of surfactant to co-surfactant in S_{mix} was varied as 1:1, 2:1 and 3:1. The oil was added to S_{mix} at 10:0, 9:1, 8:2, 7:3, 6:4, 5:5, 4:6, 3:7, 2:8, and 1:9 ratio with constant agitation. To the resultant mixtures, water was added drop wise until persistent haziness was observed. A maximum of 250 ml water was used for titration considering it as infinite dilution. The pseudoternary phase diagram was plotted using Chemix Software and microemulsification region was compared for selection of optimum S_{mix} ratio [32].

2.5. Preparation and optimization of FBX and ACL L-SMEDDS using D-optimal mixture design

In the present study, D-Optimal mixture design of experiment was used to optimize the formulation. This experimental design was used as a statistical tool to quantify relationship between critical formulation variables and responses measured. The independent variables and their respective levels were selected based on the preliminary screening studies of SMEDDS components. Table 1 represents the independent variables and response variables along with respective constraints. For the preparation of L-SMEDDS, FBX (40 mg) and ACL (100 mg) were weighed accurately and dissolved in the predetermined quantities of oil and S_{mix} suggested from the design batches. All the ingredients were uniformly mixed by vortexing to obtain uniform, clear, transparent L-SMEDDS which were further characterized for CQAs.

2.5.1. Globule size (R1)

The L-SMEDDS were microemulsified in 250 ml phosphate buffer pH 6.8 and allowed to stabilize for an hour. The resulting microemulsions were filled in clear disposable sizing cuvettes and the globule size were measured using ZetaSizer (Nano ZS, Malvern Instruments, UK) equipped with a He-Ne laser at 633 nm and scattered light detector at an angle of 90°.

2.5.2. % Transmittance (R2)

The L-SMEDDS were microemulsified in 250 ml phosphate buffer pH 6.8 and allowed to stabilize for an hour. The percent transmittance (%T) of samples were analysed at 650 nm wavelength in UV–Visible spectrophotometer (UV 1700, Shimadzu, Japan). Phosphate buffer pH 6.8 as used as a blank by adjusting its transmittance as 100%.

2.5.3. Statistical analysis

Polynomial equations including main and interaction terms were generated for two response variables using multiple linear regression analysis (MLRA) approach. Considering 95% confidence interval and 5% level of significance, the model and model terms were considered significant if the respective p value found <0.05. The general form of the polynomial equation was represented by Eq. 2.

$$Y = \beta_0 + \Sigma\beta_i X_i + \Sigma\beta_{ij} X_i X_j Y = \beta_0 + \Sigma\beta_i X_i + \Sigma\beta_{ij} X_i X_j + \Sigma\beta_{ijk} X_i X_j X_k \quad (2)$$

Where Y is the predicted response, β_o is the model coefficient, β_i is the linear regression coefficient of the main effects, β_{ij} is the regression coefficient of the two factor interaction effect, β_{ijk} is the regression coefficient of the three factor interaction effect, and X_i, X_j, and X_k are the independent variables. The interaction terms, show how response changes when two or three factors are simultaneously changed. The best fitting model was chosen based on the coefficient of determination R^2, adjusted R^2, predicted R^2 and adequate precision [33]. The validation of the generated model was done by conducting two experiments by varying the independent variables at values other than that of the model. % Bias (percent relative error) between predicted values (PV) and experimental values (EV) for each response was calculated using Eq. 3.

$$\%\text{Bias} = (\text{PV} - \text{EV})/\text{PV} * 100 \quad (3)$$

2.6. Selection of solid adsorbent and preparation of S-SMEDDS

Aerosil® 200, Aeroperl® 300 and Neusilin® US2 were screened for their oil adsorption capacity. The optimised L-SMEDDS formulations of FBX and ACL were separately mixed with a glass pestle to obtain homogeneous mass. The amount of adsorbent was added in increments of 50 mg until the blend exhibited free flowing characteristics. The adsorbent which was required in the least quantity to render the blend free flowing, was selected as solid adsorbent for further studies. Prepared FBX and ACL solid SMEDDS blends were transferred into another porcelain bowl and mixed properly. The flow properties of the prepared S-SMEDDS were measured. Finally after evaluation of powder blend it was filled in hard gelatin size "000" enteric capsules.

2.7. Characterization of L-SMEDDS/S-SMEDDS formulation

2.7.1. Self-emulsification time

The self-emulsification time of the optimised L-SMEDDS of FBX and ACL was evaluated using USP type II (paddle) dissolution apparatus. Briefly, 250 ml phosphate buffer pH 6.8 was maintained at 37 ± 1 °C in 500 ml vessels of dissolution apparatus with paddle rotating at 50 rpm. A single dose of L-SMEDDS was added to each vessel and time required to obtain visually clear, transparent phase was considered as self-emulsification time [34].

2.7.2. Thermodynamic stability testing

The optimised S-SMEDDS formulation was dispersed in 250 ml phosphate buffer pH 6.8 and allowed to stabilize for one hour. The dispersion was subjected to different thermodynamic stability testing conditions. S-SMEDDS was subjected to heating cooling cycle; freeze thaw cycle and centrifugation test. Physical stability was monitored throughout the test and also phase separation or any turbidity in microemulsion

Table 1
Formulation variables and their levels for D-Optimal Mixture design.

Independent variables	Coded levels		Actual levels (%)	
	Low	High	Low	High
Amount of oil (A)	−1	1	10	20
Amount of Surfactant (B)	−1	1	53	60
Amount of Co-surfactant (C)	−1	1	26	30
Response variables				**Constraints**
Globule size (R1)				Target <100 nm
% Transmittance (R2)				Maximize

was observed. The formulation was tested at three Heating cooling cycles between 4 °C and 45 °C with storage at each temperature for not <24 h. The formulation was then subjected to centrifugation test in which, formulation was centrifuged at 3500 rpm for 30 min. The formulation was further subjected to freeze thaw stress testing by freezing at −21 °C and thawing at 25 °C; with storage at each temperature for not <48 h. The formulation was inspected for any kind of possible instability [35].

2.7.3. Globule size and surface morphology

The S-SMEDDS formulation was dispersed into 250 ml phosphate buffer pH 6.8 and the resulting microemulsion was allowed to stabilize for one hour. In order to separate adsorbent particles, the dispersion was filtered using 0.45 μ nylon membrane filter (Whatman®) to get visually clear filtrate.

The filtrate was analysed for globule size as described earlier. Uniform dispersion of S-SMEDDS incorporating 40 mg FBX and 100 mg ACL in phosphate buffer pH 6.8 was used for the morphology study using TEM. Approximately 2 μl of sample was deposited on the carbon-coated copper grid (300 mesh, 3 mm), excess of sample was removed using blotting paper and it was air dried. The sample was then observed under operating acceleration voltage of 100 kv.

2.7.4. Cloud point measurement

In order to measure the cloud point, the S-SMEDDS formulation was treated to obtain clear filtrate as mentioned in Section 2.9.2. The filtrate was subjected to heating under water bath with the temperature increasing gradually. The sample was observed visually for a sign of turbidity and the temperature was recorded. The temperature at which the turbidity was produced is considered as cloud point.

2.7.5. Drug content

Drug content of FBX and ACL was determined in the developed S-SMEDDS formulation. 500 mg of accurately weighed S-SMEDDS was added to 10 ml methanol in order to dissolve drugs. The suspension was filtered through PVDF 0.22 μm syringe filter. The concentration of FBX and ACL present in the filtrate was determined using developed simultaneous estimation method by UV spectrophotometry at 315 nm and 277 nm λ_{max} respectively. The test was performed in triplicate and the results are expressed as mean ± SD.

2.7.6. In vitro drug release study

One end of pre-activated dialysis bag (MWCO 12 kD, Hi Media Laboratories Pvt. Ltd) was clamped, S-SMEDDS equivalent to 40 and 100 mg of FBX and ACL respectively was filled in it and 10 ml of phosphate buffer pH 6.8 was added to induce microemulsification. The other end was clamped preventing any leakage and the dialysis bag was tied with the rotating paddle submerged in 250 ml phosphate buffer pH 6.8 at 50 rpm speed and 37 ± 0.5 °C temperature. 3 ml samples were drawn at predetermined time intervals and replenished with the same volume of fresh diffusion medium. The release profile of FBX and ACL from formulations was compared with suspensions of both the drugs. The concentration of FBX and ACL release from S-SMEDDS was determined using simultaneous estimation method by UV spectrophotometry at 315 nm and 277 nm λ_{max} respectively.

2.7.7. Stability study

The stability study of optimised S-SMEDDS formulation was carried out at room temperature and at accelerated conditions (40 ± 2 °C and 75 ± 5% RH) for 3 months as per ICH guidelines [36]. The enteric capsules filled with S-SMEDDS were packed in count of 30 into high density polyethylene (HDPE) bottle and tightly closed using child resistant closure. The formulation was analysed at zero, one, two and three month time intervals for physical appearance, drug content and globule size.

2.8. In vivo pharmacokinetic study

In vivo experimental protocol was approved by Institutional Animal Ethics Committee (IAEC Protocol number: MSU/IAEC/2015–16/1610; Date of Clearance: 4-Apr-2016) and designed as per the guidelines of Committee for the Purpose of Control and Supervision of Experiments on Animals (CPCSEA). Sprague-Dawley rats of 250–300 g were procured for the pharmacokinetic study. The rats were fasted overnight and divided into three treatment groups ($n = 6$). Animals of group I and II received marketed formulations of FBX and ACL respectively while the group III animals received optimised S-SMEDDS formulation. Animal dose was calculated using Eq. 4 as per United States Food and Drug Administration guidelines [37].

$$\text{Animal Dose (mg/kg)} = \text{Human Dose (mg/kg)} * \text{Human Factor/Animal Factor} \quad (4)$$

The developed S-SMEDDS formulation was compared with marketed FBX tablet (FEBUGET 40) and marketed ACL tablet (AKILOS-100). The quantities of marketed formulations and S-SMEDDS formulation of FBX and ACL equivalent to 4.11 and 10.27 mg/kg respectively were dispersed in 3 ml phosphate buffer pH 6.8 and were administered in rat duodenum 2 cm below pylorus with 27 G needle using surgical procedure. Post-operative care of the animals was taken as per the protocol. Blood samples (0.5 ml) were collected under mild anaesthesia from the retro-orbital plexus at 1, 3, 6, 9, 12 and 24 h time points into microcentrifuge tubes. Blood samples were centrifuged at 3500 rpm for 10 min at 4 °C and the harvested plasma was frozen at −20 °C until analysis using developed HPLC method. Pharmacokinetic parameters were calculated by non-compartmental analysis using Kinetica 5.1 software. The values of relative bioavailability of the S-SMEDDS to the marketed tablet formulations of both the drugs were calculated by the following equation:

$$\text{Relative bioavailability} = \left[(AUC_{total})_{\text{combined S-SMEDDS}} / (AUC_{total})_{\text{Marketed formulation}}\right] * 100 \quad (5)$$

2.9. Final risk assessment

The effectiveness of the risk control strategy employed was evaluated by comparison of RPN before and after its implementation. As described in Section 2.3, final risk assessment was performed. RPN was calculated for each of the risk factors and were compared with the RPN before implementation of control strategy.

3. Results

3.1. Establishment of QTPP and selection of CQAs for FBX and ACL S-SMEDDS

The QTPP was laid down as shown in Table 2 for various elements like dosage form, dosage strength, route of administration, pharmacokinetics, stability and container closure system. Globule size and % T were selected as the CQAs considering the limned QTPP as the base.

3.2. Risk assessment using FMEA method

Table 3 enlists the factors that were considered in the development of FBX and ACL SMEDDS while performing FMEA. The criticality of the factor was defined as per their RPN score; i.e. the

Table 2
QTPP of FBX and ACL self-microemulsifying drug delivery system.

QTPP elements	Target	Justification
Dosage form	S-SMEDDS filled enteric capsule	S-SMEDDS are known to carry lipophilic drugs in oil and S-mix and spontaneously get microemulsified in GI fluid to enhance solubility and thereby bioavailability of drugs. The enteric capsule prevents S-SMEDDS release into stomach and facilitates its release confined to intestine thereby protecting stomach from the adverse effects of ACL (NSAIDS).
Dosage strength	FBX 40 mg ACL 100 mg	40 and 100 mg are the unit recommended dose of FBX and ACL respectively.
Route of administration	Oral	Oral route is most preferred and patients-friendly.
Pharmacokinetics	Higher AUC with lesser T_{max}	Represents improved bioavailability with fast onset of action desired to achieve better therapeutic efficacy
Container closure system	HDPE child resistant container	Being moisture resistant, HDPE retains integrity and quality of capsules stored.
Stability	Stable at room temperature	No need of cold chain management hence, less cost of transportation and storage.

RPN ≥ 40 was considered as high risk, ≥20 to <40 was considered as medium risk and <20 was considered as low risk.

3.3. Screening of formulation components based on saturation solubility studies

Screening of oil, surfactant and co-surfactants was done based on saturation solubility and the results are graphically represented in Fig. 1. Saturation solubility studies in different oils revealed that both FBX and ACL exhibited maximum solubility (16.04 ± 0.07 and 35.23 ± 0.32 mg/ml respectively) in Capmul MPGO. Different types of surfactants for peroral use were studied to determine their ability to solubilize FBX and ACL. The solubility of both FBX and ACL was found maximum in Kolliphor EL which were 62.47 ± 0.13 and 220.35 ± 0.64 mg/ml respectively. Similarly, the solubility of both FBX and ACL was found maximum in Transcutol HP i.e. 70.10 ± 0.11 and 442.99 ± 0.70 mg/ml respectively. Hence, Caprol MPGO, Kolliphor EL and Transcutol HP were finalised as oil, surfactant and co-surfactant respectively for further formulation development.

3.4. Selection of surfactant: co-surfactant (S_{mix}) ratio based on pseudoternary phase diagram

The S_{mix} ratio at which pseudoternary phase diagram showed greater microemulsion region was selected for further study. As observed in Fig. 2, S_{mix} ratio of 2:1 exhibited maximum microemulsion region as compared to 3:1 and 1:1 S_{mix} ratios. In all the three water titrations, oil and S_{mix} in the ratio of 1:9 and 2:8 proportions were showing visually clear and transparent solution up to infinite dilutions. Upper and lower limits of oil, surfactant and co-surfactant were selected by varying oil:S_{mix} from 1:9 to 2:8 and at the same time keeping S_{mix} ratio 2:1 as constant.

3.5. Statistical analysis and optimization of L-SMEDDS using D-optimal mixture design

The volume of the mixture of oil and S_{mix} (2:1) in the ratio of 2:8 required to incorporate 40 mg FBX and 100 mg ACL was determined and fixed at 0.7 ml and 0.4 ml for FBX and ACL respectively. The experimentally obtained results of both the response variable i.e. globule size and % transmittance were added to the statistical design matrix (Table 4) and polynomial equations were generated to quantify the effect of the formulation variable on the response variables.

To determine significant factors (at 5% level of significance) affecting the response variables, *p* values generated from the software were used. Model R^2, Adjusted R^2 and Predicted R^2 values for each response variable is shown in Table 5.

Polynomial equations for FBX (Eqs. 6 and 7) and ACL (Eqs. 8 and 9) SMEDDS were generated from the software.

For FBX

$$R1 = 148.73A + 675.16B + 2251.48C - 1334.72AB - 3656.58AC - 366.86BC \quad (6)$$

$$R2 = 98.57A + 38.37B - 1.95C + 84.57AB + 148.87AC + 48.60BC - 382.60ABC \quad (7)$$

For ACL

$$R1 = 102.67A + 277.58B + 311.97C - 250.37AB - 361.72AC - 124.15BC \quad (8)$$

Table 3
Risk assessment using FMEA to identify criticality of failure modes.

Formulation/process parameter component	Failure mode	Failure effect	S*	Potential causes or root of failure	O*	Detectability Method or Control	D*	RPN*
Organoleptic properties of L-SMEDDS	Hazy solution or visible precipitates	Compromised quality of the formulation	5	Impurities, Improper selection of excipient	4	Visual inspection	2	40
Oil	Improper selection and concentration	Improper drug loading and Destabilization of SMEDDS	5	Improper selection and concentration	5	Visual Detection, Globule size, % Transmittance	2	50
Surfactant	Improper selection and concentration	Impaired self-emulsification time, Destabilization of SMEDDS	5	Improper selection and concentration	5	Emulsification time, Globule size, % Transmittance	2	50
Co-surfactant	Improper selection and concentration	Destabilization of SMEDDS, Hampered drug loading	5	Improper selection and concentration	5	Thermodynamic stability testing, Globule size, % Transmittance	2	50
Micromeritics of S-SMEDDS	Poor flow properties	Non-uniform capsule filling	5	Inappropriate adsorbent, Poor adsorption of L-SMEDDS by adsorbent	3	Angle of Repose, Carr index, Hausner ratio, weight uniformity test	2	30
Packaging	Insufficient to protect drug from temperature, humidity and shipping	Stability	5	Inappropriate Packaging Material	4	Assay of active ingredients	2	40

* S, severity; O, occurrence; D, detectability; RPN, risk priority number.

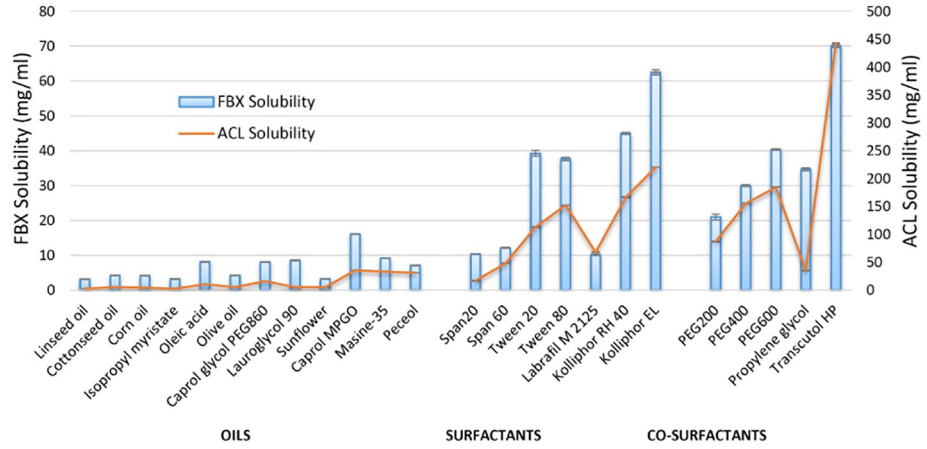

Fig. 1. Saturation solubility study of FBX and ACL in oils, surfactants and co-surfactants. Values are mean ± SD ($n = 3$).

$$R2 = 97.71A + 74.00B + 57.89C + 38.67AB + 64.89AC + 65.12BC - 128.39ABC \quad (9)$$

Based on the results of the responses, software suggested quadratic model as best fitting for all the response variables. The mean globule size was ranged between 101.4 and 1372 nm for FBX SMEDDS and 71.3 to 286.7 nm for ACL SMEDDS. The values of % T were ranged from 37.3 to 99.2 for FBX SMEDDS and 82.2 to 99.5 for ACL SMEDDS. The diverse ranges of the response variable indicate that the responses were sensitive towards the studied factor. To identify the significant model terms analysis of variance (ANOVA) was performed for each parameter. The intensity of the effect of the independent variable on the response variable was denoted by the value associated with the respective terms in the MLR equation. Larger coefficient means the respective model term has more potent influence on the responses. A positive sign of coefficient indicates an increase in the response while a negative term indicates a decrease in the response upon an increment in the respective independent model term. Coefficients with p value <0.05 had a significant effect on the measured response.

The potential interaction between various arrangements of the independent variables that can affect the response variables were studied and are graphically represented as response surface plots (Fig. 3). The results of check point analysis batches are shown in Table 6.

The values of % Bias between experimental and predicted values of the check point batches are varying from −6.97 to 8.47. The optimum values (Table 7) for three independent variable were selected by putting constraints for globule size to be minimum and % T to be maximum with desirability one.

Overlay plots were generated by superimposing contour plots of responses R1 and R2 from the software which displays the area of desired response values in the factor space also known as desirability plots (Fig. 4).

Desirability plots show high and low desirability areas of the responses obtained using various combinations of the independent variable. The experimental and predicted values of optimised formulation for each response are shown in Table 7.

3.6. Selection of solid adsorbent

The minimum quantities of Aerosil® 200, Aeroperl® 300 and Neusilin® US2 required to obtain free flowing powder blend for FBX L-SMEDDS were 400, 350 and 250 mg respectively Similarly, for ACL L-SMEDDS the value obtained were 200, 150 and 150 mg respectively. The best powder flow characteristics using minimum quantity of adsorbent were obtained in the case of Neusilin® US2. The micromeritic properties of the optimised S-SMEDDS formulations are given in Table 8.

3.7. Characterization of L-SMEDDS/S-SMEDDS formulation

3.7.1. Self-emulsification time

The optimised FBX and ACL L-SMEDDS formulations showed self-emulsification time of 11 ± 2 s and 17 ± 2 s respectively in phosphate buffer pH 6.8.

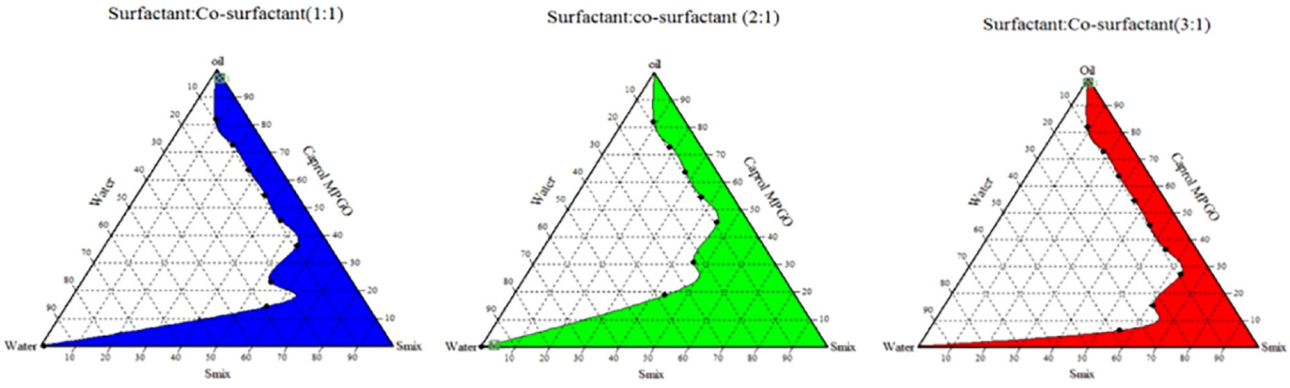

Fig. 2. Pseudoternary phase diagrams with different Smix ratio.

Table 4
Randomized batches of FBX and ACL L-SMEDDS as per D-optimal mixture design.

Batch no.	FBX loaded L-SMEDDS					ACL loaded L-SMEDDS				
	A	B	C	R1[a]	R2[a]	A	B	C	R1[a]	R2[a]
1	140.0	364.0	196.0	873.3 ± 1.2	46.2 ± 1.3	80.0	216.0	104.0	235.5 ± 1.7	83.3 ± 0.9
2	98.0	392.0	210.0	153.9 ± 2.7	97.3 ± 2.0	80.0	212.0	108.0	255.7 ± 6.5	82.2 ± 1.9
3	119.0	399.0	182.0	491.6 ± 4.2	55.1 ± 1.0	72.4	218.0	109.6	171.2 ± 2.9	89.3 ± 2.1
4	126.0	364.0	210.0	311.6 ± 2.4	56.9 ± 2.1	68.0	212.0	120.0	179.5 ± 4.9	87.8 ± 2.4
5	140.0	378.0	182.0	1372.0 ± 2.0	38.2 ± 1.4	60.4	232.0	107.6	121.8 ± 3.6	93.3 ± 2.0
6	70.0	420.0	210.0	117.6 ± 2.4	97.1 ± 2.6	68.0	228.0	104.0	149.1 ± 6.8	88.4 ± 4.1
7	126.0	364.0	210.0	371.4 ± 3.2	69.6 ± 1.5	56.0	240.0	104.0	105.7 ± 3.3	97.8 ± 1.4
8	114.8	389.2	196.0	231.6 ± 4.3	90.8 ± 3.5	80.0	216.0	104.0	286.7 ± 2.4	83.1 ± 2.1
9	127.4	376.6	196.0	437.5 ± 2.2	58.9 ± 4.6	59.4	225.0	115.6	115.8 ± 2.3	96.3 ± 2.0
10	84.0	420.0	196.0	60.4 ± 1.8	99.2 ± 0.6	48.0	240.0	112.0	71.3 ± 2.9	99.5 ± 0.1
11	70.0	420.0	210.0	94.6 ± 3.3	98.9 ± 1.1	40.0	240.0	120.0	109.4 ± 3.1	97.7 ± 1.2
12	98.0	420.0	182.0	112.6 ± 2.4	98.2 ± 0.1	52.4	232.0	115.6	119.3 ± 2.1	97.8 ± 1.5
13	98.0	420.0	182.0	101.4 ± 1.4	98.4 ± 1.2	56.0	240.0	104.0	101.2 ± 3.1	98.0 ± 0.4
14	140.0	364.0	196.0	1057 ± 9.1	37.3 ± 3.6	80.0	212.0	108.0	283.8 ± 1.7	82.8 ± 3.3
15	99.4	404.6	196.0	125.9 ± 2.4	93.8 ± 2.0	40.0	240.0	120.0	92.5 ± 2.2	98.1 ± 1.1
16	140.0	378.0	182.0	1127.0 ± 7.0	37.7 ± 3.5	68.0	212.0	120.0	162.5 ± 2.8	90.2 ± 3.2

A = Amount of oil (μl); B = Amount of Surfactant (μl); C = Amount of Co-surfactant (μl); R1 = Mean globule size (nm); R2 = Mean % T.
[a] Values are represented in mean ± SD ($n = 3$).

3.7.2. Thermodynamic stability testing

The combined S-SMEDDS formulation was subjected to three thermodynamic stability tests and results are summarised in Table 9.

3.7.3. Globule size and surface morphology

The value of globule size as mean ± SD ($n = 3$) of the combined S-SMEDDS formulation was found to be 87.41 ± 4.16 nm. The morphology of FBX and ACL combined S-SMEDDS formulation is presented in Fig. 5. Along with the oil globules, presence of Neusilin® US2 particles can be seen in the TEM (Jeol, JEM – 1011, USA) image of S-SMEDDS formulation.

3.7.4. Cloud point measurement

The cloud point value as mean ± SD ($n = 3$) of the optimised S-SMEDDS formulation was found to be 66.0 ± 0.57 °C.

3.7.5. Drug content

The optimised S-SMEDDS formulation of FBX and ACL showed drug content of 98.0 ± 0.75 (39.2 ± 0.30 mg) and 98.0 ± 0.83% (98.0 ± 0.83 mg) respectively.

3.7.6. In vitro drug release study

The release of FBX and ACL from suspensions and combined S-SMEDDS formulation is shown in Fig. 6. The graphs show comparatively higher drug release of both the drugs from S-SMEDDS formulation than from the suspension.

Table 5
Results of statistical analysis of D-optimal mixture design for FBX and ACL L-SMEDDS formulations.

Sources	*p* values*			
	FBX L-SMEDDS		ACL L-SMEDDS	
	R1	R2	R1	R2
Model	<0.0001	<0.0001	<0.0001	<0.0001
Linear mixture	<0.0001	<0.0001	<0.0001	<0.0001
AB	0.009	0.0087	0.0376	0.0123
AC	0.0222	0.0472	0.2589	0.0065
BC	0.7982	0.1775	0.6784	0.0151
ABC	–	0.115	–	0.0249
Lack of fit	0.4572	0.0515	0.625	0.1284
	R-squared values			
Model R^2	0.9624	0.9458	0.9525	0.9826
Adjusted R^2	0.9436	0.9187	0.9287	0.9710
Predicted R^2	0.9054	0.8767	0.8889	0.9461

* Level of significance: *p* value <0.05.

3.7.7. Stability study

The results of three month stability study of FBX and ACL combined S-SMEDDS formulation are represented in Fig. 7. The study was performed in triplicates and the results are represented as mean ± SD. The physical appearance of the formulation was remained unchanged during three month stability testing.

3.8. In vivo pharmacokinetic study

The values of various pharmacokinetics parameters for FBX and ACL marketed formulation and combined SMEDDS formulation are shown in Table 10.

Comparative mean plasma concentration profile is shown in Fig. 8. The optimised S-SMEDDS formulation of FBX and ACL exhibited 1.87 and 4.19 fold increase in the relative bioavailability respectively.

3.9. Final risk assessment

Comparative evaluation of RPN before and after implementation of risk management strategy is depicted in Fig. 9.

4. Discussion

FBX is a potent, non-purine, selective xanthine oxidase inhibitor used for the treatment of chronic gout and hyperuricemia. Gout flare is the side effect of FBX treatment which appears at the initiation of the therapy due to rapid dissolution of urate crystals. ACL is widely used nonsteroidal anti-inflammatory drug (NSAID) for the treatment of gout flare [9,38]. Hence, an attempt has been made to develop combination of FBX and ACL in single S-SMEDDS formulation. Increased awareness of QbD tools and risk management approaches for the formulation development led to its greater penetration into research and industry for the rational understanding of the process and/or formulation parameters [39]. The present investigation, therefore, involved QbD based systematic development of the combined S-SMEDDS formulation employing risk assessment using FMEA method, risk analysis and control strategy to mitigate the risk. Based on the prior knowledge and therapeutic objective, the targets for QTPP were set. Globule size and % T were selected as critical among other quality attributes due to their potential to represent overall quality of target product as described in QTPP. It was very clear from the FMEA analysis that oil, surfactant and co-surfactant were three formulation parameters which have RPN ≥40

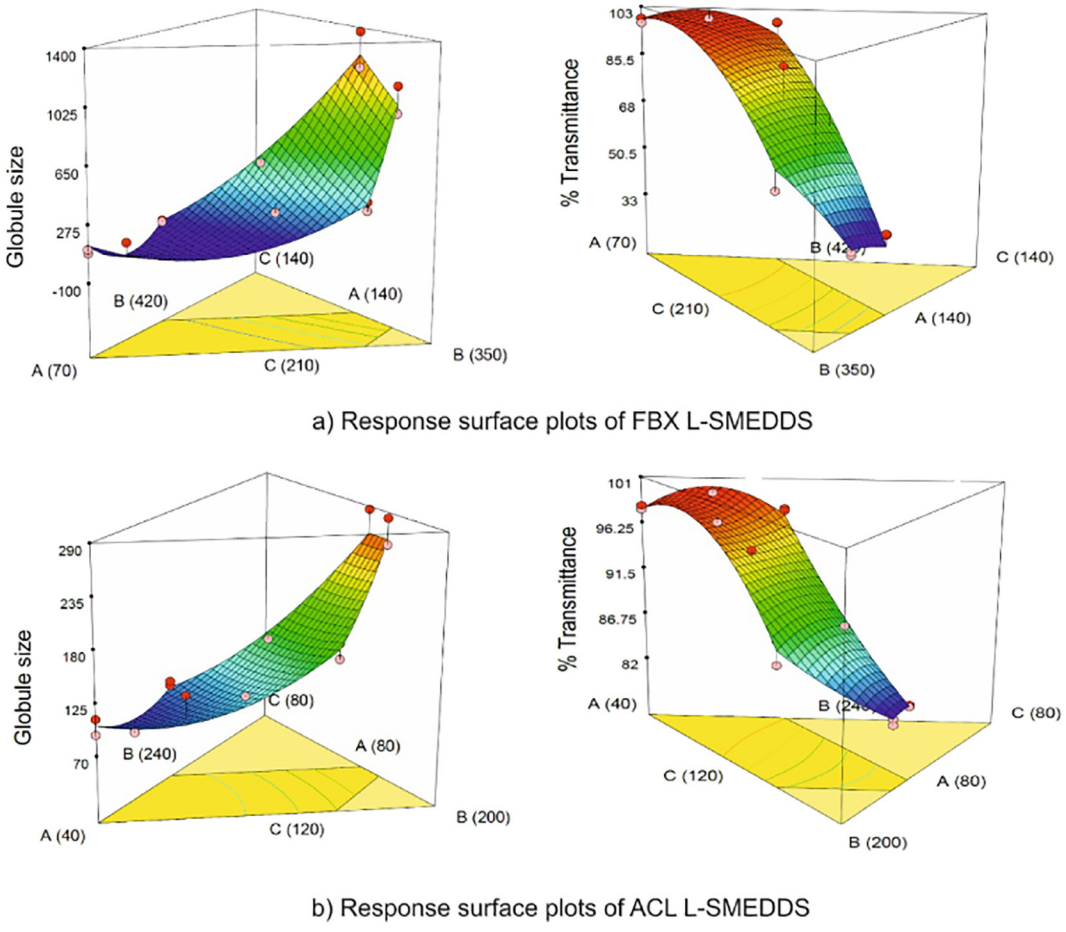

Fig. 3. Response surface graphs a) FBX L-SMEDDS; b) ACL L-SMEDDS.

and required thorough investigation and optimization. The effects of these three high risk factors in the formulation development were studied using D-Optimal mixture design of experiment. Organoleptic properties of SMEDDS and packaging were also high risk factors while micromeritics of the S-SMEDDS was a moderate risk factor. These factors are discussed further.

Solubility of the drug candidate in oil, surfactant and co-surfactant was considered as the most essential step in the formulation of SMEDDS. In the present study, solubility of FBX and ACL was found to be maximum in Caprol MPGO. Higher solubility of the drug in oil may lead to lowering the concentration of the surfactant and co-surfactant required. Hence, Caprol MPGO was selected for further studies. Likewise, the solubility of both the drugs was found maximum in Kolliphor EL which is a non-ionic surfactant and Transcutol HP which is reported to be widely used as a solubilizer and absorption enhancer [40]. Almost identical behaviour for solubility profile of both the drugs in oil, surfactant and co-surfactant might be due to their analogous physicochemical properties.

Pseudoternary phase diagram, representing phase behaviour of different formulation components, is crucial for the development of lipid-based formulation, which self-disperses as thermodynamically stable drug carrier in GI lumen [41]. From Fig. 2, it is clearly seen that the largest microemulsion region was obtained for S_{mix} ratio 2:1, indicating efficient emulsification capability of Kolliphor EL and Transcutol HP blend at this ratio.

The effect of variables which were ranked higher RPN during initial risk assessment was studied using randomized D-Optimal mixture design for the establishment of a design space without bias. The quadratic model was suggested by the design expert software as the best fit for the experimental results of globule size and % T for the SMEDDS of both the drugs. The response surface graph of the globule size of FBX

Table 6
Check point batches for validation of the model.

	Responses	Check point batches	Factors[a]			Experimental value	Predicted value	% Bias
			A	B	C			
FBX	R1	1	100	400	200	62.37	68.14	8.47
		2	130	380	190	783.30	732.23	−6.97
	R2	1	100	400	200	92.70	94.95	2.37
		2	130	380	190	59.77	56.36	−6.05
ACL	R1	1	70	220	110	235.10	223.02	−5.41
		2	50	230	120	137.40	149.44	8.06
	R2	1	70	220	110	85.44	88.91	3.91
		2	50	230	120	99.00	99.03	0.03

[a] A = Amount of oil (μl); B = Amount of Surfactant (μl); C = Amount of Co-surfactant (μl).

Table 7
Values of independent variables of optimised formulations of FBX and ACL L-SMEDDS.

		FBX L-SMEDDS	ACL L-SMEDDS
Independent variables	Oil (A)	101.11	49.48
	Surfactant (B)	388.88	237.82
	Co-surfactant (C)	210.00	112.69
Globule size (R1)	Predicted	53.13	88.37
	Experimental[a]	58.89 ± 1.33	85.49 ± 1.67
	% Bias	−9.69	3.26
% T (R2)	Predicted	99.37	99.47
	Experimental[a]	99.67 ± 0.23	99.61 ± 0.30
	% Bias	−0.29	−0.14

[a] Values are represented as mean ± SD ($n = 3$).

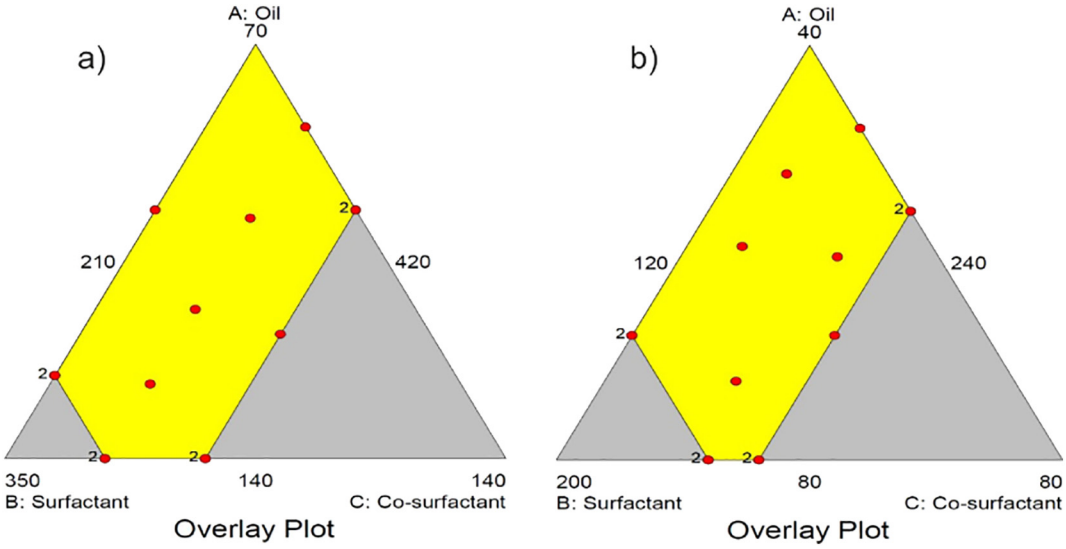

Fig. 4. Overlay plots showing design space for a) FBX L-SMEDDS and b) ACL L-SMEDDS.

L-SMEDDS showed increase in the globule size with decrease in the amounts of surfactant and co-surfactant. It is evident from the slope and the curve of the surface plot, that the surfactant alone is not sufficient to reduce the globule size to nanometric range. The higher values of the interaction terms AB and AC suggest that surfactant works with co-surfactant to reduce the size of the oil globules [42]. From the *p* values of the individual terms of Eq. 6, the linear mixture along with interaction effects of oil with surfactant and with co-surfactant were found to impact significantly on globule size. Relatively higher magnitude of the interaction effect of Caprol MPGO and Transcutol HP in the Eq. 6 suggests more prominent effect for reduction in globule size. The response surface graph of % T of FBX L-SMEDDS shows that highest level of transmittance was achieved when Kolliphor EL and Transcutol HP both were at high concentration. From the polynomial equation generated (Eq. 7), it is evident that all the three interaction effects (AB, AC and BC) are positively contributing to the value of % T. However from the *p* values of the model terms of Eq. 7, linear mixture and interaction effect of Caprol MPGO with Transcutol HP and with Kolliphor EL were found significantly affecting the response. Comparatively higher magnitude of the coefficient of the interaction term AC in the Eq. 7, shows prominent effect of Transcutol HP with Caprol MPGO for the improvement in % T. The response surface graph for globule size of ACL L-SMEDDS shows, decrease in globule size at higher concentrations of Kolliphor EL and Transcutol HP. Polynomial equation of globule size of ACL L-SMEDDS (Eq. 8) shows that all the interaction effects contributes to reduce the globule size. However from the *p* values of the individual polynomial terms of Eq. 8, only linear terms and interaction effect of Caprol MPGO with Kolliphor EL were found significantly affecting the response. The response surface graph of % T of ACL L-SMEDDS showed that with increase in the concentration of surfactant and co-surfactant, % T of the SMEDDS increases up to certain level. Moreover, the value of % T increases with decreasing amount of Caprol MPGO up to certain level. The *p* values of the polynomial terms of the Eq. 9 show linear mixture as well as interaction effects AB, AC, BC and ABC terms significantly affecting the response.

The fundamental property of the microemulsion is an ultra-low interfacial tension between the oil and water phases. The significant effect of Kolliphor EL as a surfactant in reducing the globule size and increasing the % T values might be attributed by its ability to sufficiently reduce o/w interfacial tension thereby lowering the energy required to increase the surface area; so that spontaneous dispersion of oil droplets occurs and the system becomes thermodynamically stable [43]. Moreover, being non-ionic emulsifier, Kolliphor EL generally considered safer than ionic surfactants [44,45]. The interaction effects of surfactant and co-surfactant with oil, played important role in reducing the globule size. This may be due to the fact that spontaneous microemulsion formation requires extremely low o/w interfacial tensions. However, in most cases, extremely low values of the o/w interfacial tension cannot be achieved by a single surfactant since the critical micelle concentration (CMC) is reached before a low value of interfacial tension is achieved. Above the CMC, surfactant molecules start forming micelles and remain ineffective for further reduction of interfacial tension and thereby globule size. The curvature of the response surface graph of quadratic model best represents the above fact. Addition of a co-surfactant as a second surface active species is an effective way to further decrease o/w interfacial tension [32,46].

The results of validation check point batches reveal reasonable agreement between the predicted and the experimental values, due to low value of the bias was found. Thus it can be stated that the equations reasonably prompt the influence of the selected formulation variables on the responses under study. The formulation optimization was done using desirability value. It has been reported that the globule size is one of the most important characteristics affecting the rate and extent of drug release [47]. The smaller the globule size, larger the surface area available for drug release. Hence, the goal for the optimization of globule size was set to minimum. % T value directly represents any undesirable interaction in the

Table 8
Micromeritic properties of the combined S-SMEDDS formulation.

Powder characteristics	Results	Inference
Bulk density (gm/ml)	0.516 ± 0.005	–
Tapped density (gm/ml)	0.573 ± 0.01	–
Carr index	9.95 ± 0.007	Excellent
Hausner ratio	1.11 ± 0.006	Excellent
Angle of repose	33.50 ± 1.23	Good

Values are represented as mean ± SD ($n = 3$)

Table 9
Results of thermodynamic stability testing of S-SMEDDS formulation.

Test	Observations
Heating cooling cycle	Remain clear without any sign of turbidity
Centrifugation test	No phase separation
Freeze thaw stress testing	Formulation did not produce any precipitation or color change

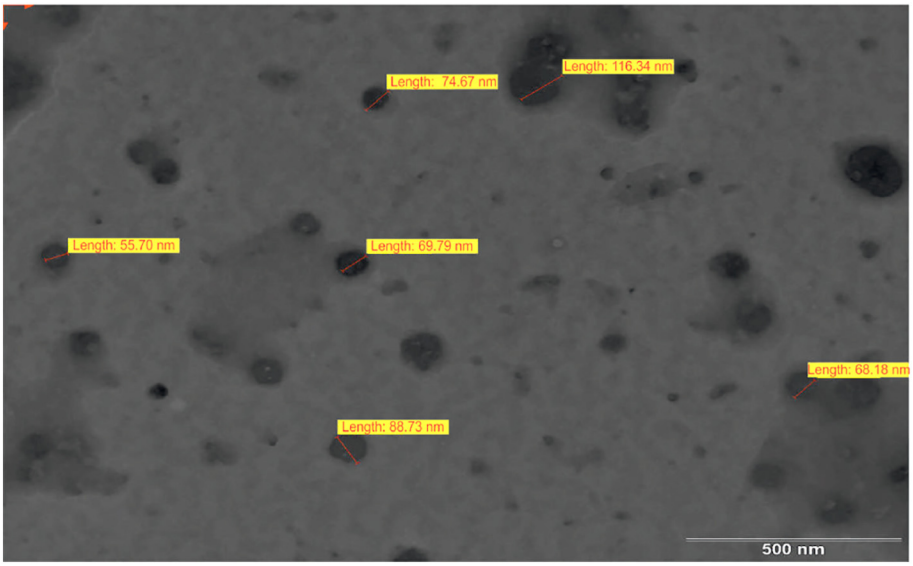

Fig. 5. TEM image of FBX and ACL combined S-SMEDDS formulation.

formulation e.g. drug precipitation and emulsion cracking etc. Therefore, the desired value of % T was set for the maximum. Experimental design was used for multiple responses therefore it is necessary to obtain a region called design space that provides optimum values of the factors. The design space is the acceptable region of the range of independent variables within which the product quality could be ensured for the desired QTPP. The risk mitigation and control strategy can be considered as an integrated framework of how quality is ascertained depending upon understanding of the process and product knowledge. Overlay plot (Fig. 4a and b) were obtained by superimposing contour plots of responses R1 and R2 which displayed the area of feasible response values in the factor space. The region highlighted in yellow color is designated as design space as a slight variation in the critical variables within this area will not affect the final response. Those regions which do not fit the optimization criteria are shaded grey. The risk mitigation strategy was established based on the design space plot. Operating the concentration ranges of high risk variables in the design space used to ensure the product quality embedded with desired globule size and % T. Moreover, monitoring the values of response variables i.e. globule size and %T; falling within the pre-fixed constraints is also an essential part of the risk mitigation strategy.

The organoleptic properties of the L-SMEDDS were evaluated visually for all the batches. It was observed that there was no sign of turbidity and drug precipitation noted for any of the L-SMEDDS batch. Therefore, the risk and criticality of this failure mode is low and under control of the process. For the development of robust formulation and to overcome the problem of metastable formulation, thermodynamic stability testing was performed. Heating and cooling of the emulsion exerts stress on two different phases of the emulsion. Heating the emulsion may cause surfactant to deactivate and ultimately coalescence of the oil globules. Moreover, heating causes density difference between dispersed and continuous phases which may cause emulsion to crack. Centrifugation provides force that acts on the dispersed phase based on the density difference between dispersed and continuous phase, which may lead to coalescence of the oil globules when the centrifugal force dominates repellent forces. Freezing and thawing processes imparts potential stress since both dispersed and continuous phases behaves differently during freezing and thawing processes with respect to their freezing point. The optimised formulation was found stable against all three thermodynamic stability testing conditions. The results of the thermodynamic stability tests are in favour of proper selection of excipients and the concentration ranges thereof; hence justifying goals of the QTPP.

The optimised L-SMEDDS formulation was adsorbed on Neusilin® US2 (magnesium aluminometasilicate) which was found the best adsorbent among screened silicates derivatives due to its highly porous nature along with good flow properties. The amount of adsorbent required to adsorb specified quantity of the L-SMEDDS incorporated the required dose of both the drugs which results in free flowing S-SMEDDS was optimised and kept constant. Hence, the risk involved for the failure mode of micromeritics of S-SMEDDS is low and was under control of the process.

Self-emulsification ability of the SMEDDS is directly related to the spontaneous formation of microemulsion when comes in the contact with the aqueous environment. Very low self-emulsification time of the optimised L-SMEDDS formulations favours spontaneous emulsification upon dilution with aqueous media. Cloud point measurement is more important to determine storage stability of

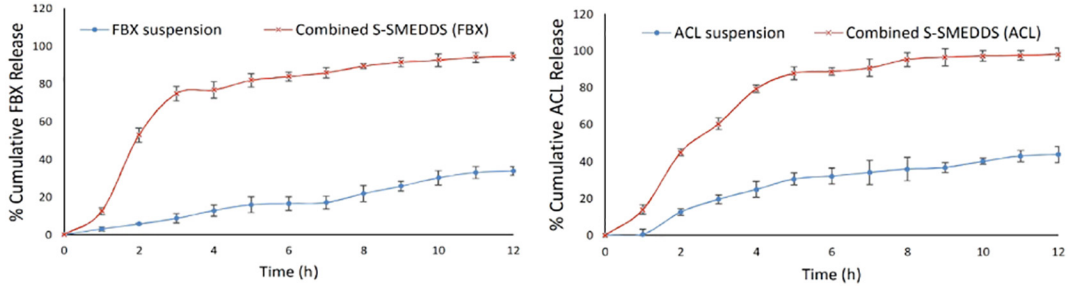

Fig. 6. In vitro drug release from drug suspensions of FBX and ACL in comparison with combined S-SMEDDS formulation.

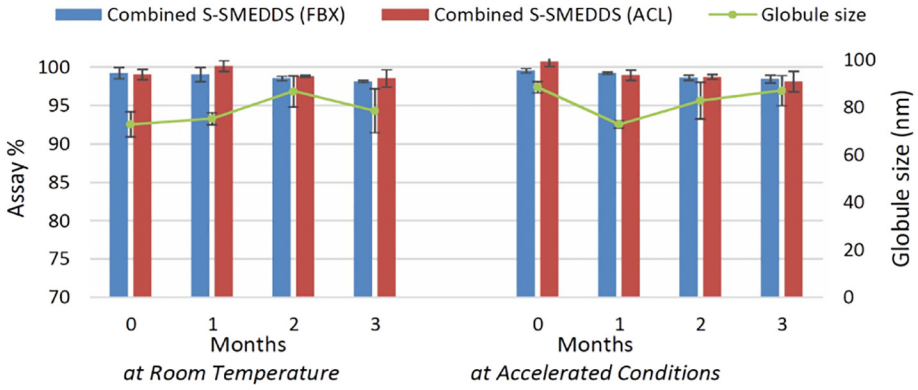

Fig. 7. Three month stability study of FBX and ACL combined S-SMEDDS at room temperature and at accelerated conditions.

the microemulsions. Exposing formulations at temperatures significantly higher than the cloud point may result in phase separation and instability. The optimised S-SMEDDS showed relatively higher cloud point than the physiological temperature. The morphological observation using TEM revealed that the microemulsion had uniformly distributed spherical oil globules along with the solid particles of Neusilin® US2. The globule size appeared to be in good agreement with the result obtained from globule size analysis using dynamic light scattering. Significantly higher in vitro drug release of FBX and ACL from S-SMEDDS in comparison to the drug suspensions may be due to smaller globule size and the greater availability of drugs in dissolved form in the case of SMEDDS formulation. The stability data suggested that the SMEDDS formulation was stable for at least three months revealing the low and under controlled risk of the product failure conferring to the selected packaging material. The in vivo pharmacokinetic data revealed that the relative bioavailability of FBX and ACL S-SMEDDS in combination form was improved 1.87 and 4.19 fold respectively. Improved saturation solubility of FBX and ACL in SMEDDS has contributed to increased dissolution rates as evidenced from in vitro drug release study which ultimately leads to improved bioavailability of BCS class II drugs. The hydrophobic drugs with low molecular weight are largely absorbed by the trans cellular routes. However, the formulation composition of SMEDDS, especially surfactant enhances tight-junction permeability and improves absorption of the drug through epithelial cells. SMEDDS formulation creates dispersion of very small droplets of oil with large surface area in GI lumen, which may also be responsible for improved absorption. Furthermore, SMEDDS, a lipid-based formulation, is considered to be partially absorbed via the lymphatic route as well, this may reduce the possibility of hepatic first pass metabolism and therefore enhance the bioavailability of drugs. The final risk assessment revealed that the RPN for all the failure modes after implementation of control strategy (Fig. 9) were below level of 20 suggesting significant reduction in the risk associated with the failure modes.

5. Conclusion

The S-SMEDDS technology was adopted here as a simple, easily scalable and cost-effective way to combine FBX and ACL in a single formulation and simultaneously improve their oral bioavailability. QbD coupled risk management approach was utilized for the development of S-SMEDDS where oil, surfactant and co-surfactant were identified as high risk factors based on the RPN score. As a part of control strategy, D-Optimal Mixture design was utilized to thoroughly understand the complex interfacial phenomena taking place among these factors to form microemulsion. The experimental design was validated using check point analysis and the optimum concentrations of the variables were obtained from the software within the developed design space. The final risk assessment revealed that the risk associated with the critical factors has been significantly reduced. In vitro characterization proved thermodynamic stability of the microemulsion along with improved drug release from the S-SMEDDS formulation. In vivo studies of the optimised S-SMEDDS formulation has shown 1.87 and 4.19 folds increase in the oral bioavailability for FBX and ACL respectively suggesting the possibility of dose reduction of both the drugs. The developed S-SMEDDS thus expected to improve patient compliance and will hopefully serve as gilt-edged formulation as a combined dosage form. After all, QbD coupled risk management has served a scientific and sagacious approach for systematic understanding of interfacial interactions involved in the self microemulsification of FBX and ACL loaded S-SMEDDS.

Table 10
Pharmacokinetic parameters of combined S-SMEDDS and marketed tablets of FBX and ACL.

Pharmacokinetic parametzers	Marketed tablet FBX	Marketed tablet ACL	FBX and ACL combined S-SMEDDS	
			FBX	ACL
C_{max} (ng/ml)	1651.63 ± 220.17	1166.84 ± 170.39	2375.94 ± 361.41	4230.55 ± 102.81
T_{max} (h)	1.00	3.00	3.00	6.00
AUC (ng/ml*h)	9786.07 ± 1113.65	5679.23 ± 549.18	13,642.19 ± 1144.60	22,546.07 ± 2870.11
AUC total (ng/ml*h)	11,379.97 ± 1569.3	6900.98 ± 781.88	21,302.95 ± 1953.51	28,913.84 ± 4253.23
$T_{1/2}$ (h)	4.24 ± 0.63	3.79 ± 0.57	10.10 ± 0.96	6.09 ± 1.03
MRT (h)	6.39 ± 1.10	7.60 ± 0.88	12.81 ± 0.92	8.89 ± 0.85
Relative Bioavailability	–	–	187.20	418.98

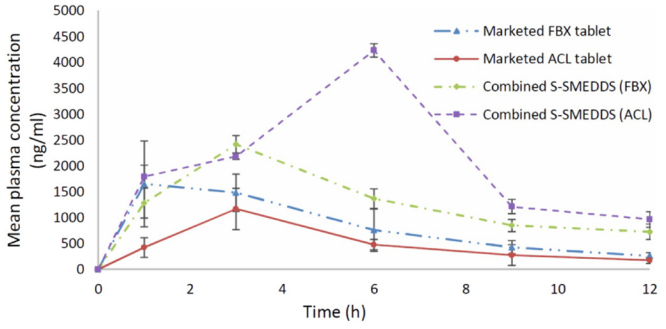

Fig. 8. Comparative plasma drug concentration-time profile of combined S-SMEDDS and marketed tablets of FBX and ACL. Values are mean ± SD ($n = 6$).

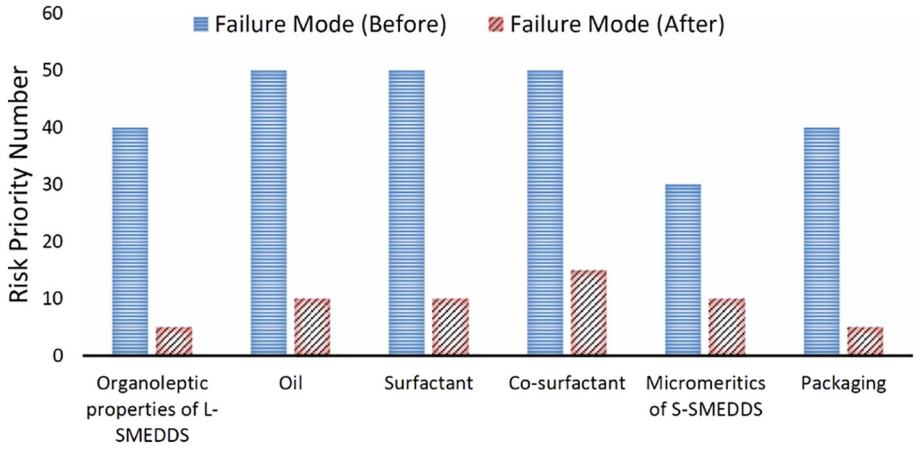

Fig. 9. RPN number of failure mode before and after implementation of control strategy.

Acknowledgement

The authors are highly grateful to Ami Drugs and Speciality Chemicals Pvt. Ltd., India and Centurion Lab., India for providing gift samples of Febuxostat and Aceclofenac respectively. The authors greatly appreciate generous support from industries that provided respective gift samples of the excipients. Authors declare no funding source had involved in the present research work.

Conflict of interest

Authors declare no conflict of interest.

References

[1] L.A. MacFarlane, S.C. Kim, Gout: a review of nonmodifiable and modifiable risk factors, Rheum. Dis. Clin. N. Am. 40 (2014) 581–604.
[2] J.A. Singh, S.G. Reddy, J. Kundukulam, Risk factors for gout and prevention: a systematic review of the literature, Curr. Opin. Rheumatol. 23 (2011) 192.
[3] J. Tayar, M. Lopez-Olivo, M. Suarez-Almazor, Febuxostat for Treating Chronic Gout (Review)DOI 2012.
[4] H.R. Schumacher, M.A. Becker, R.L. Wortmann, P.A. MacDonald, B. Hunt, J. Streit, C. Lademacher, N. Joseph-Ridge, Effects of febuxostat versus allopurinol and placebo in reducing serum urate in subjects with hyperuricemia and gout: a 28-week, phase III, randomized, double-blind, parallel-group trial, Arthritis Care Res. 59 (2008) 1540–1548.
[5] H.K. Grewal, J.R. Martinez, L.R. Espinoza, Febuxostat: drug review and update, Expert Opin. Drug Metab. Toxicol. 10 (2014) 747–758.
[6] L.I. Faruque, A. Ehteshami-Afshar, N. Wiebe, L. Tjosvold, J. Homik, M. Tonelli, A systematic review and meta-analysis on the safety and efficacy of febuxostat versus allopurinol in chronic gout, Semin. Arthritis Rheum. 43 (2013) 367–375.
[7] M.A. Becker, H.R. Schumacher Jr., R.L. Wortmann, P.A. MacDonald, D. Eustace, W.A. Palo, J. Streit, N. Joseph-Ridge, Febuxostat compared with allopurinol in patients with hyperuricemia and gout, N. Engl. J. Med. 353 (2005) 2450–2461.
[8] S. Tiwari, H. Dwivedi, K.M. Kymonil, S.A. Saraf, Urate crystal degradation for treatment of gout: a nanoparticulate combination therapy approach, Drug Deliv. Transl. Res. 5 (2015) 219–230.
[9] D. Ward, E. Veys, J. Bowdler, J. Roma, Comparison of aceclofenac with diclofenac in the treatment of osteoarthritis, Clin. Rheumatol. 14 (1995) 656–662.
[10] A. Pareek, N. Chandurkar, V. Sharma, M. Desai, S. Kini, G. Bartakke, A randomized, multicentric, comparative evaluation of aceclofenac–paracetamol combination with aceclofenac alone in Indian patients with osteoarthritis flare-up, Expert. Opin. Pharmacother. 10 (2009) 727–735.
[11] M.E. Ernst, M.A. Fravel, Febuxostat: a selective xanthine-oxidase/xanthine-dehydrogenase inhibitor for the management of hyperuricemia in adults with gout, Clin. Ther. 31 (2009) 2503–2518.
[12] R. Khosravan, B. Grabowski, J.T. Wu, N. Joseph-Ridge, L. Vernillet, Effect of food or antacid on pharmacokinetics and pharmacodynamics of febuxostat in healthy subjects, Br. J. Clin. Pharmacol. 65 (2008) 355–363.
[13] F. Shakeel, W. Ramadan, S. Shafiq, Solubility and dissolution improvement of Aceclofenac using different Nanocarriers, J. Bioequiv. Available 1 (2009) 39–43.
[14] B.S. Kuchekar, V.B. Divekar, S.C. Jagdale, I. Gonjari, Solubility enhancement and formulation of rapid disintegrating tablet of Febuxostat Cyclodextrin complex, J. Pharm. Res. 1 (2013) 168–175.
[15] K. Dua, K. Pabreja, M.V. Ramana, V. Lather, Dissolution behavior of β-cyclodextrin molecular inclusion complexes of aceclofenac, J. Pharm. Bioallied Sci. 3 (2011) 417–425.
[16] B.K. Ahuja, S.K. Jena, S.K. Paidi, S. Bagri, S. Suresh, Formulation, optimization and in vitro–in vivo evaluation of febuxostat nanosuspension, Int. J. Pharm. 478 (2015) 540–552.
[17] S.L. Prabu, S. Sharavanan, S. Govindaraju, T. Suriyaprakash, Formulation development of Aceclofenac Nanosuspension as an alternative approach for improving drug delivery of poorly soluble drugs, Int. J. Pharm. Sci. Nanotechnol. 6 (2013) 2145–2153.
[18] S. Mutalik, P. Anju, K. Manoj, A.N. Usha, Enhancement of dissolution rate and bioavailability of aceclofenac: a chitosan-based solvent change approach, Int. J. Pharm. 350 (2008) 279–290.
[19] D. Maddileti, S.K. Jayabun, A. Nangia, Soluble Cocrystals of the xanthine oxidase inhibitor Febuxostat, Cryst. Growth Des. 13 (2013) 3188–3196.
[20] S. Shinde, S. Patil, F. Mevekari, A. Satpute, An approach for solubility enhancement: solid dispersion, Int. J. Adv. Pharm. Sci. 1 (2010).
[21] R. Dass, S. Jaiswal, G. Gupta, Formulation and evaluation of febuxostat fast disintegrating tablet, Am. J. Pharm. Res. 4 (2014).
[22] S. Prachi, S.K. Prajapati, U.K. Sharma, S. Shivhare, A. Akhtar, A review on self micro emulsifying drug delivery system: an approach to enhance the oral bioavailability of poorly water soluble drugs, Int. Res. J. Pharm. 3 (2012) 1–6.
[23] A. Tan, S. Rao, C.A. Prestidge, Transforming lipid-based oral drug delivery systems into solid dosage forms: an overview of solid carriers, physicochemical properties, and biopharmaceutical performance, Pharm. Res. 30 (2013) 2993–3017.
[24] B. Singh, R. Kumar, N. Ahuja, Optimizing drug delivery systems using systematic "design of experiments." Part I: fundamental aspects, Crit. Rev. Ther. Drug Carrier Syst. 22 (2005) 27–105.
[25] S. Jain, Quality by design (QBD): a comprehen-sive understanding of implementation and challenges in pharmaceuticals development, Int J Pharm Pharm Sci 6 (2014) 29–35.
[26] S.L. Lee, T.F. O'Connor, X. Yang, C.N. Cruz, S. Chatterjee, R.D. Madurawe, C.M. Moore, X.Y. Lawrence, J. Woodcock, Modernizing pharmaceutical manufacturing: from batch to continuous production, J. Pharm. Innov. 10 (2015) 191–199.
[27] X.Y. Lawrence, G. Amidon, M.A. Khan, S.W. Hoag, J. Polli, G. Raju, J. Woodcock, Understanding pharmaceutical quality by design, AAPS J. 16 (2014) 771–783.
[28] R. Fahmy, R. Kona, R. Dandu, W. Xie, G. Claycamp, S.W. Hoag, Quality by design I: application of failure mode effect analysis (FMEA) and Plackett–Burman design of experiments in the identification of "main factors" in the formulation and process design space for roller-compacted ciprofloxacin hydrochloride immediate-release tablets, AAPS PharmSciTech 13 (2012) 1243–1254.
[29] C. Vora, R. Patadia, K. Mittal, R. Mashru, Risk based approach for design and optimization of stomach specific delivery of rifampicin, Int. J. Pharm. 455 (2013) 169–181.
[30] Y. Hiyama, Quality Overall Summary Mock P2, http://www.nihs.go.jp/drug/section3/English%20Mock%20QOS%20P2%20R.pdf March 2009 (accessed 24.03.2015).
[31] C. Vora, R. Patadia, K. Mittal, R. Mashru, Risk based approach for design and optimization of site specific delivery of isoniazid, J. Pharm. Investig. 45 (2015) 249–264.
[32] N. Parmar, N. Singla, S. Amin, K. Kohli, Study of cosurfactant effect on nanoemulsifying area and development of lercanidipine loaded (SNEDDS) self nanoemulsifying drug delivery system, Colloids Surf. B: Biointerfaces 86 (2011) 327–338.
[33] P.P. Shah, R.C. Mashru, Y.M. Rane, A. Thakkar, Design and optimization of mefloquine hydrochloride microparticles for bitter taste masking, AAPS PharmSciTech 9 (2008) 377–389.
[34] S. Kamboj, V. Rana, Quality-by-design based development of a self-microemulsifying drug delivery system to reduce the effect of food on Nelfinavir mesylate, Int. J. Pharm. 501 (2016) 311–325.
[35] F. Shakeel, N. Haq, M. El-Badry, F.K. Alanazi, I.A. Alsarra, Ultra fine super self-nanoemulsifying drug delivery system (SNEDDS) enhanced solubility and dissolution of indomethacin, J. Mol. Liq. 180 (2013) 89–94.
[36] ICH Harmonised Tripartite Guideline, Stability Testing of new Drug Substances and Products Q1A(R2). https://www.ich.org/fileadmin/Public_Web_Site/ICH_Products/Guidelines/Quality/Q1A_R2/Step4/Q1A_R2__Guideline.pdf, 2015 (accessed 24.03.2015).

[37] USFDA, Guidance for industry: estimating the maximum safe starting dose in initial clinical trials for therapeutics in adult healthy volunteers, Center for Drug Evaluation and Research (CDER), 2005 DOI.
[38] T. Soni, C. Nagda, T. Gandhi, N. Chotai, Development of discriminating method for dissolution of aceclofenac marketed formulations, Dissolut. Technol. 15 (2008) 31.
[39] R.A. Lionberger, S.L. Lee, L. Lee, A. Raw, X.Y. Lawrence, Quality by design: concepts for ANDAs, AAPS J. 10 (2008) 268–276.
[40] E.B. Basalious, N. Shawky, S.M. Badr-Eldin, SNEDDS containing bioenhancers for improvement of dissolution and oral absorption of lacidipine. I: development and optimization, Int. J. Pharm. 391 (2010) 203–211.
[41] D. Patel, K.K. Sawant, Oral bioavailability enhancement of acyclovir by self-microemulsifying drug delivery systems (SMEDDS), Drug Dev. Ind. Pharm. 33 (2007) 1318–1326.
[42] A. Gurram, P.B. Deshpande, S.S. Kar, U.Y. Nayak, N. Udupa, M. Reddy, Role of components in the formation of self-microemulsifying drug delivery systems, Indian J. Pharm. Sci. 77 (2015) 249.
[43] S. Chen, D.F. Evans, B. Ninham, Properties and structure of three-component ionic microemulsions, J. Phys. Chem. 88 (1984) 1631–1634.
[44] M. Kahlweit, R. Strey, G. Busse, Microemulsions: a qualitative thermodynamic approach, J. Phys. Chem. 94 (1990) 3881–3894.
[45] H. Hofland, J. Bouwstra, J. Verhoef, G. Buckton, B. Chowdry, M. Ponec, H. Junginger, Safety aspects of non-ionic surfactant vesicles: a toxicity study related to the physicochemical characteristics of non-ionic surfactants, J. Pharm. Pharmacol. 44 (1992) 287–294.
[46] R.J. Hunter, Introduction to Modern Colloid Science, Oxford University Press, first ed., 1993
[47] S. Gupta, S. Chavhan, K.K. Sawant, Self-nanoemulsifying drug delivery system for adefovir dipivoxil: design, characterization, in vitro and ex vivo evaluation, Colloids Surf. A Physicochem. Eng. Asp. 392 (2011) 145–155.

Taylor & Francis
Taylor & Francis Group

Journal of Macromolecular Science, Part B
Physics

ISSN: 0022-2348 (Print) 1525-609X (Online) Journal homepage: http://www.tandfonline.com/loi/lmsb20

Development and In Vitro Characterization of Capecitabine-Loaded Alginate–Pectinate–Chitosan Beads for Colon Targeting

Namrata Patel, Jagruti Desai, Praveen Kumar & Hetal P. Thakkar

To cite this article: Namrata Patel, Jagruti Desai, Praveen Kumar & Hetal P. Thakkar (2016) Development and In Vitro Characterization of Capecitabine-Loaded Alginate–Pectinate–Chitosan Beads for Colon Targeting, Journal of Macromolecular Science, Part B, 55:1, 33-54, DOI: 10.1080/00222348.2015.1110551

To link to this article: http://dx.doi.org/10.1080/00222348.2015.1110551

Accepted author version posted online: 21 Oct 2015.
Published online: 21 Oct 2015.

JOURNAL OF MACROMOLECULAR SCIENCE®, PART B: PHYSICS
2016, VOL. 55, NO. 1, 33–54
http://dx.doi.org/10.1080/00222348.2015.1110551

Taylor & Francis
Taylor & Francis Group

Development and In Vitro Characterization of Capecitabine-Loaded Alginate–Pectinate–Chitosan Beads for Colon Targeting

Namrata Patel, Jagruti Desai, Praveen Kumar, and Hetal P. Thakkar

Pharmacy Department, Faculty of Technology and Engineering, The Maharaja Sayajirao University of Baroda, Vadodara, Gujarat, India

ABSTRACT

Colon-targeted capecitabine beads were formulated by an ionotropic gelation method. The sodium alginate to pectin ratio and chitosan concentration were optimized using a 3^2 full factorial design. Analysis of response surface plots allowed the identification of an optimized formulation with high drug entrapment and controlled release. Insignificant differences in observed and predicted values for responses validated the optimization method. Optimized beads possessed an average diameter of 1395 μm and good flow properties. Their production as spherical beads having a smooth surface was confirmed by scanning electron microscopy. Fourier transform infrared spectroscopy revealed the compatibility of drug with added excipients, while differential scanning calorimetry study confirmed complete drug entrapment in polymer matrix. Higher swelling of beads in phosphate buffer pH 7.4 was obtained in comparison to pH 6.8. An in vitro wash off test indicated 70% mucoadhesion by the beads. In vitro dissolution studies of beads loaded into enteric-coated capsules revealed negligible release in simulated gastric and intestinal fluid, followed by 49.23% release in simulated colonic fluid, in 4 h. The optimized beads were found to be stable for three months at 25 ± 2°C/60 ± 5% RH. In conclusion, the formulated beads showed colon-specific controlled release properties, and thus could prove to be effective for colon cancer treatment.

ARTICLE HISTORY
Received 8 April 2015
Accepted 4 October 2015

KEYWORDS
capecitabine; colorectal cancer; experimental design; oral delivery

Introduction

Colon cancer is the third most commonly diagnosed cancer in men (10% of the total) and the second most commonly diagnosed in women (9.2% of the total) worldwide; in 2012, it accounted for 8.5% of the total cancer mortality.[1] Treatment of metastatic colorectal cancer with chemotherapy is a palliative approach. But complete responses to front-line chemotherapy are rarely observed, and partial responses are observed in less than 25% of patients.[2,3] Introduction of drugs, such as Irinotecan and Oxaliplatin, have led to enhancement in the therapy of colorectal cancer.[4] However, both of these agents can have significant toxicity (gastrointestinal toxicity, myelosuppression, and neurotoxocity) and require repeated

CONTACT Hetal P. Thakkar hetal_thakkar11@yahoo.com Pharmacy Department, Faculty of Technology and Engineering, The Maharaja Sayajirao University of Baroda, Vadodara 390 001, Gujarat, India.

Color versions of one or more figures in this article can be found online at www.tandfonline.com/lmsb.

clinical visits and/or infusion pumps for administration on a long-term basis. Oral chemotherapeutic agents, such as capecitabine, tegafur, eniluracil, emetifur, 9-aminocamptothecin, and 9-nitrocamptothecin, are also used in the treatment of colorectal cancer. Administration of oral chemotherapeutic agents has several advantages, including the potential for greater patient convenience as well as acceptance and significant cost savings in terms of both treatment costs and loss in wages incurred by patient and family during physician visits.[5]

Capecitabine, an orally administered prodrug, is enzymatically converted into active 5-fluorouracil in tumor, where it inhibits DNA synthesis and slows down growth of tumor tissue.[4] It has a plasma half life of 0.85 h and oral bioavailability of 40%. It is administered at a high dose of 1250 mg/m^2 twice a day for colorectal cancer.[4] Such a high frequency and dose leads to serious side effects such as hand and foot syndrome, vomiting, pain in stomach, fever, or infection. capecitabine gets degraded in the acidic environment of the stomach, causing a significant loss of the drug before it reaches the colon. The nonspecific release of the drug throughout the gastrointestinal tract is also responsible for its side effects. Hence, targeting of the drug in the colon and its controlled release after it reaches the colon are very important requirements to reduce side effects and frequency of administration. Various formulations, such as microspheres,[6] nanoparticles,[7] and hydrogel microspheres,[8] have been reported to achieve controlled release for capecitabine. However, we know of no reports of colon targeting and controlled release of capecitabine. Using colon-specific delivery, the drug could be delivered to the site of action for the treatment of local conditions of the colon, such as colon cancer and inflammatory bowel disease, and hence lower doses of drug may be required to achieve therapeutic levels.[9,10] To achieve colon-specific drug delivery, different approaches have been tried, including time-, pH-, pressure-, and bacteria-dependent delivery systems. Major drawbacks associated with these systems include lack of specificity in the onset of drug release (DR) and premature drug release before the delivery device arrives the colon.[11,12] Natural polysaccharides, such as pectin, chitosan, and dextran, are widely used for the development of colon-specific delivery.[13] Pectins are polysaccharide components of plant cell walls made of linear polymers of d-galacturonic acid residues having varying degrees of methyl ester substituents.[14] They become degraded only when their solubility is reduced, and hence major efforts have been focused on water resistance and still enzymatically active pectin derivatives.[15,16]

The beads formulated using mucoadhesive excipients, such as sodium alginate and chitosan, have been reported to increase the gastrointestinal residence time and permit controlled release.[17] Pectin, a polysaccharide, is reported to degrade selectively the presence of pectinase enzyme (present only in the colon region), and hence could be used for colon targeting.[18] Moreover, acid sensitive drugs, such as capecitabine, incorporated into beads could be protected from gastric juice, alter the residence time, and mask a bitter or unpleasant taste of the drug.[19] Various anticancer drugs have already been incorporated into beads, including irinotecan,[20] 5-flourouracil[21] and paclitaxel.[22]

In the design of the colon-targeted beads, the concentration of polymers play a critical role in developing an optimized batch. Hence, a concept of design of experiments with a 3^2 full factorial design was used for optimization. Since all possible combinations using such full factorial design could be evaluated, a greater precision was obtained in estimating the overall main factor effects.[23]

In this investigation, an attempt was made to develop a formulation which would deliver the drug specifically to the colon, and, at the same time, give controlled release in a manner

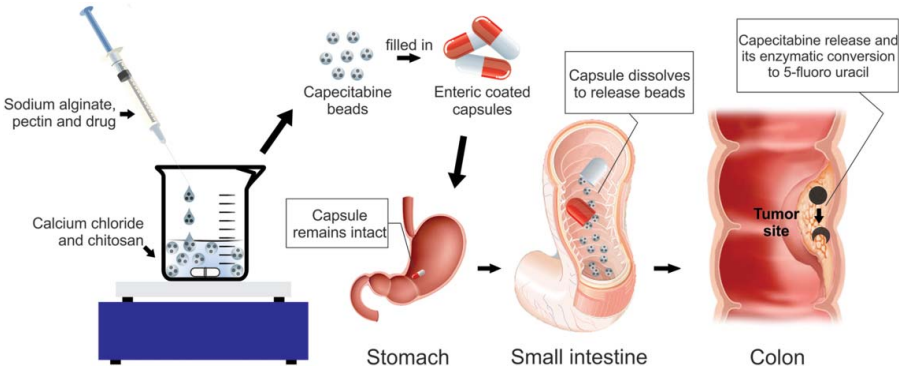

Figure 1. Diagrammatic representation of method of beads preparation and mechanism of drug transport to tumor site.

as depicted in Fig. 1. Factorial design was used to optimize two independent variables, viz., sodium alginate to pectin ratio and chitosan concentration. The effects of these variables on the percentage of entrapment efficiency (%EE) and %DR were studied.

Materials

Capecitabine was gifted by Dishman Pvt. Ltd., India. Sodium alginate and calcium chloride were purchased from SD Fine Chemicals, India. Pectin was obtained as a gift sample from Herb and Fox, Germany. Pepsin (1:1000), pancreatin, and pectinase enzymes were procured from Himedia, India. Colorectal cancer cell line (HT29) was purchased from National Center for Cell Science, India. MTT [3-(4,5 dimethylthiazol-2-yl)-2,5-diphenyltetrazolium bromide] dye, Dulbecco's modified eagle's medium (DMEM), fetal bovine serum (FBS), trypsin–ethylenediaminetetraacetic acid (EDTA) solution, penicillin–streptomycin solution and trypan blue were also purchased from Himedia, India. Chitosan was gifted by Mahtani Chitosan Pvt. Ltd., India. Dimethyl sulfoxide (DMSO) and the reagents for preparing buffer solutions as well as simulated fluids were purchased from S.D. Fine Chemicals, India.

Methods

Formulation of capecitabine beads

The beads were prepared by an ionotropic gelation technique.[24] Briefly, capecitabine, sodium alginate, and pectin were weighed accurately based on the factorial design values (Table 1) and transferred into a beaker containing 15-mL deionized water. The drug:polymer (mixture of sodium alginate and pectin) ratio of 1.5:1 was kept constant in all batches. The mixture was stirred using a magnetic stirrer for 30 min to obtain homogenous solution-A. Calcium chloride (5%) was dispersed in 35-mL deionized water in a beaker and continuously stirred for 15 min. To this, 10 mL of solution containing varying amounts of chitosan (dissolved in 2% glacial acetic acid with pH adjusted to 4.5 ± 1) was added to obtain solution-B. Then solution-A was extruded into solution-B through a hypodermic syringe with a 20-G needle (0.6-mm internal diameter) under continuous stirring. The formed beads were stirred for 30 min at 25 rpm to complete gelation reaction, and then filtered, washed

Table 1. Experimental plan of 3^2 full factorial design with observed values for different batches.

	Independent variables		Dependent variables					
Batch No.	Sodium alginate to pectin ratio, X_1	Chitosan concentration, X_2 (%)	Entrapment efficiency, Y_1 (%)*			Drug release*, Y_2 (%)		
F1	1:2 (0)	1.5 (0)	60.84 ± 1.59			67.11 ± 2.71		
F2	1:1 (−1)	2 (1)	65.24 ± 0.65			57.12 ± 2.76		
F3	1:3 (1)	1.5 (0)	52.33 ± 0.69			62.75 ± 3.08		
F4	1:3 (1)	2 (1)	61.73 ± 1.61			48.67 ± 2.54		
F5	1:2 (0)	1.5 (0)	59.56 ± 1.31			65.65 ± 2.57		
F6	1:3 (1)	1 (−1)	41.23 ± 0.72			80.25 ± 3.12		
F7	1:2 (0)	1.5 (0)	61.51 ± 1.02			66.59 ± 2.89		
F8	1:2 (0)	1.5 (0)	61.23 ± 1.04			67.26 ± 2.89		
F9	1:2 (0)	2 (1)	71.05 ± 0.73			50.81 ± 2.14		
F10	1:1 (−1)	1.5 (0)	58.05 ± 0.24			72.10 ± 2.13		
F11	1:1 (−1)	1 (−1)	43.38 ± 1.60			89.74 ± 3.75		
F12	1:2 (0)	1 (−1)	48.29 ± 0.64			83.59 ± 2.69		
Optimized batch	1:2.01	2	Observed*	Predicted	%Error[a]	Observed*	Predicted	%Error[a]
			69.29 ± 0.32	70.11	1.17	49.43 ± 0.13	51.31	3.36

*Mean ± SD, n = 3.
[a] %Error = [(Observed value − predicted value)/Predicted value] × 100.
(−1) = low level, (0) = mid level, (1) = high level.

using distilled water, and dried overnight. The unentrapped drug fraction present in the filtrate was estimated for mass balance characterization using a UV spectrophotometer at a maximum absorbance of 239.5 nm.[25] The formulated beads were stored in a desiccator until used.

Experimental design

To design colon-specific beads, it was essential to recognize major parameters in the formulation since these variables could affect the properties of the desired formulation. Hence, for the optimization of the formulation, a concept of design of experiments was used.[26] Different batches of beads were planned based on 3^2 full factorial experimental design (Design Expert®, version 8.0.3, Stat-Ease Inc., USA). For these experiments two factors were evaluated, each at three levels, and experimental trials were performed for all nine possible combinations. The independent variables selected were sodium alginate:pectin ratio (X_1) and chitosan concentration (X_2). Their levels, along with their actual and coded values, are shown in Table 1. Twelve batches of beads (including four center points) were formulated, as shown in Table 1. Percentage of drug entrapment efficiency (Y_1) and %DR (Y_2) were taken as response parameters (dependent variables). The following polynomial equation was generated by the design:

$$Y = \beta_0 + \beta_1 X_1 + \beta_2 X_2 + \beta_{12} X_1 X_2 + \beta_{11} X_1^2 + \beta_{22} X_2^2, \quad (1)$$

where β_0 is an intercept, X_1 and X_2 are the coded levels of independent factors, β_1 and β_2 are coefficients of X_1 and X_2 respectively, β_{11} and β_{22} are coefficients of quadratic terms, and β_{12} represents the coefficient of interaction.

Percentage of drug entrapment efficiency

Ten milligram of the dried beads were accurately weighed and allowed to swell for 24 h in 10-mL phosphate buffer pH 7.4. After 24 h, the solution was stirred using a magnetic stirrer for 2 h to allow complete breakage of beads. Then the solution was filtered through Whatman filter paper and analyzed at 239.5 nm using UV visible spectrophotometer,[25] and the amount of capecitabine in the total beads was calculated using the calibration curve method. Absorbance of the filtrate was measured and the percentage of drug entrapment efficiency (%EE) was calculated as given in Eq. (2):

$$\%\mathrm{EE} = \frac{\text{Actual quantity of drug present in beads}}{\text{Theoretical content of drug}} \times 100. \tag{2}$$

Micromeritic studies

Average bead size was determined using an optical microscopy technique. In all measurements 50 beads were examined, and each experiment was carried out in triplicate. The angle of repose of a pile of beads to determine their flow-ability was measured by a fixed base cone method. Briefly, the prepared beads were allowed to fall freely through a funnel fixed at 1 cm above the horizontal flat surface until the apex of the conical pile just touches the tip of the funnel. The average base radius of the cone was measured and the angle of repose was calculated using Eq. (3):

$$\text{Angle of repose}(\theta) = \tan^{-1}\left(\frac{\text{Cone height}}{\text{Average radius of cone base}}\right). \tag{3}$$

Bulk and tapped densities, as measures of the pack-ability of beads, were measured in a 10-mL graduated cylinder, to which 1 gm of sample was added, the volume occupied by the sample was noted, and the bulk density was calculated (Eq. (4)). The cylinder was tapped for 100 times and the volume occupied was again measured to calculate the tapped density (Eq. (5)):

$$\text{Bulk density} = \frac{\text{Weight of sample}}{\text{Volume occupied by sample before tapping}}, \tag{4}$$

$$\text{Tapped density} = \frac{\text{Weight of sample}}{\text{Volume occupied by sample after tapping}}. \tag{5}$$

The Carr's index and the Hausner's ratio were also calculated as measures of the powder flow properties using Eqs. (6) and (7) respectively:

$$\text{Carr's index} = \frac{(\text{Tapped density} - \text{bulk density})}{\text{Tapped density}} \times 100, \tag{6}$$

$$\text{Hausner's ratio} = \frac{\text{Tapped density}}{\text{Bulk density}}. \tag{7}$$

Microscopic studies

The beads were analyzed microscopically using an optical microscope (Nikon Digital Sight, DS-Fi20, Japan) to study their shape. The surface morphology of the beads was studied using scanning electron microscopy (SEM; JSM-5610LV, JEOL Ltd., Japan). For SEM, the samples were attached to sample stubs, silver coating was done, and these were viewed using an accelerating voltage of 15 kV and a magnification of 15,000×.

Compatibility of capecitabine with excipients

Drug-polymer interactions were studied using FT-IR spectroscopy. The studies were performed for free drug, placebo beads, and drug-loaded beads. The IR spectra of the pellets, obtained by pressing the sample–potassium bromide powder mixture by a press, were recorded using an alpha FT-IR spectrophotometer (Bruker Optik GmBH, Germany).

Thermal analysis

Differential scanning calorimetry (DSC) was used to check the entrapment of capecitabine inside beads using a DSC-60/TA-60WS thermal analyzer (Shimadzu, Japan) at a heating rate of 10°C per minute in the range of 30 to 300°C in an inert nitrogen atmosphere with a flow rate of 50 mL/min. DSC thermograms were recorded for pure drug, placebo beads, and drug-loaded beads.

Swelling index

The swelling index was studied by measuring percentage of water uptake by beads. Accurately weighed 50 mg of beads were allowed to swell in phosphate buffer pH 6.8 or 7.4 at 37°C for 4 h. The excess surface-adhered liquid drops were removed by blotting and the swollen beads were weighed again. The study was carried out for all batches in triplicate and the swelling indices of all batches were calculated using Eq. (8),[27]

$$\text{Swelling index} = \frac{(\text{Weight of swollen beads} - \text{initial weight})}{\text{Initial weight}} \times 100. \quad (8)$$

Mucoadhesivity study by In vitro wash-off test[28]

Rat colonic mucosa was used for this study. The mucosa was removed, cut into 2-cm^2 pieces, and rinsed with phosphate buffer pH 7.4. Pieces of wet rat colonic mucosa were mounted on glass slides with acrylate glue. Fifty beads were counted and spread over the surface of wet mucosa. The glass slide was then connected to a support and hung on the arm of a USP tablet disintegration test apparatus. The disintegrating test apparatus was operated such that the tissue specimen was given regular up and down movements in the beaker containing phosphate buffer at pH 6.8. The temperature was maintained at 37 ± 5°C throughout the study. The number of beads still adhering to the tissue were counted at the end of 6 h and

the percentage of mucoadhesion was calculated as per Eq. (9):

$$\% \text{ Mucoadhesion} = \frac{\text{Number of adhered beads}}{\text{Total number of applied beads}} \times 100. \quad (9)$$

In vitro Drug Release

The in vitro release of capecitabine from beads and from a marketed immediate release tablet (Xeloda®, Roche Inc., Philippines) was performed using USP type I and type II dissolution test apparatus respectively. Weighed amounts of beads filled in enteric-coated capsules were added to the basket, and dissolution was run at 75 rpm, 37 ± 0.5°C throughout the study. The dissolution media used was 900 mL of simulated gastric fluid (SGF) for the first 2 h, simulated intestinal fluid (SIF) for the next 3 h, and, lastly, simulated colonic fluid (SCF) for 4 h. Samples, measuring 5 mL, were collected at predetermined time intervals for analysis. Fresh media was replenished to maintain the bath volume. After performing the drug release study, the data were fitted to various models to understand the release mechanism of the drug from the formulation. The best model was analyzed by its correlation coefficient (R^2) value. An R^2 value nearest to 1 indicates the best release model. Different models applied for drug release were zero-order release, first-order release, Higuchi's model, Hixon–Crowell's model, and Korsmeyer–Peppas' model.[29]

In vitro cytotoxicity study

The anticancer potential of capecitabine beads was evaluated and compared with its marketed tablet (Xeloda®, Roche Inc., Philippines) using the MTT-based cytotoxic assay on the HT29 colorectal cancer cells. The MTT assay involves colorimetric estimation of purple-colored formazan developed via reduction of yellow-colored MTT dye by mitochondrial dehydrogenase within living cells, and, thereby, gives a direct estimate of the number of viable cells. Briefly, 5×10^3 cells/mL in their exponential growth phase were plated in 96-well flat-bottom tissue culture plates and incubated at 37°C with 5% CO_2 in an incubator for 24 h to allow the cells to adhere and grow as a monolayer. Concurrently, optimized formulation of capecitabine beads and the marketed Xeloda® tablet (equivalent to 400-mg drug) were incubated in simulated body fluids in the same way as adapted for in vitro drug release studies, and 5-mL samples were withdrawn at 1-h interval starting from zero time for the estimation of capecitabine concentration and its cytotoxicity. In the well plates, when a monolayer was formed, the supernatant was removed, the monolayer washed once with phosphate buffer saline at pH 7.4, and 100-μL of the above-mentioned samples were added to cells in the well plate. The plate was then incubated at 37°C and 5% CO_2 for 4 h. At the end of the exposure period, the medium was removed from all the wells, and the wells were washed with phosphate buffer saline at pH 7.4. Then 50 μL of MTT dye solution (1 mg/mL) was added to all wells and incubated for 4 h. After 4 h the plate was taken out and the medium, along with MTT, was removed from the wells without disturbing formazan crystals. Cell lysis and solubilization of formazan crystals were obtained by adding 200 μL of DMSO to all the wells and their absorbance were measured using a microplate reader at a wavelength of 540 nm.

Stability studies

To conduct the stability study, an optimized batch was prepared and filled into hard gelatin enteric-coated capsules in stability chamber at 25 ± 2°C and 60 ± 5% RH and at accelerated conditions of 40 ± 2°C and 75 ± 5% RH. At intervals of 0, 1, 2, and 3 months, the formulations were characterized for percentage of drug content and in vitro drug release as per the procedures mentioned in above sections.

Statistical analysis

Statistical optimization was performed using Design-Expert® version 8.0.3 (Stat-Ease Inc., USA). All measured data were expressed as mean ± standard deviation (SD). All other data were analyzed by simple statistics.

Results

When an aqueous solution of sodium alginate and pectin containing capecitabine is dropped into a counter-ions solution (calcium), the metallic calcium ions rapidly diffuse into alginate/pectin solution droplets because of their smaller size than polymeric ions, and bind to unoccupied binding sites on these polymers to form gelled beads instantaneously. This ionotropic gelation process resulted in spherical beads with mean diameters of 4–5 mm before drying.

Experimental design

The observed values of two response variables, viz., %EE and %DR for all 12 batches of factorial design are shown in Table 1. The selected independent variables were found to influence the two responses measured. All batches showed entrapment efficiency in the range of 41.23 to 71.05% and drug release from 48.67 to 89.74% in 9 h. For both responses, the various models fitted were linear, two-factor interaction, quadratic, and cubic models, and their values obtained are shown in Table 2. The cubic models gave the highest R^2 value but were aliased, and hence the quadratic models having higher R^2 compared with the rest of the models were selected. Using the ANOVA provision available in the software, the polynomial equations involving the main effects and interaction factors were determined based on various statistical parameters as shown in Table 3. The full quadratic model was further reduced by omitting the interactive term X_1X_2, which was found insignificant (p-value > 0.05) for both response variables (Table 3). The effect of independent variables on %EE could be described by the following quadratic equation: $Y_1 = 60.98 - 1.90X_1 + 10.85X_2 - {X_1}^2 - 1.70\ {X_2}^2$, while the equation for %DR was generated as follows: $Y_2 = 66.49 - 4.55X_1 - 16.16X_2 + 1.26\ {X_1}^2 + 1.03\ {X_2}^2$. In the equation, positive values indicate that the response increases with the factor and vice versa.[30] Chitosan concentration (X_2) showed the greatest influence on both responses, as indicated by its highest exponent in the equation. It directly affected %EE, while it inversely affected %DR.

The reduced quadratic model of Y_1 showed R^2, adjusted R^2, and predicted R^2 values to be 0.9918, 0.9871, and 0.9721 respectively (Table 2). Adequate precision of 45.395 was obtained while standard deviation (SD) and coefficient of variation were 1.02 and 1.78% respectively. For response Y_2, the reduced model showed R^2, adjusted R^2, and predicted R^2 values to be

Table 2. Model fit summary statistics.

Models		R^{-2}	Adjusted R^{-2}	Predicted R^{-2}	SD	Remarks
Response (Y_1)						
Linear		0.8275	0.7892	0.6397	4.11	—
2FI		0.8280	0.7636	0.1604	4.35	—
Cubic		0.9964	0.9901	0.8691	0.89	Aliased
Quadratic	Full	0.9923	0.9859	0.9463	1.06	Suggested
	Reduced[#]	0.9918	0.9871	0.9721	1.02	
Response (Y_2)						
Linear		0.9922	0.9905	0.9832	1.21	—
2FI		0.9924	0.9895	0.9591	1.27	—
Cubic		0.9987	0.9964	0.9540	0.74	Aliased
Quadratic	Full	0.9986	0.9974	0.9948	0.64	Suggested
	Reduced[#]	0.9984	0.9975	0.9959	0.62	—

[#]By omitting insignificant model terms (p-value > 0.05) from full quadratic model.

0.9984, 0.9975, and 0.9959 respectively (Table 2). Adequate precision of 103.511 was obtained while SD and coefficient of variation were 0.62 and 0.92% respectively.

With the help of the software, the response surface analysis plots were constructed as three-dimensional (3D) model graphs to understand the interaction effects of two independent variables on the responses. The graphs of %EE and %DR obtained are shown in Figs. 2 (a) and (b). The amount of unentrapped drug of different batches varied from 28.90–58.70% (Table 4), while the optimized batch gave 30.7% free drug.

Micromeritic studies

Micromeritic properties were determined for all batches, and the results, as shown in Table 4, were found to be within limits. The angle of repose between 20° and 30°, Carr's index between 12 and 20, and Hausner's ratio less than 1.25 indicate good flow properties.[6] The average particle size was found to be in the range of 1090 to 1493 μm. It can be seen that as the polymer concentration was increased, the particle size also increased significantly.

Table 3. Regression coefficients and p-values for different quadratic model terms.

	Full model				Reduced model			
	Y_1		Y_2		Y_1		Y_2	
Source	Regression coefficient	p-value	Regression coefficient	p-value	Regression coefficient	p-value	Regression coefficient	p-value
Model	—	<0.0001	—	<0.0001	—	< 0.0001	—	<0.0001
Intercept	60.98	—	66.49	—	60.98	—	66.49	—
X_1	−1.90	0.0047	−4.55	<0.0001	−1.90	0.0026	−4.55	<0.0001
X_2	10.85	<0.0001	−16.16	<0.0001	10.85	< 0.0001	−16.16	<0.0001
X_1X_2	−0.34	0.5458	0.26	0.4442	—	—	—	—
X_1^2	−6.18	<0.0001	1.26	0.0178	−6.18	< 0.0001	1.26	0.0128
X_2^2	−1.70	0.0395	1.03	0.0376	−1.70	0.0290	1.03	0.0296
Lack of fit	—	0.2865	—	0.6952	—	0.3482	—	0.7319

X_1: Sodium alginate to pectin ratio; X_2: chitosan concentration (%).

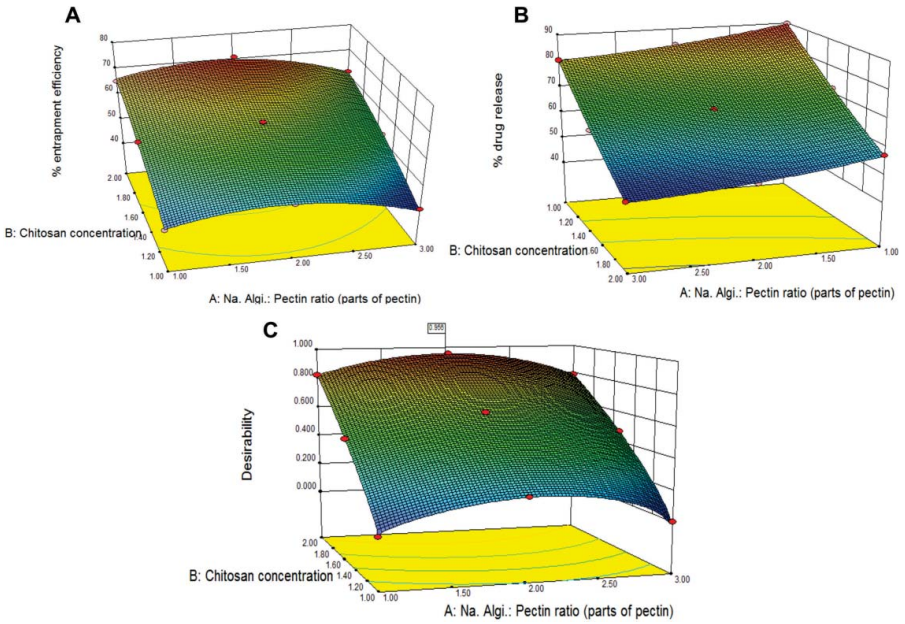

Figure 2. Response surface plot (3D) showing effect of sodium alginate:pectin ratio and chitosan concentration on (a) %EE, and (b) %DR. (c) Desirability plot of optimized variables.

Microscopic studies

An optical microscopic image of the optimized formulation (Fig. 3) shows that the beads were almost spherical in shape. Moreover, its SEM image (Fig. 4) depicts their smooth surface.

FT-IR study

FT-IR spectra of capecitabine, blank beads, and drug-loaded beads were recorded, and the graphs obtained are shown in Fig. 5. The capecitabine FT-IR spectra gave major peaks at 1757, 1333, 1242, and 1117 cm^{-1}. These peaks were found absent in the blank beads, while they were found to be present in the drug-loaded beads spectra.

DSC study

Differential scanning calorimetry thermograms of capecitabine bulk powder, blank beads, and drug-loaded beads were recorded and graphs obtained are shown in Figs. 6(a)–(c) respectively. Capecitabine pure drug gave a sharp peak at 121.9°C and a number of other peaks at higher temperature, while they were not found in blank beads and drug-loaded beads.

Swelling index

The results of swelling index for all batches are shown in Table 5. The swelling index was found to be higher in phosphate buffer pH 7.4 as compared with phosphate buffer pH 6.8

Table 4. Results of characterization of different batches.

Batches and their composition									
Code	X_1[#]	X_2[#]	Free drug[*] (%)	Average particle size (μm)	Angle of repose[*]	Bulk density[*] (g/cm^3)	Tapped density[*] (g/cm^3)	Carr's index[*] (%)	Hausner's ratio[*]
F1	1:2	1.5	39.10 ± 1.27	1322.61	23.65 ± 0.02	0.585 ± 0.009	0.725 ± 0.009	19.35 ± 1.13	1.24 ± 0.02
F2	1:1	2	34.36 ± 1.69	1431.11	25.24 ± 0.05	0.590 ± 0.009	0.726 ± 0.005	18.69 ± 1.63	1.23 ± 0.02
F3	1:3	1.5	52.33 ± 0.69	1400.11	24.72 ± 0.04	0.581 ± 0.004	0.720 ± 0.012	19.34 ± 0.98	1.24 ± 0.01
F4	1:3	2	38.20 ± 1.87	1493.11	28.72 ± 0.03	0.660 ± 0.009	0.772 ± 0.008	14.55 ± 0.96	1.17 ± 0.01
F5	1:2	1.5	40.44 ± 1.83	1329.58	23.63 ± 0.03	0.637 ± 0.002	0.764 ± 0.006	16.70 ± 0.87	1.20 ± 0.01
F6	1:3	1	58.70 ± 1.23	1188.38	22.68 ± 0.02	0.605 ± 0.003	0.695 ± 0.003	12.90 ± 0.74	1.15 ± 0.01
F7	1:2	1.5	38.40 ± 1.54	1326.25	23.68 ± 0.02	0.660 ± 0.010	0.766 ± 0.004	13.75 ± 1.78	1.16 ± 0.02
F8	1:2	1.5	38.70 ± 1.28	1322.21	23.67 ± 0.03	0.653 ± 0.003	0.758 ± 0.004	13.89 ± 0.48	1.16 ± 0.01
F9	1:2	2	28.90 ± 1.58	1467.38	26.80 ± 0.09	0.631 ± 0.005	0.764 ± 0.004	17.49 ± 0.72	1.21 ± 0.01
F10	1:1	1.5	41.90 ± 1.36	1234.88	23.43 ± 0.31	0.665 ± 0.003	0.772 ± 0.005	13.90 ± 0.40	1.16 ± 0.01
F11	1:1	1	56.58 ± 1.61	1090.11	20.25 ± 0.10	0.685 ± 0.004	0.801 ± 0.006	14.55 ± 1.16	1.17 ± 0.02
F12	1:2	1	51.72 ± 1.64	1141.88	20.58 ± 0.12	0.657 ± 0.005	0.755 ± 0.004	12.94 ± 0.52	1.15 ± 0.01
Optim. batch	1:2.01	2	30.70 ± 0.26	1395.76	25.98 ± 0.07	0.602 ± 0.01	0.736 ± 0.05	18.20 ± 1.51	1.22 ± 0.09

[*]Mean ± SD, n = 3.
[#]X_1: Sodium alginate to pectin ratio; X_2: Chitosan concentration (%).

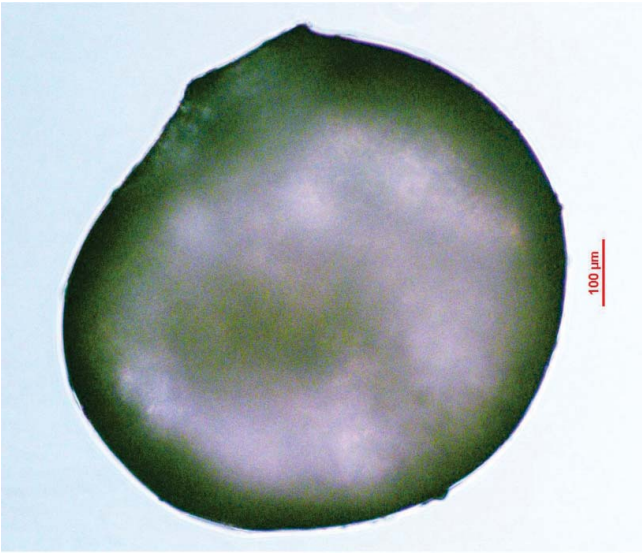

Figure 3. Optical microscopic image of a bead of optimized formulation.

for all batches. Pectin and chitosan had negative effects on the swelling index and the effect was more pronounced for changes in the concentration of chitosan.

Mucoadhesivity study by in vitro wash-off test

Percentage of mucoadhesion for different batches of beads are shown in Table 5. It could be seen from the results that the highest mucoadhesion of 76% was observed with batch F2 containing the highest concentration of chitosan (2%) and the least pectin amount. The least mucoadhesion of 20%, was observed with batch F12 containing least chitosan (1%) and the pectin amount at mid level.

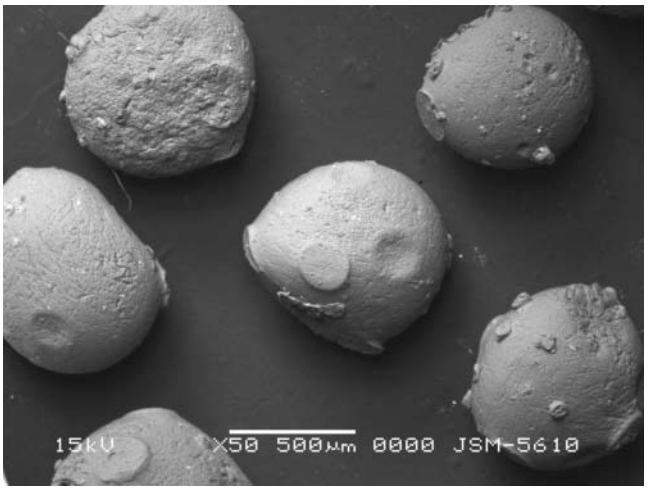

Figure 4. SEM image of optimized formulation beeds.

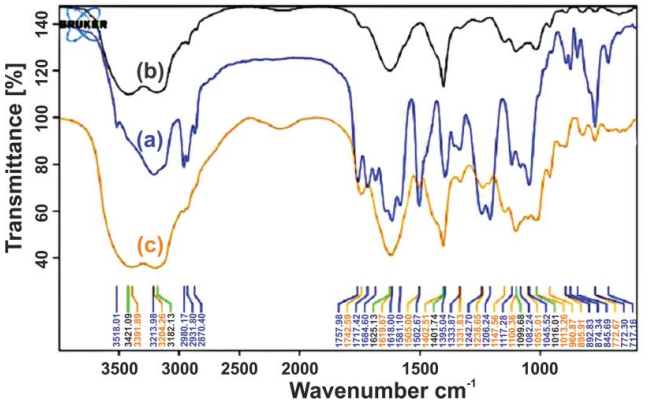

Figure 5. FT-IR spectra of (a) free drug, (b) blank beads, and (c) drug-loaded beads.

In vitro drug release

Comparative dissolution studies were carried out for all batches and the cumulative percentage of capecitabine release was plotted against time (*t*). The graph obtained is shown in Fig. 7. There was no release in SGF in 2 h. Upon change of media to SIF, the drug started to release slowly and by the completion of 5 h, the drug release varied only up to 2% release in different batches. When the media was again replaced by SCFt 9 h, the release in different batches varied from 48 to 89% (Table 1; Fig. 7). Further, upon applying different kinetic models to the data of optimized formulation, the highest R^2 value of 0.8428 was found for the zero-order release model (Table 6). On the other hand, for the first order, Higuchi's, Hixson–Crowel, and Korsmeyer–Peppas models, R^2 values were found to be 0.7253, 0.7126, 0.8019 and 0.7931 respectively. The value of diffusion exponent, *n*, was 2.1905, indicating a super case II transport mechanism.

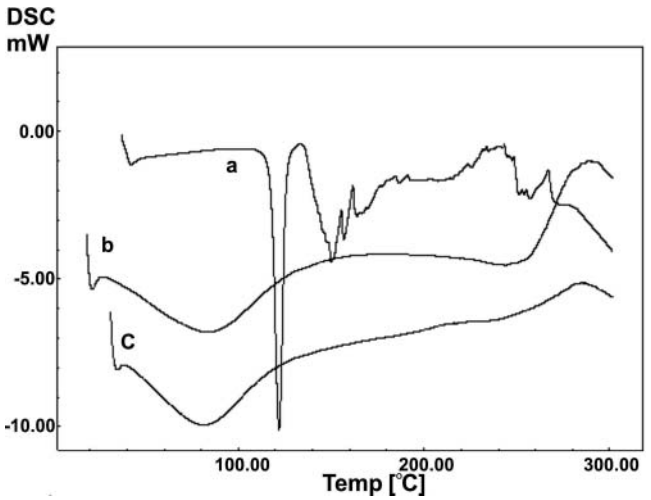

Figure 6. DSC thermograms of (a) capecitabine, (b) blank beads, and (c) drug-loaded beads.

Table 5. Results of swelling and mucoadhesion studies of different batches of beads.

Batches and their composition			Swelling index in phosphate buffer pH 6.8*	Swelling index in phosphate buffer pH 7.4*	Mucoadhesion (%)
Code	X_1#	X_2#			
F1	1:2	1.5	612 ± 2.58	1906 ± 3.50	48
F2	1:1	2	376 ± 2.87	1534 ± 3.46	76
F3	1:3	1.5	574 ± 2.81	1754 ± 2.35	36
F4	1:3	2	244 ± 1.99	1122 ± 2.90	64
F5	1:2	1.5	620 ± 5.29	1935 ± 3.12	46
F6	1:3	1	712 ± 1.67	2376 ± 2.61	12
F7	1:2	1.5	632 ± 1.54	1926 ± 2.54	48
F8	1:2	1.5	647 ± 2.64	1941 ± 2.59	48
F9	1:2	2	292 ± 2.02	1329 ± 2.67	72
F10	1:1	1.5	668 ± 2.57	2172 ± 2.18	56
F11	1:1	1	867 ± 2.44	2703 ± 2.30	28
F12	1:2	1	792 ± 2.19	2529 ± 1.52	20
Optimized batch	1:2.01	2	267 ± 2.22	1607 ± 2.78	70

* Mean ± SD, n = 3.
# X_1: Sodium alginate to pectin ratio; X_2: Chitosan concentration (%).

In vitro cytotoxicity study

Blank beads did not show any cytotoxicity against HT-29 cells whereas the optimized beads did. Hence, the formulation can be effectively tested for its anti-cancer property. The marketed Xeloda tablet showed rapid dissolution and achieved maximum drug concentration in 1 h. Consequently, a quick decline in the percentage viability of HT-29 cells to 6.67%

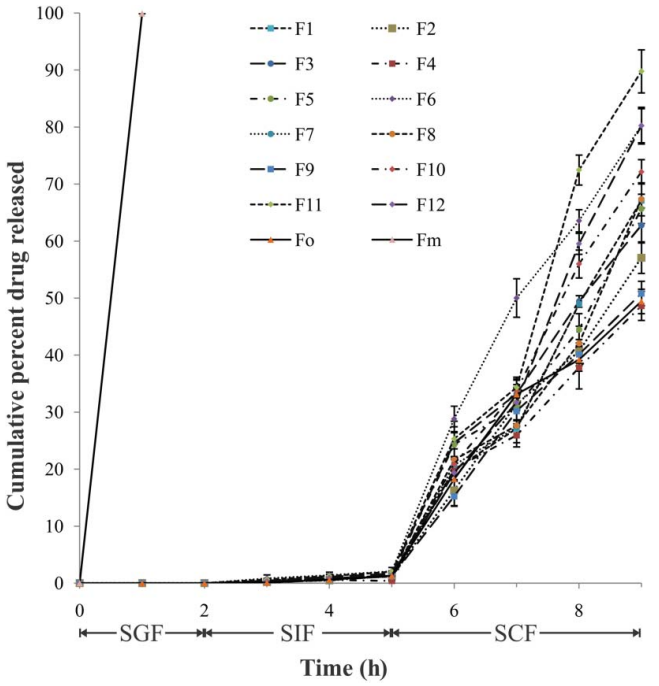

Figure 7. In vitro drug release profile of optimized and marketed formulation.

Table 6. Kinetics and mechanism of drug release from optimized capecitabine-loaded beads.

Release models	Equations	R^2	n	Release mechanism
Zero order	$M_t = Kt$	0.8428	—	($n = 0.5$): Fickian diffusion
First order	$\ln[1-(M_t/M_0)] = -Kt$	0.7253	—	($0.5 < n < 1.0$): Non-Fickian diffusion
Higuchi	$M_t = K\sqrt{t}$	0.7126	—	($n = 1.0$): Case II (zero-order) transport
Hixson–Crowel	$\sqrt[3]{M_0} - \sqrt[3]{M_t} = Kt$	0.8019	—	($n > 1.0$): Super case II transport
Korsmeyer–Peppas	$\ln(M_t/M_0) = \ln K + n \ln t$	0.7931	2.1905	

M_0 = Initial amount of drug present, M_t = amount of drug released at time t, K = release rate constant, n = diffusion exponent.

(93.33% cell death) was observed (Fig. 8). On the other hand, the optimized beads showed only 3.67% cell death (96.33% cell viability) at the end of 6 h, which was increased gradually to 67.92% (32.08% cell viability) in the next 3 h because of increased drug release in SCF.

Stability study

The results of stability studies at 25°C, 60% RH and 40°C, 75% RH of the optimized formulation are shown in Table 7. There were no significant changes in drug content and drug release for the changes in both storage temperatures and related RH conditions.

Discussion

In recent years, the use of natural polymers as carriers that are degraded specifically by colonic bacteria seems to be the most promising method for colonic delivery of drugs.[13,31] Among such polymers, pectin shows high specificity for colonic drug release, but since it

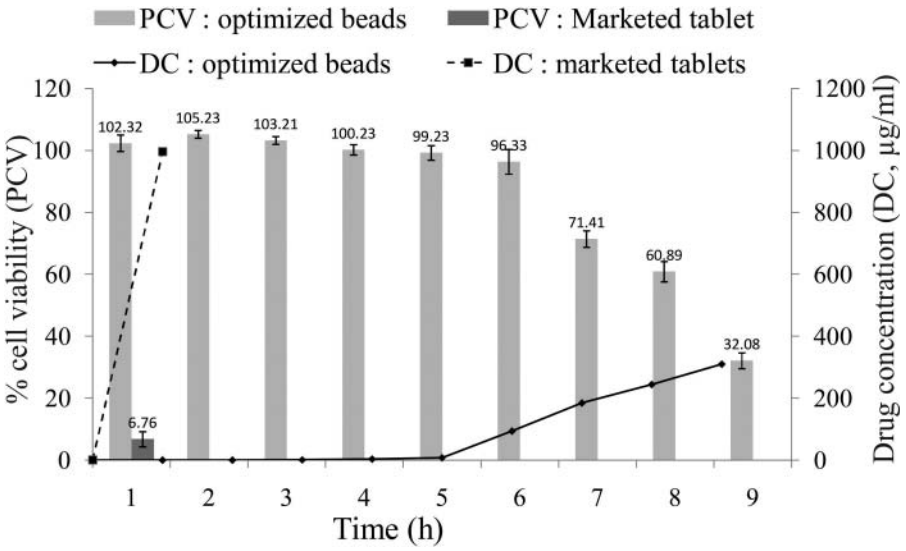

Figure 8. In vitro cytotoxicity profile of optimized and marketed formulation correlating drug concentration and percentage of cell viability up to 9 h.

Table 7. Stability study data for different storage conditions of optimized capecitabine-loaded beads; storage in air prior to testing.

	Drug content* (%)		Drug release* (%)	
Time (months)	25 ± 2°C/60 ± 5% RH	40 ± 2°C/75 ± 5% RH	25 ± 2°C/60 ± 5% RH	40 ± 2°C/75 ± 5% RH
0	63.12 ± 0.37	63.12 ± 0.37	51.52 ± 0.12	51.52 ± 0.12
1	63.06 ± 0.39	62.46 ± 0.31	51.47 ± 1.58	50.87 ± 0.08
2	62.92 ± 1.21	62.34 ± 0.29	50.63 ± 1.34	50.73 ± 0.31
3	62.80 ± 1.68	62.30 ± 0.98	50.44 ± 1.59	50.07 ± 1.54

* Mean ± SD, $n = 3$.

exhibits high solubility and swelling in aqueous media, it is unable to effectively prevent drug release during transit through the upper gastrointestinal tract.[32] To overcome this difficulty, calcium ions were used in the present investigation; they form intermolecular cross-links with pectin and alginate, resulting in an "egg-box" structure. Additional use of chitosan in calcium–pectinate beads has already been recognized as stabilizing the "egg-box" structure and thereby reducing the problem of drug leaching during bead preparation.[16] Moreover, use of sodium alginate along with pectin resulted in an increase in capecitabine entrapment. Hence, we formulated the beads using a combination of polymers: sodium alginate and pectin along with chitosan. Now in order to get capecitabine beads with high entrapment and controlled colonic release, concentrations of sodium alginate, pectin, and chitosan were statistically optimized via factorial design. Accordingly, 12 batches were taken as per the 3^2 full factorial design with varying sodium alginate/pectin ratio and chitosan concentration (X_2). For measuring the response, two parameters were selected – %EE and %DR. Quadratic models were found to best fit both responses because of their higher R^2 values than for other models (Table 2), and hence were further evaluated statistically by applying one-way ANOVA (considering $p < 0.05$ as statistically significant). "Model p-value" of <0.0001 for both Y_1 and Y_2 implied that the fitted quadratic models were significant (Table 3). There is only 0.01% chance that the large model p-value could occur due to noise. Model terms X_1, X_2, X_1^2, and X_2^2 had a p-value of <0.05 (Table 3) for both responses Y_1 and Y_2 and hence were considered significant. "Lack of fit F-value" of 1.69 and 0.52 for Y_1 and Y_2, respectively, indicated that lack of fit was not significant relative to pure error. There were 34.82% and 73.19% chances of large "lack of fit F-value" for Y_1 and Y_2, respectively, which could occur due to noise. Nonsignificant lack of fit is desirable.[33] The values of correlation coefficient of the generated polynomial equations for Y_1 and Y_2 were found to be 0.9918 and 0.9984 respectively, indicating good fits. The closeness of predicted R^2 to the adjusted R^2 was within the desirable range of 0.2 (Table 2). These were 45.395 for Y_1 and 103.51 for Y_2, indicating an adequate signal. Further, polynomial equations were generated for both responses using the software as described in the Experimental Design section. It was found that in the polynomial equation generated for Y_1, chitosan concentration (X_2) had a higher and positive effect on Y_1 in comparison with sodium alginate:pectin ratio (X_1), which showed a negative effect. Exponents of X_1 and X_2 in the polynomial equation generated for Y_2 had minus signs, indicating that both factors showed a negative effect on %DR. A higher value of the exponent of X_2 (−16.16) indicated that chitosan concentration has a more significant effect on the %DR than the exponent of X_1 (−4.55).

The influence of both factors on the responses were further elucidated by the response surface method. This method is a widely used approach for the development and

optimization of formulations to understand as fully as possible the effects of factors and their levels on a model to predict the responses inside the domain. The response surface method generally gives 2D contour graphs and 3D response surface graphs. The latter is more useful for understanding the main effects and the interaction effects of factors on responses.[34,35] Therefore, 3D graphs were generated for both the responses. In the case of Y_1 it was found that on increasing pectin concentration, the entrapment efficiency increased up to an optimum value and then with further increase in pectin concentration, it decreased. During gelation, alginate and pectin bind with calcium to form calcium–alginate, calcium–pectinate, and calcium–alginate–pectinate networks[36] that may be required as protective layers to maximize the drug entrapment. An initial increase in %EE with increasing pectin fraction signified that the pectinate network was more effective in the prevention of diffusion of drug than the alginate network. However, beyond the optimum pectin level, a further increase in pectin caused reduction in %EE, which indicated the need for a ratio of both polymers. Moreover, on increasing the chitosan concentration, %EE increased significantly. This may be due to the fact that higher chitosan concentration results in the formation of a denser matrix structure that probably decreases the loss of drug to the curing medium. In addition, electrostatic attraction between the negatively charged capecitabine and the positively charged chitosan also becomes stronger, promoting the drug entrapment.[16]

As shown by the response surface plot for Y_2 (Fig. 2b), as the pectin and chitosan concentration was increased, the %DR decreased. Diffusion media penetrated into the chains of alginate, forming hydrogen bridges through the hydroxyl and –COO groups of alginate. As a result, the beads became hydrogel and their diameter increased, resulting in the diffusion of drug. Increasing pectin ratio with decreasing sodium alginate resulted in decreased drug release. This may be due to the alginate beads having insufficient cross-linking density to prevent drug molecules from diffusing out. Moreover, increasing chitosan also decreased the drug release. This was expected since on increasing pectin and chitosan amounts, the interaction between the three polymers increased cationic chitosan ($–NH^{3+}$) complexes with anionic sodium alginate and pectin (–COO), forming the egg-box structures, which decreased the diffusion of drug outwards from the interiors of the beads, leading to decreased drug release.[37]

To obtain optimized formulation, numerical optimization was performed in the software. Desirabilities were fed into the software as constraints for responses. The optimum formulation was based on set criteria of maximum drug entrapment and minimum drug release. Figure 2(c) shows the desirability (0.956) of the optimized formulation predicted by the software; the predicted values were in the sodium alginate:pectin ratio of 1:2.01 and 2% chitosan concentration. This new batch of beads was formulated as per the same procedure, and the responses were measured. The observed values of the responses are shown in Table 1 along with the percentage error to validate the method. The observed values were close to the predicted values of the software, which proves the validity of the optimization method of the software.

The results of micromeritic studies indicated that an increase in chitosan concentration led to an increase in particle size. Moreover, increasing the pectin concentration also resulted in a slight increase in particle size. This phenomenon could be due to the fact that both alginate and pectin bind with chitosan, resulting in an increase in viscosity of the extruded solution that ultimately increased the emulsion droplet size and hence led to the increased beads size.

The morphological evaluation of the optimized batch was done by optical microscopy and SEM analysis. These images confirmed that the formulated beads were spherical in shape with a relatively smooth surface texture. Moreover, in the SEM images, no drug crystals were found on bead surfaces, which indicate that the drug particles were present in the form of a finely dispersed state in the polymeric matrix of beads. Similar results were found previously for ibuprofen buoyant beads formulation[38] and cloxacillin-loaded alginate beads.[34]

The chemical compatibility between capecitabine and other formulation components (excipients) was ensured using an FT-IR study. In the spectrum of capecitabine there are sharp peaks at 1757, 1333, 1242, and 1117 cm^{-1} corresponding to C=O stretching vibrations (pyrimidine carbonyl), C-N bending vibrations, N-H bending vibrations (tetrahydro furan), and C-F stretching vibrations respectively.[39] These peaks were absent in blank beads, while they were found in drug-loaded beads. This confirms that no chemical interaction was found between the drug and polymers, thus confirming drug compatibility with these excipients.

Thermal analysis of capecitabine bulk powder and capecitabine-loaded beads was conducted using DSC. These experiments measure the heat gain or loss from chemical or physical changes within a sample as a function of temperature. In the DSC thermogram of capecitabine there was a sharp endothermic peak at 121.9°C, which nearly corresponded to the melting point of capecitabine (116–118°C). This peak was absent in the thermogram of loaded beads formulation, confirming complete drug entrapment in polymer matrix. Similar results were obtained in piroxicam-loaded pectin–alginate beads.[40]

Swelling of beads was studied and the swelling index was calculated for all batches. When beads come in contact with aqueous media, the polymers imbibed water and swelled due to the presence of physical–chemical cross-links in the hydrophilic polymer network. These cross-links prevented the dissolution of polymers, thus maintaining the physical integrity of beads. The swelling behavior of polymers in beads has been reported as one of the significant factors for controlling the drug release in drug delivery systems.[41] An optimum amount of cross-linking is required to maintain a balance between swelling and dissolution.[42] Moreover, the swelling behavior of polymers in beads depends on the pH, ionic strength, and ionic composition of medium.[43] Therefore, swelling studies were carried out in different pH conditions. It was found that an increase in pectin and chitosan concentrations in beads resulted in decreased swelling. The reason may be that the swelling of dry beads is mainly attributed to the hydration of hydrophilic groups of alginate. The presence of chitosan might reduce the interaction of Ca^{2+} with the media, thus reducing the swelling, while pectin also has lesser hydrophilicity, leading to lesser swelling. At higher pH (media pH 7.4), significantly higher swelling was found for all batches as compared with pH 6.8 ($p < 0.05$; Table 5), which might be the reason that the presence of phosphate ions at higher pH displaces Ca^{2+} ions within the beads. This may result in increased swelling as compared with that at pH 6.8.[44,45]

Many polymers exhibit properties of adhesion with mucous membranes, and hence a mucoadhesivity study was performed for all formulation batches. As can be seen from the results (Table 5), the mucoadhesion order of polymers was found to be chitosan > sodium alginate > pectin. The basis of mucoadhesion could be described in terms of electronic theory: electron transfer occured between the positively charged chitosan and sodium alginate polymers of the formulation and the negatively charged mucus glycoprotein network. This led to the formation of an electrical double layer that resulted in adherence to beads for a

longer time. Moreover, increased polymer concentrations resulted in increased viscosity of gel that was formed and ultimately led to higher adhesion. This helps in the release of drug in a sustained manner before the beads were eroded away.[45]

The formulated beads were tested in an in vitro dissolution study under conditions mimicking the stomach, the small intestines, and the colon to evaluate the potential of this formulation for colon-specific drug delivery. The results showed that due to enteric capsules drug release was effectively suppressed in SGF pH 1.2 with no release (Fig. 7). Further, in SIF pH 6.8, the enteric-coated capsules started to dissolve and the beads came in contact of physiological fluid with near neutral pH. Owing to the presence of pectin, there was only about 2% release in all batches (Fig. 7). This release might be due to the presence of drug on the outer surface of beads. Later, when the media was replaced by SCF that contained pectinase, the pectin started to be digested by enzyme, resulting in an initial burst release starting at 5 h and varying from 15 to 28% in different batches by the 6th h (Fig. 7). Subsequently, controlled release was observed up to 9 h with slower release in batches containing higher amounts of pectin and chitosan. This was expected since cationic chitosan complexes with anionic alginate and pectin form an egg box structure whose density increases with increasing concentration of polymers. This resulted in decreased diffusion of drug outwards from the interiors of beads, leading to decreased drug release. Moreover, the chitosan chains contained amine groups protonated by acetic acid, such as present in chitosan acetate. At physiological pH some of the amine groups might be deprotonated and those that remain protonated acted as a barrier for the penetration of media and drug release. This resulted in drug release at a slow rate, and hence higher chitosan led to controlled drug release. The release of drug followed zero order and super case II (relaxational) transport mechanisms (Table 6). This was in accordance with a published report suggesting relaxational release associated with stress and state-transition in hydrophilic polymers which swell in water or biological fluids and lead to polymer disentanglement and erosion.[46] In the case of the currently marketed sample, the tablet released up to 99.62% of drug within an hour due to the absence of any matrix or other system that could control the release.

In vitro cell cytotoxicity was performed using the MTT assay for blank and drug-loaded beads. The non-cytotoxicity found for blank beads indicated their safe use as a drug delivery system. The marketed sample released the total drug in 1 h, leading to high cell death; 6.67% cell viability was obtained, which means that 93.33% cell death of HT-29 cells occurred using the marketed sample. In the case of optimized beads, there was less cytotoxicity (3.67% cell death) up to 6 h. This means that beads meant for colon targeting would show much less cytotoxicity before they reach the colon region. Moreover, after 6 h, there was high cell death, up to 67.92% from 6 to 9 h (cell viability – 32.08%; Fig. 8), depicting good cytotoxicity at the colon despite slow drug release.

The result of stability studies showed that there was no significant change in the percentage of drug content and in vitro drug release of capecitabine-loaded beads immediately after production to three months of storage prior to the tests (Table 7), indicating that the developed formulations were stable.

Conclusions

In order to impose spatial as well as temporal control over capecitabine delivery for the treatment of colonic cancer, alginate–pectin–chitosan beads containing capecitabine were

prepared successfully. The formulation with an alginate:pectin ratio of 1:2.01 and chitosan concentration of 2% w/v was considered optimum based on their most desirable in vitro characteristics, viz., 69.29% EE and 49.43% DR in SCF in 4 h. Smooth surface spherical beads with no evident drug crystals were observed in the SEM images of optimized batch. The disappearance of drug's endothermic peak in DSC of optimized batch reflected complete entrapment and miscibility or dispersion of drug in polymer matrix. Compatibility among the excipients was established using infrared spectroscopy. Optimized beads were also found to possess a higher swelling index in phosphate buffer at pH 7.4 than at pH 6.8, as well as substantial mucoadhesion (70%). In vitro MTT assay indicated considerable toxicity (67.92% cell death) by optimized beads during 4 h of drug release (49.43%) in SCF. The results suggested the suitability of capecitabine-loaded beads as a colon-targeted delivery system. However, pharmacokinetic and targeting studies are still needed to give us a better idea of the performance of formulated beads in vivo.

Acknowledgment

The authors acknowledge the Technology Information, Forecasting and Assessment Council (TIFAC), Department of Science & Technology, Government of India, New Delhi for providing research facilities to the team.

References

1. Ferlay, J.; Soerjomataram, I.; Dikshit, R.; Eser, S.; Mathers, C.; Rebelo, M.; Parkin, D.M.; Forman, D.; Bray, F. Cancer incidence and mortality worldwide: sources, methods and major patterns in GLOBOCAN 2012. Int. J. Cancer **2015**, *136*, E359–386.
2. Parkin, D.M.; Bray, F.; Ferlay, J.; Pisani, P. Estimating the world cancer burden: Globocan 2000. Int. J. Cancer **2001**, *94*, 153–156.
3. Cohen, A.; Minsky, B.; Schilsky, P., Colorectal cancer. In *Cancer: Principles & Practice of Oncology*; DeVita, V.T., Hellman, S. and Rosenberg, S.A., Eds.; Lippincott Williams & Wilkins: Philadelphia, PA, **2005**, pp. 929–977.
4. Sharma, S.; Saltz, L.B. Oral chemotherapeutic agents for colorectal cancer. Oncologist **2000**, *5*, 99–107.
5. DeMario, M.D.; Ratain, M.J. Oral chemotherapy: rationale and future directions. J. Clin. Oncol. **1998**, *16*, 2557–2567.
6. Narasimha Rao, R.; Sampath Kumar, M.; Dileep Kumar, K.; Vineeth, P. Formulation and evaluation of capcitabine microspheres. Int. J. Pharm. Technol. **2011**, *3*, 2598–2632.
7. Latha, A.; Selvamani, P.; Naveenkumar, P.; Ayyanar, P.; Silambarasi, T. Formulation and evaluation of capecitabine nanoparticles for cancer therapy. Int. J. Biol. Pharm. Res. **2012**, *3*, 477–487.
8. Agnihotri, S.A.; Aminabhavi, T.M. Novel interpenetrating network chitosan-poly(ethylene oxide-g-acrylamide) hydrogel microspheres for the controlled release of capecitabine. Int. J. Pharm. **2006**, *324*, 103–115.
9. Gao, S.Q.; Sun, Y.; Kopeckova, P.; Peterson, C.M.; Kopecek, J. Antitumor efficacy of colon-specific HPMA copolymer/9-aminocamptothecin conjugates in mice bearing human-colon carcinoma xenografts. Macromol. Biosci. **2009**, *9*, 1135–1142.
10. Laroui, H.; Dalmasso, G.; Nguyen, H.T.; Yan, Y.; Sitaraman, S.V.; Merlin, D. Drug-loaded nanoparticles targeted to the colon with polysaccharide hydrogel reduce colitis in a mouse model. Gastroenterology **2010**, *138*, 843–853.
11. Kumar, P.; Mishra, B. Colon targeted drug delivery systems – an overview. Curr. Drug Delivery **2008**, *5*, 186–198.
12. Van den Mooter, G. Colon drug delivery. Expert Opin. Drug Delivery **2006**, *3*, 111–125.

13. Vandamme, T.F.; Lenourry, A.; Charrueau, C.; Chaumeil, J. The use of polysaccharides to target drugs to the colon. Carbohydr. Polym. **2002**, *48*, 219–231.
14. Sinha, V.R.; Kumria, R. Polysaccharides in colon-specific drug delivery. Int. J. Pharm. **2001**, *224*, 19–38.
15. Liu, L.; Fishman, M.L.; Kost, J.; Hicks, K.B. Pectin-based systems for colon-specific drug delivery via oral route. Biomaterials **2003**, *24*, 3333–3343.
16. Sriamornsak, P. Investigation of pectin as a carrier for oral delivery of proteins using calcium pectinate gel beads. Int. J. Pharm. **1998**, *169*, 213–220.
17. Shu, X.Z.; Zhu, K.J. Controlled drug release properties of ionically cross-linked chitosan beads: the influence of anion structure. Int. J. Pharm. **2002**, *233*, 217–225.
18. Aydin, Z.; Akbuga, J. Preparation and evaluation of pectin beads. Int. J. Pharm. **1996**, *137*, 133–136.
19. Rajesh, K.S.; Khanrah, A.; Biswanath, S. Release of ketoprofen from alginate microparticles containing film forming polymers. J. Sci. Ind. Res. **2003**, *62*, 985–989.
20. Iliescu, R.I.; Andronescu, E.; Ghitulica, C.D.; Voicu, G.; Ficai, A.; Hoteteu, M. Montmorillonite-alginate nanocomposite as a drug delivery system – incorporation and in vitro release of irinotecan. Int. J. Pharm. **2014**, *463*, 184–192.
21. Olukman, M. Release of anticancer drug 5-Fluorouracil from different ionically crosslinked alginate beads. J. Biomater. Nanobiotechnol. **2012**, *3*, 469–479.
22. Kobayashi, M.; Sakane, M.; Abe, T.; Ikoma, T.; Ochinai, N. Anti-tumor effect of a local delivery system; hydroxyapatite-alginate beads of paclitaxel. Bioceram. Dev. Appl. **2012**, *2*, 1–3.
23. Deming, S.N.; Morgan, S.L., Data handling in science and technology. In *Experimental design: a chemometric approach*, B.G.M. Vandeginste and S.C. Rutan (Eds.), 2nd rev. and expanded ed.; Elsevier: New York, NY, **1993**, xv, 437 p.
24. Takka, S.; Gurel, A. Evaluation of chitosan/alginate beads using experimental design: formulation and in vitro characterization. AAPS Pharm. Sci. Tech. **2010**, *11*, 460–466.
25. Prashanthi, D.; Raj Kumar, B.; Nagarajan, G.; Methusala, R.J.; Prasanthi, A. A new analytical method development and validation of capecitabine in pure and tablet dosage forms by UV spectroscopy. Int. J. Med. Nanotechnol. **2014**, *1*, 48–53.
26. Gareth, A.; Lewis, D. M.; Roger, P.-T.-L., *Pharmaceutical Experimental Design*; Marcel Deckker: New York, NY, **2005**.
27. Takka, S.; Ocak, O.H.; Acarturk, F. Formulation and investigation of nicardipine HCl-alginate gel beads with factorial design-based studies. Eur. J. Pharm. Sci. **1998**, *6*, 241–246.
28. Nayak, A.K.; Pal, D.; Santra, K. Tamarind seed polysaccharide-gellan mucoadhesive beads for controlled release of metformin HCl. Carbohydr. Polym. **2014**, *103*, 154–163.
29. Patel, D.; Kumar, P.; Thakkar, H.P. Lopinavir metered-dose transdermal spray through microporated skin: permeation enhancement to achieve therapeutic needs. J. Drug Delivery Sci. Technol., **2015**, *29*, 173–180.
30. Gannu, R.; Yamsani, V.V.; Yamsani, S.K.; Palem, C.R.; Yamsani, M.R. Optimization of hydrogels for transdermal delivery of lisinopril by box-Behnken statistical design. AAPS Pharm. Sci. Tech. **2009**, *10*, 505–514.
31. Friend, D.R. New oral delivery systems for treatment of inflammatory bowel disease. Adv. Drug. Deliv. Rev. **2005**, *57*, 247–265.
32. Mura, P.; Maestrelli, F.; Cirri, M.; Gonzalez Rodriguez, M.L.; Rabasco Alvarez, A.M. Development of enteric-coated pectin-based matrix tablets for colonic delivery of theophylline. J. Drug Target **2003**, *11*, 365–371.
33. Jain, A.; Jain, S.K. Formulation and optimization of temozolomide nanoparticles by 3 factor 2 level factorial design. Biomatter **2013**, *3*, e25102.
34. Malakar, J.; Nayak, A.K.; Pal, D. Development of cloxacillin loaded multiple-unit alginate-based floating system by emulsion-gelation method. Int. J. Biol. Macromol. **2012**, *50*, 138–147.
35. Ahuja, M.; Yadav, M.; Kumar, S. Application of response surface methodology to formulation of ionotropically gelled gum cordia/gellan beads. Carbohydr. Polym. **2010**, *80*, 161–167.
36. Sandoval-Castilla, O.; Lobato-Calleros, C.; García-Galindo, H.S.; Alvarez-Ramírez, J.; Vernon-Carter, E.J. Textural properties of alginate–pectin beads and survivability of entrapped Lb. casei in simulated gastrointestinal conditions and in yoghurt. Food Res. Int. **2010**, *43*, 111–117.

37. Girhepunje, K.M.; Pillai, K.; Pal, R.S.; Gevariya, H.B.; Thirumoorthy, N. Celecoxib loaded microbeads: a targeted drug delivery for colorectal cancer Int. J. Curr. Pharm. Res. **2010**, *2*, 46–55.
38. Malakar, J.; Nayak, A.K. Formulation and statistical optimization of multiple-unit ibuprofen-loaded buoyant system using 2(3)-factorial design. Chem. Eng. Res. Des. **2012**, *90*, 1834–1846.
39. Coates, J. Interpretation of infrared spectra, a practical approach. In *Encyclopedia of analytical chemistry*; Meyers, R.A., Ed; John Wiley: Chichester, UK, **2000**, pp. 10815–10837.
40. Auriemma, G.; Mencherini, T.; Russo, P.; Stigliani, M.; Aquino, R.P.; Del Gaudio, P. Prilling for the development of multi-particulate colon drug delivery systems: pectin vs. pectin-alginate beads. Carbohydr. Polym. **2013**, *92*, 367–373.
41. Del Gaudio, P.; Colombo, P.; Colombo, G.; Russo, P.; Sonvico, F. Mechanisms of formation and disintegration of alginate beads obtained by prilling. Int. J. Pharm. **2005**, *302*, 1–9.
42. Chawla, G.; Gupta, P.; Karodia, V.; Bansal, A. Gastroretention a means to address regional variability in intestinal drug absorption. Pharm. Technol. **2003**, *27*(7), 50–68.
43. Segi, N.; Yotsuyngi, T.; Ikeda, K. Interaction of calcium-induced alginate gel beads with propranolol. Chem. Pharm. Bull. **1989**, *37*, 3092–3095.
44. Mortazavi, S.A.; Carpenter, B.G.; Smart, J.D. An investigation of the rheological behaviour of the mucoadhesive/mucosal interface. Int. J. Pharm. **1982**, *83*, 221–225.
45. Andrews, G.P.; Laverty, T.P.; Jones, D.S. Mucoadhesive polymeric platforms for controlled drug delivery. Eur. J. Pharm. Biopharm. **2009**, *71*, 505–518.
46. Singhvi, G.; Singh, M. Review: in-vitro drug release characterization models. Int. J. Pharm. Studies Res. **2011**, *2*, 77–84.